Doctoral theses at NTNU, 2023:437

Daniel Baltensperger

Optimal and Adaptive Arming of System Protection Schemes

Doctoral thesis

NTNU
Norwegian University of Science and Technology
Thesis for the Degree of Philosophiae Doctor
Faculty of Information Technology and Electrical Engineering
Department of Electric Energy

NTNU
Norwegian University of Science and Technology

Daniel Baltensperger

Optimal and Adaptive Arming of System Protection Schemes

Thesis for the Degree of Philosophiae Doctor

Trondheim, December 2023

Norwegian University of Science and Technology
Faculty of Information Technology and Electrical Engineering
Department of Electric Energy

NTNU
Norwegian University of
Science and Technology

NTNU
Norwegian University of Science and Technology

Thesis for the Degree of Philosophiae Doctor

Faculty of Information Technology and Electrical Engineering
Department of Electric Power Engineering

ISBN 978-82-326-7576-0 (printed ver.)
ISBN 978-82-326-7575-3 (electronic ver.)
ISSN 1503-8181 (printed ver.)
ISSN 2703-8084 (online ver.)

Doctoral theses at NTNU, 2023:437

Printed by NTNU Grafisk senter

Preface

This thesis is submitted in partial fulfillment of the requirements for acquiring a Ph.D. Degree at the Norwegian University of Science and Technology (NTNU) in Trondheim, Norway. The project was developed under the supervision of Prof. Kjetil Uhlen, the co-supervision of Prof. Irina Oleinikova and Prof. Petr Korba. The following projects supported the work:

- SynchroPhasor based Automatic Real-time Control (SPARC), funded by the ENERGIX Program of the Research Council of Norway, under Project 280967, and the industry partners, Statnett, Fingrid, Energinet, Svenska Kraftnat, Landsnet and GE.
- Advanced System protection schemes Applied in the Power grid (ASAP), funded by the industry partner Statnett

Acknowledgments

First and foremost, I express my gratitude to my supervisor, Kjetil Uhlen, for allowing me to work on this exciting and forward-looking topic. I benefited greatly from his expertise in electric power systems and academia. His empathic nature, constructive feedback, constant accessibility, and open-door policy were extremely beneficial throughout this Ph.D. journey. Also, thank my co-supervisors, Irina Oleinikova and Petr Korba, for their supportive and helpful manner. Thanks also to Santiago Sanchez and Salvatore D'Arco for the numerous hours in the lab and the honest, critical, but also friendly advice; I benefited a lot from your expertise. A heartfelt thank you to Hallvar Haugdal for the many humorous coffee conversations and his helpful and open-minded nature. Many thanks to Sigurd Hofsmo Jakobsen for the numerous creative and exciting conversations. I also need to thank Stefan Stanković and Susanne Ackeby for their great cooperation. I learned a lot from you, and I think we were a great team during the ASAP project. Special thanks to my office colleagues Daniel Mota, Lorrana Faria da Rocha, Han Shao, and Fanny Skirbekk, as well as all the department colleagues I cannot list here due to space constraints. Many thanks to the best landlord, Merete Hesdal, for my wonderful home and the warm Christmas invitations during the pandemic. Last but not least, I would like to thank my entire family, who have always supported me in good times and bad during this PhD project. Their encouragement and support have been very important to me, especially in times of doubt and exhaustion.

Summary

A dependable power supply is critical to the well-being of today's society. According to forecasts, this issue will become increasingly relevant and pose numerous challenges that need to be faced. The energy demand is increasing. The load pattern might change and be more temperature-sensitive and volatile. The generation will be less predictable and dictated by geography, which may necessitate energy transfers over long distances. A liberalized power market aggravates the situation, and approvals for grid expansion are progressing very slowly. Therefore, it is becoming increasingly challenging for the transmission system operator to guarantee enough margins concerning stability and thermal overload. Power system flexibility is crucial for ensuring a stable future supply.

System Protection Schemes, the subject of this dissertation, are a measure that can increase the grid's flexibility. By selectively arming schemes, the system can operate with smaller reserves and be more effective (i.e., offering more capacity and lower risk).

Control actions of such SPSs are, for example, generator rejection, load shedding, controlled separation and reconfiguration of the grid, etc.

This thesis presents three adaptive arming methods based on mathematical models and different optimization procedures. The first approach uses a bi-level optimization technique for optimally arming multiple system protection schemes considering steady-state models. This procedure aims to minimize the amount of System Protection Schemes to be armed to detect all critical contingencies while keeping the number of possible trips due to non-critical contingencies as low as possible. This avoids triggering

when unnecessary and positively influences the complexity and scheme's security. One of the challenges is that the approach involves a mixed integer non-linear optimization problem, which is difficult and time-consuming to solve.

The other two procedures presented in this thesis are event-based and predictive under-frequency load shedding, considering different dynamic models. The basic idea is to arm the protection concerning the current system state for a specific contingency, such as electric islanding. Thus, a fast scheme is proposed that requires no computation time during the post-contingency transient phase. The methods showed good results under different assumptions and could keep the quantities in the specified range. However, due to their feed-forward structure, uncertainties may be challenging, and the right granularity of the model is essential.

In this work, the focus was on adaptive algorithms that are closely related to wide-area monitoring protection and control systems that depend on synchronized phasor measurement units. For this reason, various approaches to integrating Phasor Measurement Units into a real-time laboratory were also evaluated in the framework of this thesis. IEC 61850-based Phasor Measurement Units proved promising as they are a simple and cost-effective method to realize a Wide-Area Monitoring System Hardware-in-the-Loop test platform.

Glossary

AD Automatic Differentiation.

aFRR Automatic Frequency Restoration Reserve.

AGC Automatic Generation Control.

CoI Center of Inertia.

FACTS Flexible Alternating Current Transmission System.

FCR Frequency Containment Reserves.

FD Finite Differentiation.

FFR Fast Frequency Reserves.

GNSS Global Navigation Satellite Systems.

gph graph.

GPS Global Positioning System.

HIL Hardware-in-the-Loop.

HVDC High Voltage Direct Current.

IED Intelligent Electronic Device.

IRIG-B Inter Range Instrumentation Group Timecode.

mFRR Manual Frequency Restoration Reserve.

MPC Model Predictive Control.

MU Merging Unit.

OPF Optimal Power Flow.

PD-AD Partial Decoupled Automatic Differentiation.

PDC Phasor Data Concentrator.

PMU Phasor Measurement Unit.

PTP Precision Time Protocol.

ReTeSe Relay Test Set.

RMS Root Mean Square.

ROCOF Rate of Change of Frequency.

RTDS Real-Time Digital Simulator.

RTS Real-Time Simulator.

SPS System Protection Scheme.

TSO Transmission System Operator.

TVE Total Vector Error.

UFLS Under-frequency load shedding.

UTC Coordinated Universal Time.

WAMPAC Wide Area Monitoring, Protection and Control.

Contents

List of Figures

List of Tables

Chapter 1

Introduction

Adequate and secure electricity supply is essential for a well-functioning modern society. Especially in developed countries, reliability is so high that people are often no longer aware of its importance. From an economic perspective, power interruptions have enormous consequences. In automotive production, for example, revenue lost due to power outages can quickly amount to 250'000 euros per minute [56]. Without considering social consequences such as injuries and death, a one-day blackout can lead to costs that are around 0.5% of the gross domestic product [27].

This is strengthened by the clear signs that the reliance on electrical energy is increasing sharply worldwide. The World Energy Outlook 2022 [36] projects an increase in electrical energy consumption of between 75% and 150% by 2050, based on 2021 consumption of about 24700 TWh in all scenarios analyzed. The increase in electrical loads in building services, such as cooling and heating systems, and the increase in the electric transport sector may influence the load pattern concerning temperature sensitivity and volatility [36]. Furthermore, it assumes [36] a significant worldwide increase in renewable energy generation in all scenarios. Consequently, substantially increasing variable demand and generation profiles are expected [36].

In addition to the increased, less predictable generation built at locations where it makes geographical sense, the liberalization of the power

market also contributes to power flows over long distances. This can lead to challenging operations concerning congestion management. All these mentioned aspects motivate the expansion of the power system infrastructure. However, the expansion of high-voltage transmission equipment is highly complex regarding permitting and construction. This time lag in development can lead to changes in generation and consumption happening faster than grid expansion [36]. It should also be mentioned that given the increasing consumption, the market participants expect an adequate trading capacity without a significant cost increase. However, the transmission business is very capital-intensive, which makes it challenging to find an agreement that meets the needs of all parties [14].

"Power system flexibility" is vital to tackle the challenges mentioned above. System Protection Scheme (SPS) can be seen as a tool to enhance flexibility [30]. They can be used to increase transmission capacity, trading capacity, and the reliability of supply [44]. This is also beneficial concerning costly re-dispatching as congestion management (e.g., market zone internal congestion). In more detail, SPSs allow the system to operate with smaller reserves for a limited time while carefully following a protocol for arming post-contingency remedial action. This dissertation concerns these SPSs and, more specifically, how the current arming procedure may be enhanced.

1.1 Outline of the Thesis

This very first section is essential to understand the conceptual backbone of the thesis. It is a brief presentation that outlines the primary objectives of each section and discusses their contribution to the overall manuscript.

The aim of section 1.2 is to provide the reader with a logical explanation of the identified problem based on state-of-the-art, current practice, and future trends. Based on these findings, the various research questions are derived and defined in section 1.3.

The Background section 1.2 assumes the reader is acquainted with various subject-specific topics. However, the second chapter elaborates on the most important theoretical concepts for understanding the background

section more deeply.

The following chapters are based on scientific papers published within the scope of this Ph.D. project. All chapters associated with at least one published paper follow the same structure. First, the motivation and the objectives are presented. In the second step, the methodology is presented, followed by the results and a description of the study case. The last section explains how the topic contributes to answering the research questions and the state of the art. Note that the different papers are included in the second part of this thesis. Typically, they provide more details than the text in the associated chapters.

The only chapter that does not follow this structure is Chapter 4 because the associated paper could only be submitted when the thesis was written. However, it is unclear if it will be accepted. Therefore, it is described in more detail here. Note, the submitted copy can be found in the second part for these readers who prefer a paper.

1.2 Background

1.2.1 Definitions and Fundamental Concept of System Protection Schemes

Organizations worldwide have different definitions of SPS and use different naming conventions for the protection schemes themselves and for the individual steps of the operation [57]. The variety of terminologies can be misleading and implies the importance of a clear definition of terms as they are used in the rest of this manuscript.

The name System Protection Schemes, as suggested in [22], will be referred to in this thesis. The definition presented by CIGRE [16] will be utilized. *A System Protection Scheme (SPS) or Remedial Action Scheme (RAS) is designed to detect abnormal system conditions and take predetermined, corrective action (other than the isolation of faulted elements) to preserve system integrity and provide acceptable system performance.*

It is important to note that protection systems developed by the manufacturer specifically for the protection of a device are counted here as unit

protection (e.g., over-current or distance protection relays) and not as a System Protection Scheme. SPS does not include feedback controllers that aim to maintain electric system quantities within a specific range during Normal operation. Although [16] does not categorize any overload protection that safeguards equipment as an SPS, it does categorize protection measures that enhance system capability. However, this thesis does not differentiate between the two and considers both as SPS. This approach is in alignment with the current method in Norway. The control action used in this work consists of load shedding, production disconnection, and grid reconfiguration, as Statnett uses it, the Norwegian Transmission System Operator (TSO)[58]. Besides the mentioned, Statnett employs other control measures, such as High Voltage Direct Current (HVDC) emergency control, but these are not considered here.

A simple example illustrating the current practice of operating the system with an SPS is depicted in Fig. 1.1. The transmission system operator provides a corridor for transmitting electrical energy from one area or market zone to another. A transmission capacity is offered to the market based on security criteria (e.g., N-1). Fig. 1.1 corresponds to the connection between buses 7 and 9. The control room personnel must carefully observe the flow through the cut since it may reach a critical overload limit (denoted here with S_{max}). Note that there is no information about the specific type of issue that determines the limit. It may be a thermal issue, a stability problem, or both. However, if the flow through the cut exceeds S_{max}, the system state would move from Normal to Alert state (in more detail section 2.1). Although the simple operation in the alert state would technically prove to be problem-free and techno-economically more attractive, losing either line between 7-8 would be devastating and move the system to the Emergency state. The operation in the Alert state would consequently be N-0 secure, which is unacceptable.

When an Alert case is detected, the control room personnel have two options—applying preventive, remedial action such as re-dispatching generators as congestion management or arming system protection schemes as a post-contingency corrective action. In the example illustrated in Fig. 1.1, a generator rejection scheme may be armed to change the power flow

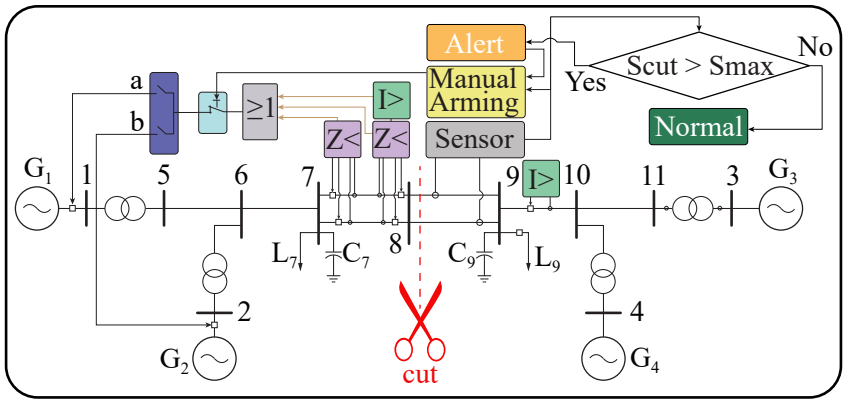

Figure 1.1: Current practice SPS. An illustrative and simplified instance of a generation rejection incorporated in the Kundur two-area model [42].

from buses 7 to 9 in case of a sudden line loss. Arming system protection schemes are advantageous compared to preventive measures because they allow the operation in a more secure Alert state, sometimes called N-1/2 secure state [14] without costly rescheduling generators.

Operating the system in the N-1/2 secure state has significant advantages. SPSs allow the use of the system more flexibly and effectively. More precisely, the trading and transmission capacity can be increased by arming SPS without expensive grid reinforcement [44].

However, this decision-making process is highly challenging and requires significant experience from the control room personnel. A risk analysis must be conducted in the control room to assess whether the SPS's possible triggering is worthwhile compared to the increase in transmission capacity [14]. One of the main objectives of this Ph.D. project is to identify possibilities for model-based optimization techniques that may assist the control room personnel in this challenging decision-making process considering modern measuring and control techniques. This leads to the following research question:

How can control room personnel benefit from modern model-based control algorithms and measurement techniques in the decision-making process of arming SPS?

1.2.2 Strengths and Challenges of System Protection Schemes

As indicated earlier, many reasons and advantages exist for using SPS, such as postponing or even avoiding grid expansion and increasing transmission capacity, as well as avoiding costly re-dispatching for congestion management. Nevertheless, SPS can also be beneficial for operating the system more meshed and consequently more resilient to faults [44]. Regarding security, the classical under frequency protection should be mentioned that reduces the risk of a frequency collapse in situations where a significant amount of generation is lost in the Nordic area [58]. Besides all these positive aspects, there is a drawback of significant importance. An operation with SPSs increases the system complexity [44],[57]. To make matters worse, the amount of SPSs in Norway is expanding [58]. Considering the complexity, the manual arming process should be mentioned explicitly. It is already the case today that large complex SPS always remain armed to reduce the complexity in the control room [44]. Besides reducing the complexity of manual arming, it reduces the dependability-based misoperation (DBM), i.e., the non-triggering when necessary [48]. However, permanent arming makes them more prone to security-based misoperation (SBM), i.e., triggering when unnecessary [48]. Given these advantages and disadvantages of permanent arming described above, it is a priori clear that permanent arming will hurt the coordination of the different SPSs.

The difficulty and relevance of adequately coordinating the individual SPSs were also emphasized by [44]. In addition to the coordination of the SPSs with each other, the coordination between SPS and control infrastructure [7] and SPS and unit protection schemes is also highly relevant [16]. An example of such a lack of coordination can be seen in Fig. 1.1. Assuming the SPS would trip generation G_1 or G_2 although G_3 and G_4 do not have enough spinning reserves, or if the post contingency situation would overload the connection between 9 and 10 in such a way that the

unit protection would isolate the line.

The formulated findings regarding the current practice raise the following research question:

How do the deterministic, model-based optimization techniques affect the coordination of SPS, the dependability, and the security? What potential challenges might arise from this approach?

1.2.3 Testing of New WAMPAC Solutions in a Laboratory Environment

The objectives of SPSs are typically more system-oriented in terms of detecting and triggering remedial measures [7]. The current practice of SPS is rather rule-based, and the different SPSs are tailored for specific contingencies. Due to the deregulated market and the increasing amount of renewable generation, the system's state may change essentially during operation. Therefore, an adaptive SPS is desirable, which, depending on the system state, would coordinate optimally and automatically calculate the minimum remedial action necessary.

Wide Area Monitoring, Protection and Control (WAMPAC) can meet these requirements. The basis for Wide-Area Protection Schemes is the Phasor Measurement Unit (PMU) [54]. They act as sensing devices and estimate typically with 50 or 60 Hz current and voltage phasors as well as frequency and Rate of Change of Frequency (ROCOF). These phasors are time stamps provided by the Global Navigation Satellite Systems (GNSS).

An example illustration of a WAMPAC that would coordinate SPSs can be seen in Fig. 1.2. Compared to the current practice shown in Fig. 1.1, time-synchronous measurements are made at different locations using PMUs. In the WAMPAC block, applications such as state estimation and optimization procedures are implemented for the optimal choice of SPSs.

Real-Time Simulator (RTS) has become essential in academia and industry. The basic idea is to calculate a time step in a mathematical model described by differential equations in time with the real-world clock time [25]. Consequently, the elapsed second of the simulation corresponds to the

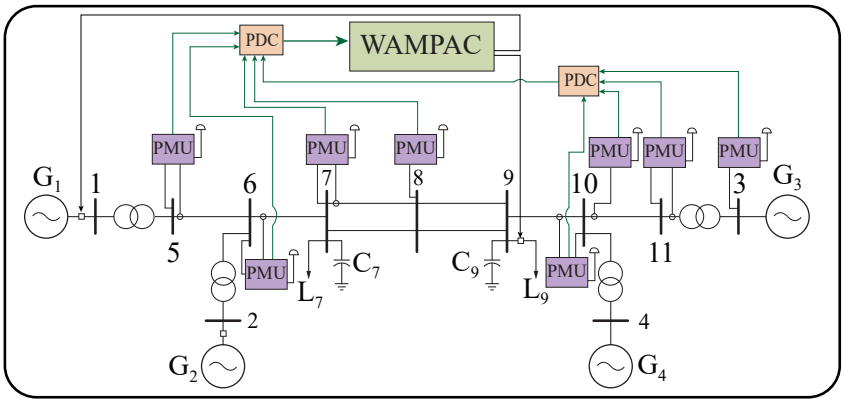

Figure 1.2: An illustrative and simplified instance of WAMPAC for coordinating load shedding and generator rejection in the Kundurs two-area model [42].

one measured in the natural environment [8]. This feature allows it to communicate via an input-output interface with external devices such as IEDs or relays. Typical practical applications are designing, rapid prototyping, teaching, and most dominant testing purposes [25].

Given the strict reliability and security requirements in the power system domain, the benefits of using RTS can also apply to WAMPAC systems. Specifically, it is valuable in testing new algorithms and accelerating the proof-of-concept process [4]. Contingencies that cannot be tested quickly in a real-world application can be evaluated, and the response of different hardware components can be studied.

However, a Hardware-in-the-Loop (HIL) lab test setup to test WAMPAC systems requires a complex laboratory setup. There are different ways to integrate WAMPAC devices into such a setup. Each option has characteristics that can influence the accuracy and overall test capacity [4], leading to the following research question:

What are the technical solutions for integrating WAMPAC devices into a

real-time setup, and how do they differ? What are the common sources of errors, and how can they be identified?

1.3 Objective, Research Questions, Publications

The objectives of this dissertation are primarily to identify how modern optimization techniques, computational methods, and measurement devices can influence the increasingly demanding decision-making process in the control room regarding the arming of SPSs. This goal leads to the research questions R1: and R2: derived in section 1.2. To answer these questions, the research papers described in the Chapters 4, 5, and 6, written in the framework of this dissertation, are used.

In addition, Chapter 3 is used to answer research question R3:.

1.3.1 Research Questions

R1: How can control room personnel benefit from modern model-based control algorithms and measurement techniques in the decision-making process of arming SPS?

R2: How do the deterministic, model-based optimization techniques affect the coordination of SPS, the dependability-based misoperation, and the security-based misoperation? What potential challenges might arise from this approach?

R3: What are the technical solutions for integrating WAMPAC devices into a real-time setup, and how do they differ? What are the common sources of errors, and how can they be identified

1.3.2 Publications

The main contributions that address the research questions are published in the following papers and further described and discussed in Chapter 3 to 6 in this thesis.

P1 D. Baltensperger, K. Uhlen, S. Sanchez-Acevedo and S. D'Arco, "Experimental Characterization of Methods for Connecting Real-Time Simulations and Synchrophasors," 2021 IEEE Madrid PowerTech, Madrid, Spain, 2021, pp. 1-6,
doi: 10.1109/PowerTech46648.2021.9494884.

P2 D. Baltensperger and K. Uhlen, "Optimal Coordination of Multiple System Protection Schemes against Critical Overload Conditions," 2022 IEEE PES Innovative Smart Grid Technologies Conference Europe (ISGT-Europe), Novi Sad, Serbia, 2022, pp. 1-5,
doi: 10.1109/ISGT-Europe54678.2022.9960423.

P3 D. Baltensperger, S. Sanchez, S. D'Arco and K. Uhlen, "Assessing Hardware in the Loop Approaches for Wide-Area Monitoring Control and Protection Devices," in IEEE Transactions on Power Delivery, vol. 38, no. 4, pp. 2724-2734, Aug. 2023,
doi: 10.1109/TPWRD.2023.3255414.

P4 D. Baltensperger and K. Uhlen, "Optimal and predictive under-frequency load shedding against critical islanding contingencies," 2023 IEEE Belgrade PowerTech, Belgrade, Serbia, 2023, pp. 1-6, doi: 10.1109/PowerTech55446.2023.10202682.

P5 D. Baltensperger, S.Stanković, S.Ackeby and K. Uhlen, "An Optimal Arming Technique for System Protection Schemes," *paper is submitted*

Chapter 2

Conceptual Foundation

The main topic of this thesis is the optimal arming and coordination of system protection schemes. The theory of SPSs is an interdisciplinary topic connecting various power system engineering areas. Since the term SPS is used in the literature for various protection schemes, the main objective of this chapter is to provide a clear definition used in this thesis and briefly introduce the relevant areas connected to the theory of SPS.

2.1 Relevant Definitions Related to Protection and Operation

In order to understand the idea of SPSs and the purpose of arming them, this first chapter introduces some definitions, which will be frequently referred to later in the document. Definitions can differ depending on the field (i.e., Power System Engineering, Protection Engineering). If so, it is mentioned here explicitly.

In the context of protection engineering, security, and dependability is, according to [2], defined as the following: "Security in protective systems is a term sometimes used to indicate the ability of a system or device to refrain from unnecessary operations. Often we use security as a generic term to indicate that the system is operating correctly. Dependability in

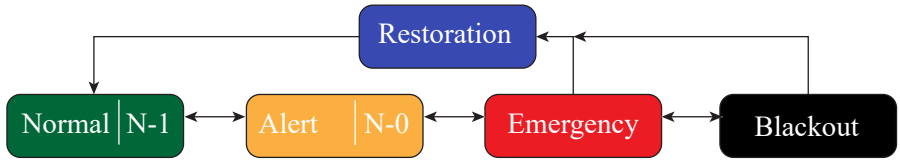

Figure 2.1: The different states together with the N-1 criteria. Note: unlike in [21], in this figure the normal state is considered N-1 secure and the alert state N-0.

protective systems is a term used to indicate the degree of certainty that the system or the device will operate when necessary." This terminology is essential, especially when considering arming, as it will be later explained.

In power system engineering, "Security" focuses on the possible contingencies the system must withstand and consequently represents the system's robustness [27]. Typically, the system should be at least N-1 secure, i.e., any contingency must result in a stable post-contingency equilibrium and no stress or current overloads. Furthermore, the often used term adequacy describes the ability of sufficient generation and grid capacity to meet the demand for electric power and energy at any given time [27].

When considering the operation of a power system, it can be helpful to categorize the system into various states where it can operate. Such a decomposition was first introduced in [43] and later extended in [23] using these states is today common practice. However, the naming of these states may vary slightly, and the representation can be different, as seen in [29]. The states can be divided into Normal, Alert, Emergency, and Restoration and directly related to security criteria such as the N-1 operation, illustrated in Fig. 2.1.

A Normal operating condition implies adequacy and enough margin such that a sufficient security level can be reached [23] (e.g., an N-1 secure operation). The Alert state implies the following: If a contingency occurs that does not push the system out of its limits, but a further additional contingency would result in significant uncertainty as to whether the TSO

can bring the system back to the normal state [21]. If it is not possible to recover from the Alert to the Normal state before another outage with sufficient severity appears, the system may move into the emergency state. In this state, the certainty is not fulfilled, and limitations are exceeded. The definition implies that the system would still be intact in this state; specifically tailored emergency control actions may bring the system back at least to the alert state [23]. If such emergency actions are initiated too late or insufficiently, the system may fail and move to the blackout state.

2.2 Flexibility

The flexibility of the power system can be directly related to uncertainty. This becomes clear when considering some potential drivers, such as the deregulated market, the increasing share of variable renewable generation, the uncertainty of fuel prices (e.g., natural gas) [3], time-consuming grid reinforcement procedures, and the increasing volume and nature of electricity demand, to name a few. This indicates that in a future power system, more flexibility is needed. A general definition given by [30] is: "Flexibility relates to the ability of the power system to manage changes". This definition was derived from a summary of the various definitions commonly used in the literature (see, for example, the collection given by [47] and [30]). However, the stated definition is an umbrella term that is difficult to grasp. Therefore, [30] proposed differentiation in terms of time, spatial extent, and physical manner [30]. This can be seen in Fig. 2.2. The flexibility of Power describes the uncertainty of the short-term system-wide power equilibrium that may be increased due to the more significant amount of variable sources, potential measure is, for example, fast frequency reserve. Flexibility of Energy, on the other hand, is more related to the long-term equilibrium where storage systems may be appropriate measures. Local uncertainties, for example, due to the increasing amount of distributed generation, may lead to more so-called Flexibility in Voltages, and Flexible Alternating Current Transmission System (FACTS) devices may be used to change the reactive power injection at selected nodes. The increasing

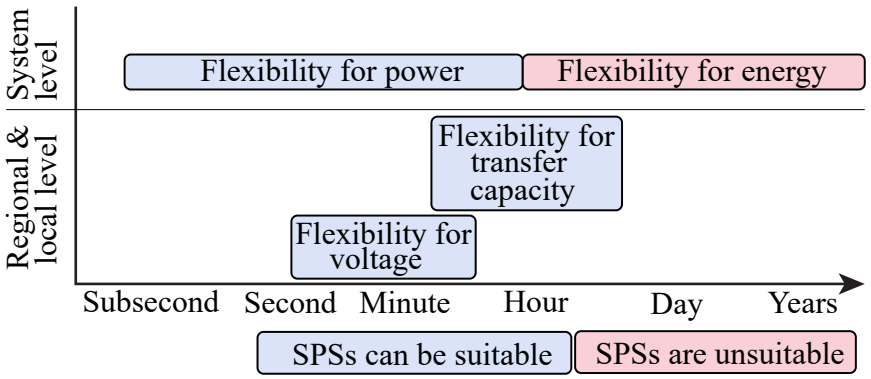

Figure 2.2: The differentiated terminology of flexibility (proposed by [30]). The illustration is based on [30] but additionally shows the categories in which SPSs might be suitable.

utilization level, with a highly fluctuating peak supply and demand, can lead to the need for more so-called Flexibility for Transfer Capacity.

SPSs can positively influence these challenges in terms of flexibility and provide added value for mastering them. However, not all types of flexibility presented above can be addressed equally well. Fig. 2.2 illustrates the categories of flexibility in which SPSs may or may not contribute, denoted by blue and red, respectively.

2.3 The Day-Ahead and Intraday Market

The electricity market, especially the intraday and day-a-head market, is essential for unit commitment and dispatch. It is a far-reaching topic in power system engineering. Although the field may seem relatively non-technical at first glance, it plays a crucial role in how power systems operate (i.e., it directly dictates the unit commitment and dispatch). SPSs can contribute to realizing a market-optimal operating condition in a technically

secure manner. For this reason, the essential aspects are briefly described here.

The Market Operator and the Transmission System Operator are two essential actors in the topic of power markets. The Market Operator that manages the Nordic power exchange is called Nord Pool [6]. It is responsible for providing a fair marketplace for trading products on the spot and in the financial markets [12]. Furthermore, Nord Pool publishes a price reference and creates incentives to avoid congestion in the power grid with a spot market price mechanism [12].

The transmission system operator's role is to provide an acceptable supply quality and the infrastructure for a well-functioning power market [14].

The day-ahead market provides an equilibrium schedule for the next day for every hour. This is important because some generating units may have long time constants and ramping constraints, so they cannot adjust their power set-points as quickly [49]. It is also beneficial for maintenance purposes that can be planned and coordinated better.

Generator units and retailer estimate their production or consumption for each hour for the next day. Based on these forecasts, they submit an offer by noon, stating how much energy and at what price they are willing to sell or buy energy. Based on the bids, an optimization problem is solved for each hour in which the so-called social welfare is maximized. At a predetermined time in the afternoon, the individual actors get the information on whether and to which price condition they were scheduled for the next day [49].

Generation and load are thus scheduled between 12 and 36 hours in advance. Naturally, there may be unforeseen deviations, such as unexpected shifts in demand or abrupt weather fluctuations. In this case, there is the intra-day market where energy can still be traded bilaterally between 5 minutes and 2 hours (depending on the country) before the operation hour [50]. However, the power available in this market may be limited. According to [6], in October 2010, the average intra-day trading volume was around 300 MW, while the average volume in the day-ahead market was around 30'000 MW.

2.4 Interplay Between Balancing Market Frequency Control

The balancing market involves an interaction between the retailer or generator companies and the transmission system operator, specifically addressing short-term deviations from the initial plan. The ultimate goal of the transmission system operator is to achieve one of their core objectives, namely, to ensure that generation and consumption are balanced the whole time. The TSO must guarantee that the frequency control always keeps the frequency within defined limits and above 49 Hz [20]. Therefore, even the reference incidence (i.e., a trip of the system's largest generator) should not trigger under-frequency load-shedding action below 48.8 Hz [20].

The regulation market is operated to ensure that the transmission system operator has sufficient reserves. Companies willing to manually increase or decrease their production or demand can participate by submitting bids. The TSO encourages market participation by adjusting prices based on day-ahead market conditions, making it financially beneficial to be available for up-regulation and down-regulation [50]. There are various pricing policies and strategies, but these will not be discussed further here since they are out of scope.

The transmission system operator provides different products that vary mainly in their activation time and the method (either manual or automatic). These products are called ancillary services and are available for frequency regulation, voltage regulation, and system restart [51]. Note only those services related to frequency regulation are briefly described here.

The Frequency Containment Reserves (FCR) are also called the spinning reserve in this thesis (especially relevant in Chapter 5). It is designed to stabilize the frequency automatically. This reserve is implemented with a droop regulation where the generators change their active power output proportionally to the frequency deviation. The technical implementation can be seen in Fig. 2.3 located in the rectangle labeled FCR, where R represents the droop. In the Nordic a distinction is made between FCR-N and FCR-D. FCR-N is active and arranged symmetrically, i.e., with the same

capacity for up and down-regulation, while the FCR-D is only designed for up-regulation [38]. The total reserve is distributed to several power plants, where most of them are hydropower plants [41]. These power plants must fulfill specific design criteria. For example, Svenska kraftnät requires 63% of its FCR-N to be ready within one minute and 100% after 3 minutes [38]. FCR-D, on the other hand, is specifically designed to keep the nadir above the minimum instantaneous frequency after an N-1 contingency [41]. If the frequency falls below 49.9 Hz, the control action will activate automatically [38].

The Automatic Frequency Restoration Reserve (aFRR) can be considered Automatic Generation Control (AGC), also called secondary or load frequency control. Note that generators participating in the FCR all feed in power proportional to the frequency deviation, regardless of where they are located. As a result, there is first a steady state frequency deviation and, second, a change in the scheduled tie-line power flows [42]. The AGC eliminates these two deviations precisely. It is a slow-acting centralized controller with an integrator part that changes the set points of the different generators (see Fig. 2.3). The controller eliminates permanent frequency deviation and unplanned tie-line flows such that only generators located in the same zone as the failed generator are used to replace it.

The Manual Frequency Restoration Reserve (mFRR) is the product that are traded in the regulation market described above. Typically it is used to restore the used aFRR and is done based on unit-commitment and dispatching considerations. It is also used if the aFRR can only partially achieve its two objectives. Another important application is the so-called re-dispatching regarding congestion management (see section 2.5) The interplay between frequency control and the markets are illustrated in Fig. 2.3.

Fast Frequency Reserves (FFR) are the Nordic region's latest additional service. This reserve was created in response to the decreasing amount of inertia in the system. Decreasing inertia indicates that the generation units' frequency response speed must become faster to keep the frequency for the reference incidence above 49 Hz. The generator units cannot become faster because the governor system physically dictates their response. For this

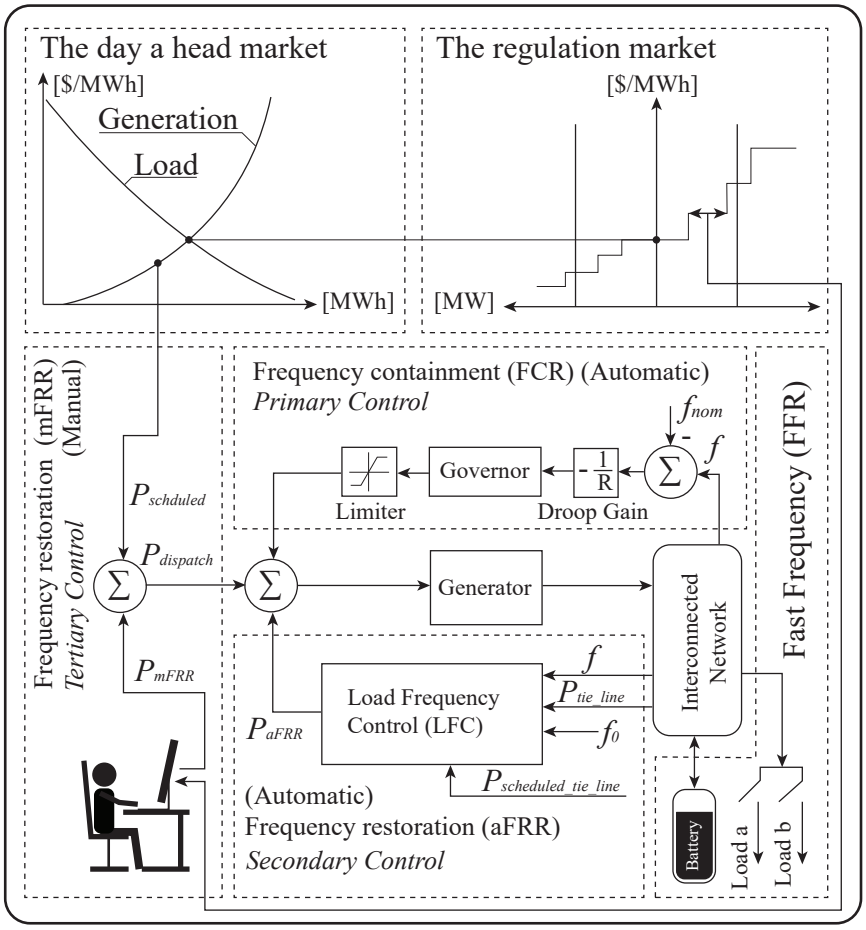

Figure 2.3: A simplified sketch of the interaction between the market and frequency control (illustration is adapted and based on [53]).

reason, the concern increases that the FCR-D is no longer fast enough, resulting in FFR [20]. Quick reaction time is crucial to be considered as a reserve provider, typically between 0.7 and 1.3 seconds, where the reserve activation is between 49.5 to 49.7 Hz [20].

The interplay between the different ancillary service products can be seen in Fig. 2.4

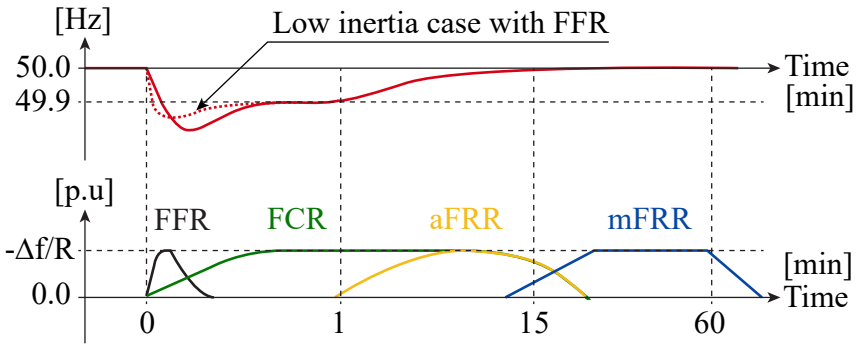

Figure 2.4: Frequency related ancillary services in operation (graphic is adapted and is based on, [60] publicly available in [1])

2.5 Loading Limits and Congestion Management

The national TSOs monitor and analyze the transmission system using state estimation and contingency analysis tools to determine the power corridors' capacity limits and ensure that the system operates within these limits [61]. The identified capacity limits are passed to the market operator and incorporated into the day-ahead market used for the planning phase.

The overloads that dictate these capacity limits can be different. A distinction is made between thermal limits, i.e., a specific maximum current in the conductor, and stability limits [61]. These limits are related to rotor angle and voltage stability limits. Which of the three limits is the most dominant depends on the point of operation, the types of loads, the unit-

commitment, and for example, grid configurations. Therefore, these factors must be determined individually by the TSO.

Besides security problems, congestion can lead to reduced competition, preventing the realization of the full potential of a deregulated electricity market [9]. In the Nordic system, there are two types of congestion management: market coupling and countermeasure [14].

In market coupling, the power system is divided into different market zones, with the zone boundaries reflecting common bottlenecks in the grid [14]. Fig. 2.5 shows the zonal pricing model in the Nordics. The idea is to implement the day-ahead market so that a uniform energy price for all zones appears in cases of no congestion. However, market participants bid in the different zones separately. If congestion occurs between multiple zones and the day-ahead market is closed separately for each zone, resulting in different prices. Transmission congestion will be offset [64].

If the congestion is inside one particular zone, the transmission system operator must re-dispatch generation and consumption to relieve the internal bottlenecks [31] which can be done by considering the bids in the regulation market [64] (i.e., participants willing to provide mFFR).

2.6 System Protection Schemes

2.6.1 Definition

Organizations worldwide work with SPSs and use different naming conventions for the protection schemes themselves but also for the steps of the operation. The variation of terminologies and definitions can, first of all, be confusing but can also be risky since one word is used for two different meanings [57].

As mentioned in section 1.2, this thesis uses the CIGRE definition [16] *A System Protection Scheme (SPS) or Remedial Action Scheme (RAS) is designed to detect abnormal system conditions and take predetermined, corrective action (other than the isolation of faulted elements) to preserve system integrity and provide acceptable system performance.*

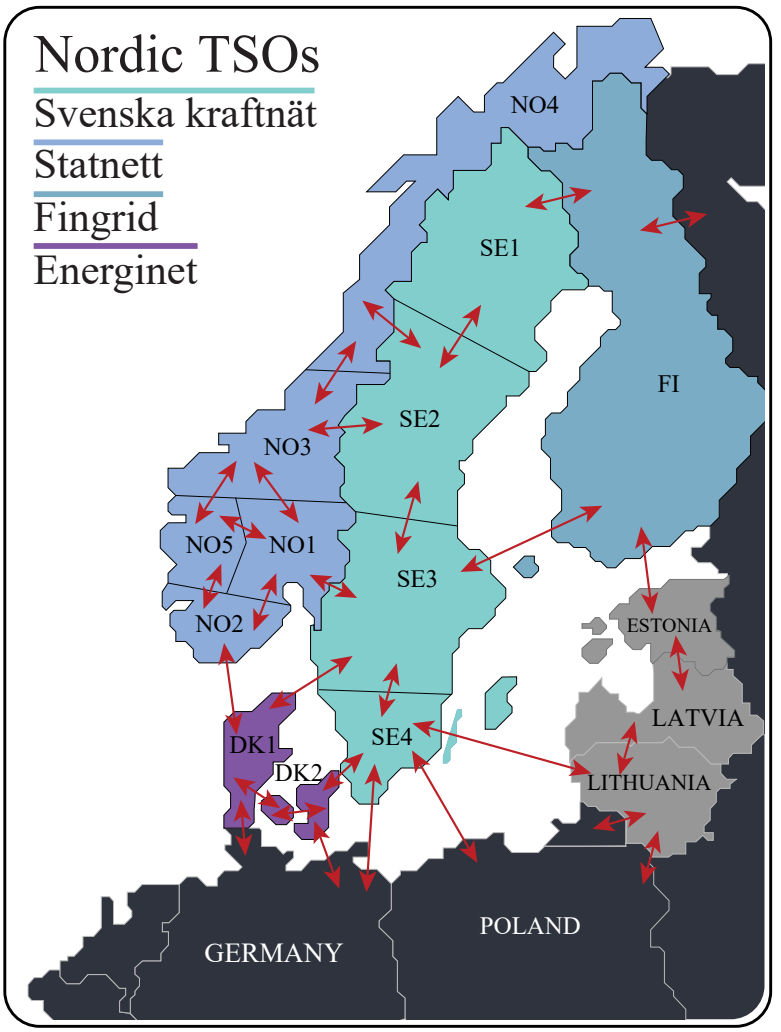

Figure 2.5: The different market zones in the Nordic region (the illustration is adapted and is based on [59])

Operating the Norwegian transmission system under N-1 secure operation is not always possible. If a contingency is detected that would cause the system to operate outside its limits, it implies the operation is in the N-0 secure (i.e., Alert) state. However, if it is possible to arm an SPS, the operation can be lifted between the Normal and Alert states, called the N-1/2 secure operation state [28]. If the particular contingency detected appears, the SPS would be triggered automatically, and the post-contingency state would go back to the Alert state but not directly to the Emergency state. Consequently, Fig. 2.1 can be extended with the N-1/2 secure operation (see Fig. 2.6) to bring this definition into the above context. The state allows to operate the system more effectively. Based on this relaxation of the N-1 criterion and subsequent expansion of the possible states, the benefits of SPS result directly. By arming SPS, the transfer capacity can be increased. This point means improving the transfer between market areas and avoiding the need for re-scheduling in market zones, a common issue with zonal pricing. Additionally, SPS can be helpful in situations where there are delays in network expansion or when individual devices require maintenance.

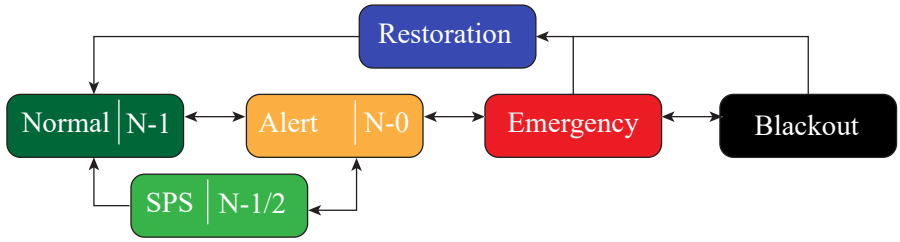

Figure 2.6: The N-1/2 secure operation state

2.6.2 Control Actions

Typical control action by system protection schemes are [16]: Generation and load rejection, turbine fast valving/generator runback, gas tur-

bine/pumping storage start-up, Under-frequency load shedding (UFLS), Undervoltage load shedding (UVLS), HVDC fast power change, automatic shunt switching, dynamic braking or braking resistor, controlled opening of interconnection/area islanding, tap changers blocking and setpoint adjustment and quick increase of generator voltage setpoint.

In the following, some of these schemes will be briefly explained in more detail, because they are relevant in the Nordics and to the thesis.

Under-Frequency Load Shedding

UFLS is a countermeasure against frequency swings appearing after a sudden mismatch in generation and consumption. Such an imbalance typically appears after a generation loss or a grid separation.

The basic idea can be seen in Fig. 2.7. The illustration shows the system's response to a loss of generation. On the right-hand side, the frequency is plotted versus the time; on the left-hand side, the frequency is plotted versus the power. The frequency is divided into a normal operation zone (blue), a frequency range where loads are shaded (orange), and an emergency zone (red). The left-hand side shows the turbine's steady state characteristics in black and grey solid. Due to the proportional primary frequency control, the first part is linear but starts dropping at some point since individual governors may reach their limit. At the maximum point, the last governor connected reaches its limit. The efficiency of the connected turbines may be frequency-dependent. This is why, for lower frequency, the power decreases [45]. This effect concludes in an upper (stable turbine curve) and a lower unstable part.

Assuming a sudden generation loss, the initial operation point $P_{L,0}$ reduces to point 2. Since the frequency is related to the speed of synchronous generators which are state variables, the frequency remains the same in the first moment. The blue solid curve shows the dynamic behavior of the system response. After reaching point 3, the first stage of loads are shed that would lead to a final steady-state equilibrium in $P_{L,1}$. However, the frequency continues to decrease and exceeds the second and third UFLS thresholds. In point 6, the frequency reaches its minimum point, also called

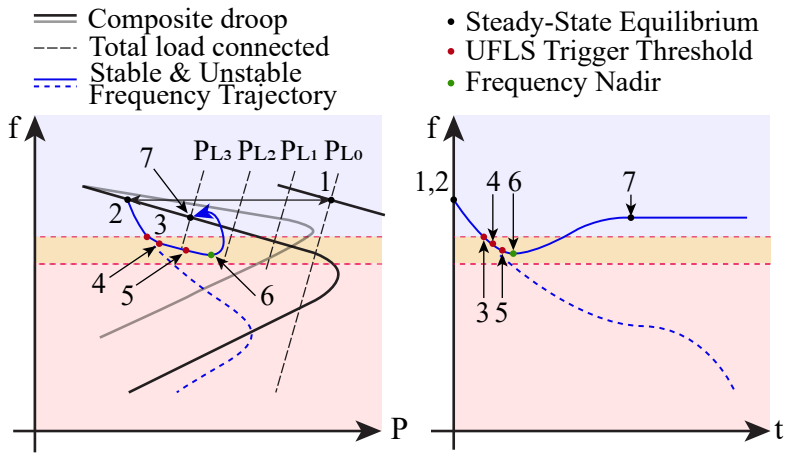

Figure 2.7: Basic frequency based UFLS (graphic is adapted and is based on [45])

the Nadir point. The final steady-state point can be seen in 7. The blue dashed curve shows the response without load-shedding remedial action. The response is too slow and crosses the unstable equilibrium.

The grey solid curve shows a situation where not enough spinning reserves are available. In this situation, it is evident that some load-shedding action must be triggered.

In summary, when considering UFLS, it is not only the steady-state properties that are important, but the dynamic behavior must also be considered. The amount of inertia as well as the speed of the frequency controller, are decisive for whether a stable equilibrium can be achieved or not [39].

The regulations for UFLS in the Nordics depend on the country. Norway distributes the amount of control action to the different regions where each area is assumed to shed between 20%-50% of the total consumption [32]. Within the Nordic System Operation Agreement (SOA), 30 % of the total loss is shed over multiple stages between 48.7 Hz and 47 Hz [32].

Grid Reconfiguration and Grid Separation

The controlled islanding of systems is a method that allows blocking different dangerous phenomena such as rotor-angle oscillations, voltage collapse, cascading problems, etc.[18]. The main idea is to find a set of lines to be disconnected such that the system can be split into multiple isolated and stable subsystems [18]. This thesis covers grid reconfiguration, a control action that can, for example, protect the lower voltage grids against large currents after losing a high voltage line by switching off particular transformers or lines.

Generator and Load Rejection

Generator rejection is a remedial action typically event-based, meaning that based on logic, a specific combination of generators is disconnected after a fault. A typical application is to protect the system against transient rotor angle instabilities.

The basic idea is that with the trip of machines, one tries to increase the electrical power of the remaining machines [16]. The situation becomes particularly clear when considering the equal-area criterion. A sudden reduction of the mechanical power due to the tripping of the machine after the fault increases the braking energy (deceleration area). This increases the chance that the rotor does not exceed the unstable equilibrium.

However, the generator and load rejection can also be used against critical thermal overload situations after losing specific lines.

2.6.3 Arming

An SPS can be prepared for triggering if a system state is reached in which a contingency would jeopardize the system concerning overload (thermal or stability). The SPS must be able to detect the contingency properly and provide sufficient remedial measures. This preactivation of an SPS is defined as arming. Arming is an important mechanism when dealing with system protection schemes. It can be done automatically or manually; some are even armed all the time [7].

The concepts and procedures presented later here will support the operator's decision regarding the arming step.

The main idea is to arm the system protection only on those operations where it could be potentially valuable rather than otherwise. This may help to avoid a so-called security-based misoperation (SBM), which corresponds to triggering when not required.

In contrast, the so-called dependability-based misoperation (DBM) corresponds to a non-triggering when required.

[48] showed, based on a specially developed reliability procedure and a realistic example, that permanent arming improves concerning the DBM but, as assumed, is significantly worse concerning the SBM.

2.6.4 Classification

SPSs can be classified according to their structure.

Response-Based

These SPSs follow a feedback structure [52]. They are not explicitly tailored for a particular contingency [52]. The input is a measured quantity, such as voltage or frequency. The conventional UFLS is an example of such a response-based SPS [52]. They are highly dependable because they respond directly to deviation despite uncertainty. However, they are relatively slow because they wait until the measured quantity reacts [52].

Event-Based

These types of SPSs follow a feedforward structure [52]. They are typically tailored for certain critical contingencies, and their design is determined using offline simulations. They are fast and typically rule-based. However, they might be sensitive with respect to uncertainty (like all feedforward controllers).

2.6.5 Adaptive System-Protection Schemes

All methods presented here are considered adaptive because they determine the best control action to be armed online on the system's current state. Arming refers to the concept described in more detail in subsection 2.6.3. Essentially, the arming process must ensure sufficient mitigation extent in the right place and that the SPS can detect the corresponding contingency accurately. This is done here based on model-based optimization techniques. However, there are two significant challenges to this control structure. First, and probably most obvious, is that a model describing the system is needed. The second challenge becomes apparent when looking at Fig. 2.8. All algorithms shown here try pre-calculating for a given system state and contingency the optimal control action. This pre-calculation is done repetitively and as fast as possible. A timeline is drawn in Fig. 2.8 to illustrate the problem. The optimization number k starts at time t_0 and ends at $t_0 + \Delta t$. After the optimization, the arming state can be updated. That point means the arming at state number k is active while optimization number $k+1$ runs. Consequently, if the operations point of the system changes quickly in relation to the computation time, the applied control action may be unsatisfactory.

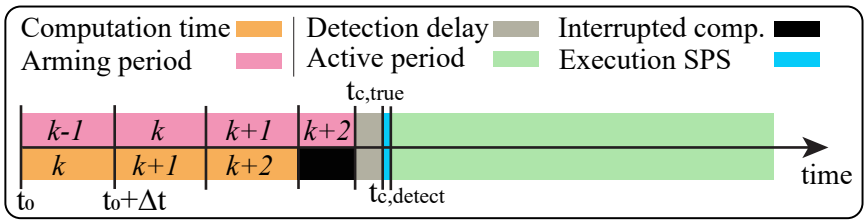

Figure 2.8: Adaptive and event-based approach for arming procedures presented in this thesis

2.7 Fundamentals About Phasor Measurement Units (PMUs)

Today, the measurement rate of the devices used for SCADA and EMS is around 1 Hz, which is too slow for measuring the dynamics appearing in the system accurately [61]. Therefore, there is a clear need for time-synchronized measurement devices with higher measuring rates. PMUs fulfill this requirement precisely. The central concept of a PMU is to estimate a synchrophasor, the frequency and rate of change of frequency (ROCOF).

According to the C37.118 standard[35], a synchrophasor is defined as follows: A sinusoidal signal $x(t) = X_m \cos(\omega t+\delta)$ can be written as a phasor $X = (X_m/\sqrt{2}) \exp(j\delta)$ [35]. Let X be a phasor representing a cosine signal with a phase δ. In addition, let δ be the phase difference between a reference cosine function with nominal frequency f_0, which is furthermore time synchronized with the Coordinated Universal Time (UTC). In this case, X is called synchrophasor [35]. The synchrophasor definition is written as a mathematical equation in (2.2) [35], whereby it should be mentioned that the magnitude $X_m(t)$ is written here as a function of the time.

$$x(t) = X_m(t) \cos\left(2\pi f_0 t + \left(2\pi \int_{t_0}^{t} (f(\tau) - f_0)\, d\tau + \delta\right)\right) \tag{2.1}$$

$$X(t) = \frac{X_m(t)}{\sqrt{2}} \exp\left(j2\pi \int_{t_0}^{t} (f(\tau) - f_0)\, d\tau + j\delta\right) \tag{2.2}$$

For the evaluation of the PMU measurements, the standard [35] defines the following three metrics. The so-called Total Vector Error (TVE) is used to evaluate the synchrophasor. The TVE is defined as written in (2.3). X_r and X_i are the theoretical true reference quantities representing the real and complex parts. $\hat{X}_r$ and $\hat{X}_i$ stand for the measured quantities.

The frequency and ROCOF error are defined according to (2.5) and (2.4).

$$TVE = \sqrt{\frac{\left(\hat{X}_r - X_r\right)^2 + \left(\hat{X}_i - X_i\right)^2}{(X_r)^2 + (X_i)^2}} \tag{2.3}$$

$$FE = |f_{\text{true}} - f_{\text{measured}}| \tag{2.4}$$

$$RFE = \left| \left(\frac{\mathrm{d}f}{\mathrm{d}t}\right)_{\text{true}} - \left(\frac{\mathrm{d}f}{\mathrm{d}t}\right)_{\text{measured}} \right| \tag{2.5}$$

As can be seen from the formula, the TVE is a number that summarizes inaccuracies in terms of phase and magnitude. Since it is sometimes advantageous to consider this separately, the phase and magnitude errors are defined separately in this thesis (see (2.6) and (2.7)).

$$E_{ang} = \hat{\varphi}_{x,1} - \varphi_x \tag{2.6}$$

$$E_{mag} = \frac{|\underline{\hat{X}}| - |\underline{X}|}{|\underline{X}|} \tag{2.7}$$

PMUs typically have a reporting rate of 50 frames per second for 50 Hz systems and 60 frames per second for 60 Hz. Other reporting rates are possible, as written in the standard [34].

A PMU setup comprises several PMUs, one or more Phasor Data Concentrator (PDC), and an accurate clock. A PDC is a node in a communication network that receives multiple streams of measurement data from PMUs and possibly other PDCs, processes the data according to their time stamp, and forwards the data as a single stream [33].

In such a communication network, time delays also occur. The delay of data from a PMU to the end PDC is called synchrophasor data latency. It comprises the PMU reporting latency, network delays, and the various PDC-latencies [35]. It is important to note that the delays experienced may differ depending on the specific setup, so it is recommended to check each system individually for its respective delays [34].

Time synchronization is essential for PMUs since inaccuracies in synchronization lead immediately to a phase error in the measurements. For this reason, the standard [35] specifies that the accuracy of the time stamp should be at least 1 μs over 100 years (which would result in a phase error of 0.018 degrees for a 50 Hz system) [35].

Typically, two different time dissemination techniques are used for PMUs to synchronize their internal clock with a primary time source. First, one uses the atomic clocks built into Global Positioning System (GPS) satellites and synchronizes the internal clock of a PMU or a master clock with that of the GPS satellites. Secondly, a network-based method (e.g., Inter Range Instrumentation Group Timecode (IRIG-B) or Precision Time Protocol (PTP)) synchronizes individual PMUs with a master clock, primarily of interest when there is no clear sky view at the location [17].

Chapter 3

Experimental characterization and evaluation of WAMPAC real-time HIL test platform

This chapter is based on the two publications P1 and P3, where it should be mentioned that P3 is a continuation of P1. The two publications contribute to answering the research question R3:. In addition, the expertise and knowledge acquired contributed to developing the publication [55], where a specific application was implemented and assessed.

3.1 Motivation and Objective

WAMPAC is a promising solution for protecting and controlling the future power grid. SPSs are, in fact, a type of WAMPAC as they, by definition, do not aim to protect a specific device but the system integrity. This is one reason the topic is highly relevant to this thesis.

Real-time simulators are favorable for testing WAMPAC systems. These

simulators enable the incorporation of actual devices into theoretical simulations, also known as hardware in the loop. HIL is beneficial since it can accelerate the development procedure and proof of concept.

The main components of such real-time WAMPAC test setup are PMUs, PDCs, precise GPS-synchronized clocks, a communication network, and converters. Before testing any WAMPAC algorithms, it is essential to evaluate the real-time setup due to its complexity and error-prone nature. Identifying various sources of error and characterizing the platform is a fundamental topic of this chapter.

There are different approaches to implementing such a WAMPAC test setup with its devices, all of which have advantages and disadvantages. This chapter presents three methods for incorporating PMUs into a WAMPAC test setup.

In the first method, the real-time simulator generates and outputs the phasors, referred to as synthetic phasors. The method is dominated by simplicity but may neglect essential points, such as concepts of the phasor estimation algorithm. One advantage is that any number of phasors can be generated.

In the second method, hardwired PMU devices estimate the phasors. This method is exceptionally realistic because it measures and processes the actual physical quantities. However, it must also be emphasized that the method is associated with relatively high laboratory costs and more considerable complexity. The number of possible phasors is given by the surrounding laboratory equipment, such as the converters, and the number of PMUs available.

The IEC 61850 standard is becoming more popular, leading to a third approach for integrating PMUs into a real-time setup. This involves using the real-time simulator to publish sampled values (SV), which an Intelligent Electronic Device (IED) then uses to calculate the phasors. This method is interesting because it involves hardware equipment such as IEDs and is more realistic than the synthetic approach. Since the method requires much less equipment (for example, no converter is needed), it is also economically appealing. The number of phasors is also limited, but only concerning the number of PMUs, not analog outputs.

The literature review conducted in the framework of the publication P3 found that most of the papers focused on either synthetic PMUs generated by the real-time simulator or hard-wired devices (for more information, see paper P3).

There is minimal literature on IEC-61850-based PMUs included in a real-time test setup. [10] is one of the literature. It shows a WAMPAC test system, including a real-time simulator that publishes sampled values and an Advanced RISC Machine (ARM)-based device that generates the phasors according to [34]. The platform can generate 64 synchrophasors and dominates through its cost-effective implementation and scalability. Besides describing the implementation, the reporting latency was analyzed. However, even though the author mentioned the possibility of generating the phasors in the Real-Time Digital Simulator (RTDS) (note the abbreviation is also the name of a company in the field), no comparison between the three approaches is presented. [11] shows a method that, besides the PMU reporting latency, can also be used for the end-to-end latency, which is highly relevant for WAMPAC applications. For measuring these latencies, a multicore microcontroller (XMOS xCORE) platform is used. It was shown that the presented method could be used for all three approaches (i.e., phasors generated in the RTDS hard-wired PMUs and PMUs subscribing to sampled values). Furthermore, it should be mentioned that the proposed technique is not limited to real-time test platforms.

To the best of the author's knowledge, the work of [26] is currently the publication most closely related to the subject described in this chapter. A performance evaluation of three commercial PMUs in a real-time setup is presented. One PMU measures analog signals, while another estimates the phasor based on sampled values. The third PMU considers analog and sampled values and processes them in parallel. Dynamic and steady-state tests were evaluated based on a reference, a synthetic PMU generated in a real-time simulator.

The overall objective of this chapter is consistent with the goal of P3:

- To provide a comparative assessment of three HIL approaches for WAMPAC testing, including synthetic synchrophasors, IEDs sub-

scribing sample values and hard-wired IEDs extending the work presented in [5].

3.2 Methodology

The WAMPAC real-time test platform is illustrated in Fig. 3.1. 1) Shows an overview of the laboratory. Sub-figure 2) illustrates the used real-time simulator (RTS) of OPAL-RT model 5600 with 12 cores. 3) displays the Merging Unit (MU)s and IEDs used in the setup. In addition, a Relay Test Set (ReTeSe) from Omicron model CM C356 is shown. This device can output analog signals as well as sampled values. In sub-figure 4) is a picture of the converter used to amplify the analog signals generated in the RTS. It is a high-bandwidth power amplifier fabricated by Egston Power with a nominal output capacity of 200 kVA. 5) the communication switch from the manufacturer Planet is shown, and sub-figure 6) depicts the measurement transformers. For more technical details, please see P3.

Fig. 3.2 represents the WAMPAC laboratory setup in a schematic diagram. Two MUs and two IEDs are included in the setup. All these devices have a software function that allows them to estimate phasors and output them as a C37.118 data frame. It is important to emphasize that the MUs used in this setup convert the analog signals to IEC 61850 sampled values and act simultaneously as PMUs. A separate computer is connected to the local area network that runs PDC software. In all tests described in this chapter, the PDC is configured not to combine the individual phasor streams into one stream as described in section 2.7 but forwards each stream separately. The master clock is time synchronized with GPS, where an antenna on the roof is used. All equipment used is time-synchronized to this master clock using PTP or IRIG-B.

This chapter proposes a three-stage procedure to evaluate this WAMPAC test system, depending on the stage, using the ReTeSe or the RTS as the source. However, the measurement block remains the same for all tests. The procedure furthermore consists of dynamic as well as static tests. Fig. 3.3 illustrates the exact test setup configuration. The two MUs estimate

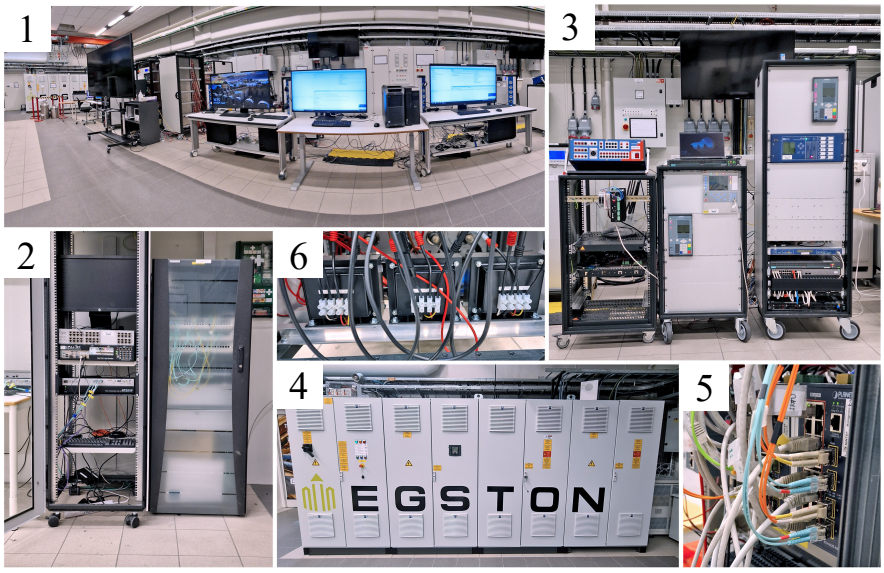

Figure 3.1: A photograph of the WAMPAC laboratory test setup

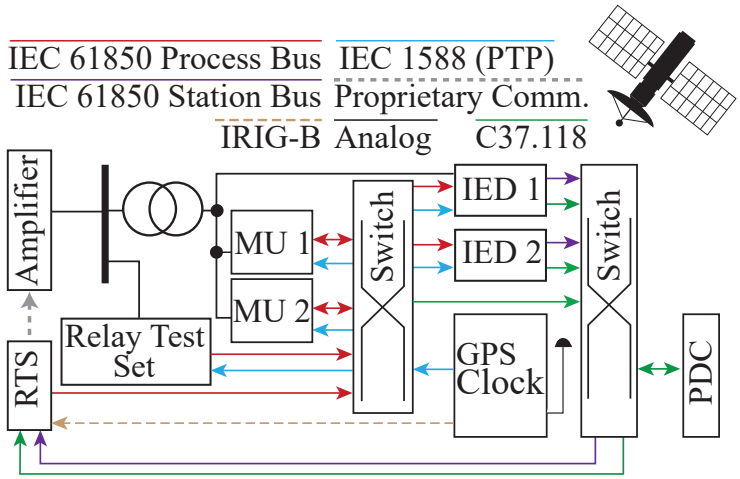

Figure 3.2: A schematic diagram of the WAMPAC laboratory setup

the phasors based on analog measurements. In addition, MU2 also publishes sampled values subscribed by IED1 and IED2. Consequently, IED1 estimates the phasors based on the sampled values and the analog measurements, while IED2 estimates the phasors based only on the sampled values. To be precise, it obtains the samples from MU2 and the respective active sources (RTS or ReTeSe).

Only switch two in Fig. 3.3 is activated in the first stage. Amplitude and phase in the ReTeSe are varied, and the measurements are stored in the RTS. In the second stage, only switches 3 and 1 are active, and the test is repeated. Thus, the effect of the measuring transformers can be observed. In the third stage, only switch 4 is activated, which implies that the RTS now acts as a source and measurement storage (i.e., it closes the loop). Unlike in stages one and two, dynamic tests can now be used for assessing the setup. The reference signal for these tests is a step in magnitude from 90% of the nominal voltage to 100%, ramping up the phase or adjusting a fixed off-nominal frequency of 0.05 Hz.

It should be noted that the real-time simulator is equipped with an

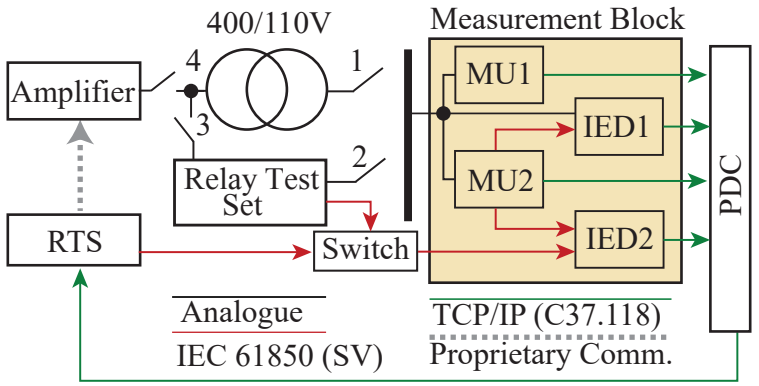

Figure 3.3: Test setup with all configuration options

internal Oregano board that is synchronized with IRIG-B, providing an accurate simulation time. This allows received phasors to be compared against simulation time or their respective timestamps.

3.3 Test Case and Results

The most relevant results are briefly shown in this section. For more results of the individual tests, please refer to the paper P3. The scenario examined here shows an incorrectly set converter acting as the source of the error.

The static tests of stage one are shown in Fig. 3.4 for a voltage of 30 volts. The IED that subscribed to the sampled values directly from the source (i.e., ReTeSe) and estimated the phasors based on them achieves the smallest TVE (see red curve IED 2). The highest TVE, on the other hand, was observed when an IED estimated phasors using sampled values subscribed by an MU that measured analog values. This can be seen by considering the TVE of MU 2, IED 1 (Subscr. MU 2), and IED 2 (Subscr. MU2) in Fig. 3.4.

The following can be concluded when considering the stage 3 results as shown in Fig. 3.5. The TVE has increased significantly compared to those

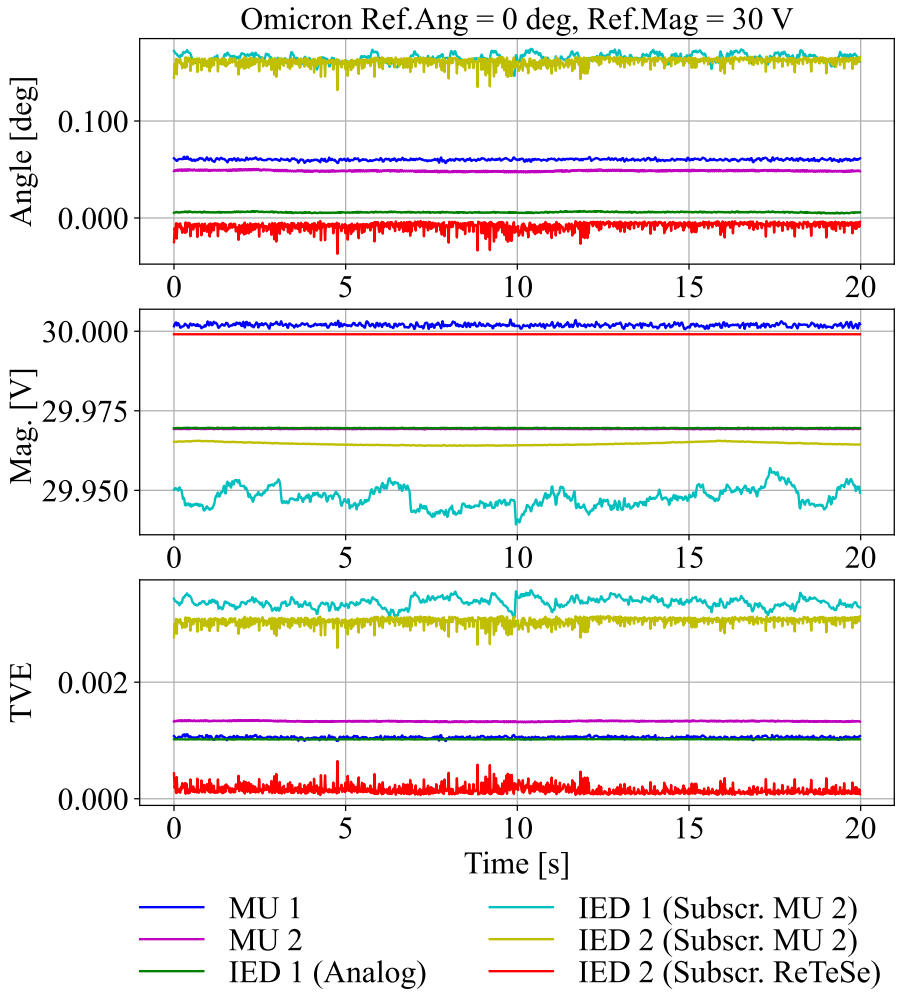

Figure 3.4: Positive sequence magnitude, phase, and TVE (without VT) for a selected operation point plotted over time

in stage 1 (see Fig. 3.4) and stage 2 (see paper P3) and is now approximately 6% for all these measurements based on the analog values. Interestingly, the measurements based on the sampled values published by the RTS still appear correct and show the best TVE. It is worth noting that the superior performance of the sampled value-based loop was also reported in [26]. Based on these findings, it is now clear that the inaccuracies measured are converter-related.

The dynamic tests for a sudden step in the magnitude can be seen in Fig. 3.7 and Fig. 3.6. Please refer to the underlying paper P3 for results regarding the off-nominal frequency test.

The purpose of displaying these results here is to present an effective method to get an estimation of the overall latency in the setup and to show the importance of taking the UTC timestamp into account in a WAMPAC test system (assuming that multiple PDCs or PMUs send separate data streams to the real-time simulator).

However, the step response is first plotted against their UTC timestamp. This can be seen in the Fig. 3.6. The reference signal is the step signal generated in the RTS (black solid line). In the real-time simulator, the sampling rate for sending and receiving is one millisecond. The PMUs used in the process have a reporting rate of 50 frames per second. As a result, a new sub-different measuring point is only available every 0.02 seconds. This explains why the synthetic phasor was obtained just before the transferred phasor. Regarding dynamics, all methods have a similar step response. Only the receiving Synthetic phasor and the MU2 (blue) seem to deviate. The overshoot behavior of MU2 can be explained by the fact that all IEDs and MUs in m-class operate with the standard C37.118-2011 except MU2. The MU2 shown is, therefore, the only device that uses the C37.118-2005 standard. The difference in the synthetic phasor can be explained by the fact that this concept is highly simplified and outputs the reference signal directly as a phasor frame. There is no estimation algorithm considered.

When plotting the magnitude and phase against the RTS simulation time available through the internal oregano board, it is possible to observe some delays between the various measurements. The plot shows the order and simulation time the data arrives. Consequently, it is the overall latency

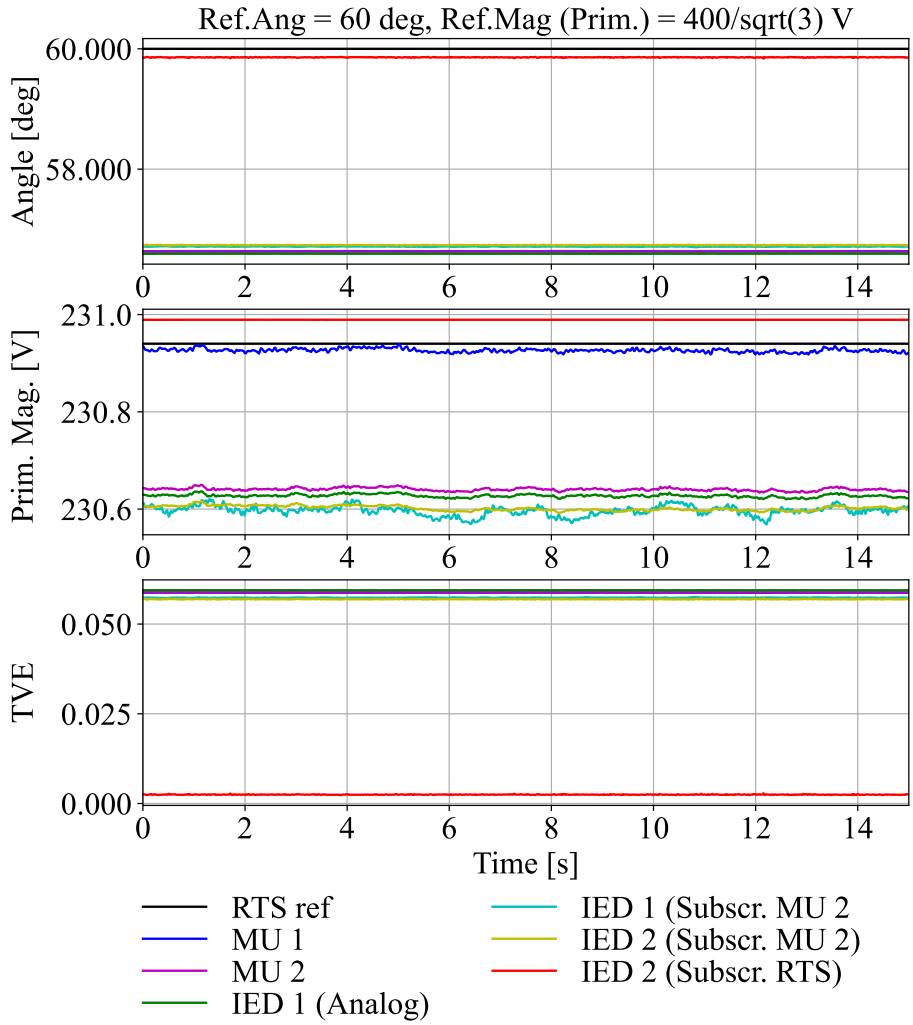

Figure 3.5: Positive sequence magnitude, phase, and TVE (with VT) for a selected operation point plotted over time (signals generated by RTS)

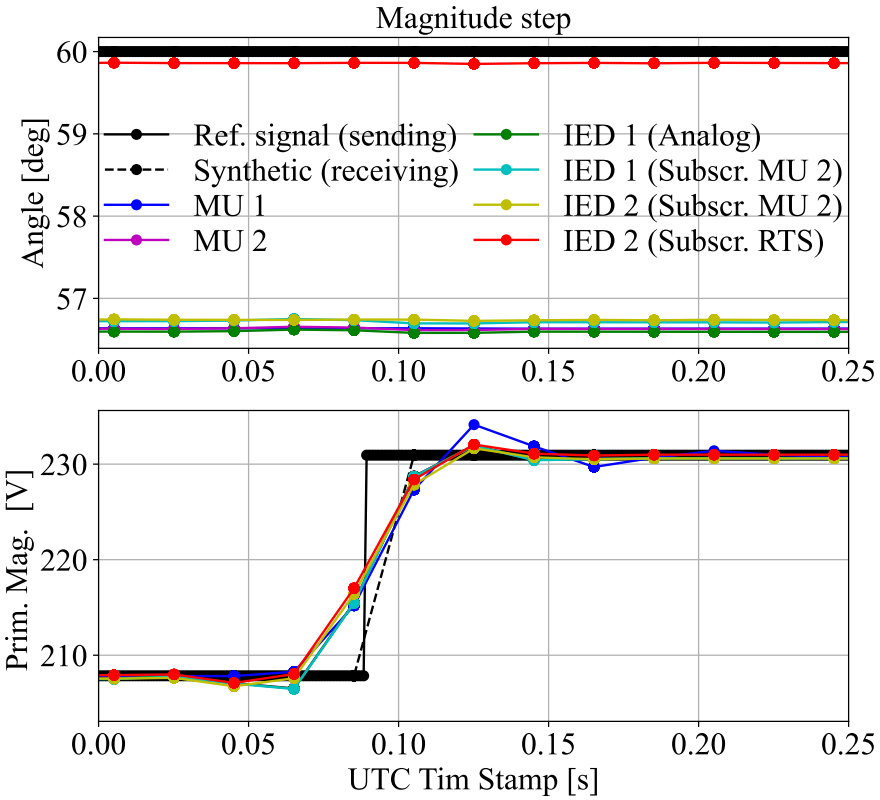

Figure 3.6: Positive sequence magnitude and phase for a magnitude step change of 10 %. Phase and magnitude versus its according UTC time stamp (Note: The plotted time stamp is shifted around UTC time 1661628567.014856815 seconds)

that is present in the platform.

3.4 Discussion and Contribution

Content contribution for answering the research question: The presented chapter can contribute to answering research questions R3: as follows:

- R3: *What are the technical solutions for integrating WAMPAC devices into a real-time setup, and how do they differ? What are the common sources of errors, and how can they be identified*
  This chapter presents three methods for implementing PMUs in a real-time WAMPAC test platform. The first approach is to generate phasors in the real-time simulator internally. It is an effective and inexpensive method since many phasors can be easily generated without purchasing expensive external equipment. However, the results may be different since the concept is somewhat simplified. For example, no phasor estimation algorithm is used here. The dynamic test implemented in the setup showed a clear difference between a real PMU and a synthetic PMU. A second method was presented where phasors were estimated based on sampled values. Two different approaches for implementing this were presented. 1) An IED receives sampled values directly from the source. This shows a minor error, but it should be mentioned that it is also a simplification because there is, for example, no analog-to-digital conversion in the loop. 2) The analog signals are sampled by a merging unit and published as IEC 61850 sampled values, and an IED estimates the phasors based on this input. The third method is to estimate the phasors directly from analog signals. The complexity increases when a converter is in the loop, and the number of outputs available at the converter limits the possible number of PMUs.

  A potential source of error identified and described in this chapter is based on conceptual confusion when using phasors without their specific time stamp (i.e., using the internal simulation time instead

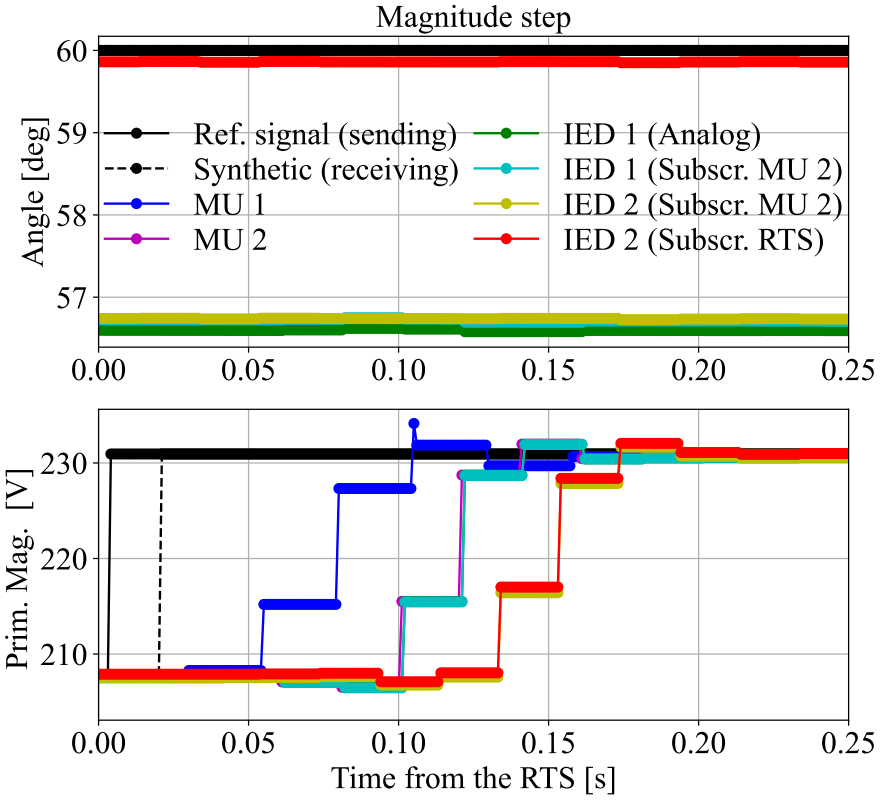

Figure 3.7: Positive sequence magnitude and phase for a magnitude step change of 10 %. Phase and magnitude versus the simulation time in the RTS

of the UTC stamp). This error may lead to unclear delays and, consequently, to an incorrect system snapshot. In addition, it should be emphasized that such a WAMPAC test setup quickly becomes complex, and there are numerous sources of error. For this reason, this chapter proposes a three-stage evaluation procedure.

Contribution:

- To emphasize the pros and cons of various methods for integrating WAMPAC devices, specifically PMUs, into a real-time simulation environment to assess WAMPAC applications. This also applies to the less commonly discussed configurations where IEC 61850-based technology is involved in the loop.

- To provide a comprehensive example of a WAMPAC test platform with a real-time simulator capable of functioning as both a merging unit and an analog signal generator. Beyond that, commercial merging units are in the loop for sampling the analog values and publishing sampled values to IEDs. These IEDs and MUs can act as PMUs and estimate phasors according to the C37.118 standard. All the listed equipment plus a high-precision signal generator (ReTeSe) is time synchronized with IRIG-B or PTP to a GPS-based master clock.

- To characterize inaccuracies that may appear when using the presented WAMPAC platform. Furthermore, to show how a second source capable of generating sampled values and analog signals may be beneficial for effectively identifying the source of the error.

- A simple procedure was presented that can be used for estimating the overall delay. This procedure is easily implemented using a real-time WAMPAC test setup, as shown here. However, it should be emphasized that the method is less accurate than the one in [11]. Furthermore, it is limited to a test setup with an RTS that includes an internal clock. However, no further equipment is needed, which is an advantage.

Chapter 4

Optimally Arming and Disarming Procedure Considering Steady-State Overload Criteria

This chapter contains a topic that has yet to be published. However, when submitting the thesis, a paper has already been submitted for a conference with the relevant content (see P5). For this reason, it is the only chapter that deviates from the basic structure and is described in more detail. The work was developed within the ASAP project with researchers from the Research Institutes of Sweden (RISE). The method is divided into three blocks, where the contribution of this dissertation is the development of the second block, named "Optimal Detection Block." For this reason, this block is described here in much more detail than the others. The content of this chapter contributes to the research questions R2:, R1:

4.1 Naming and Basic Definition

The naming and definition used in this chapter deviate slightly from the previously stated. This is because the terminology was defined within the framework of the underlying research project. Fig. 4.1 summarizes the essential concepts and devices to understand the chapter.

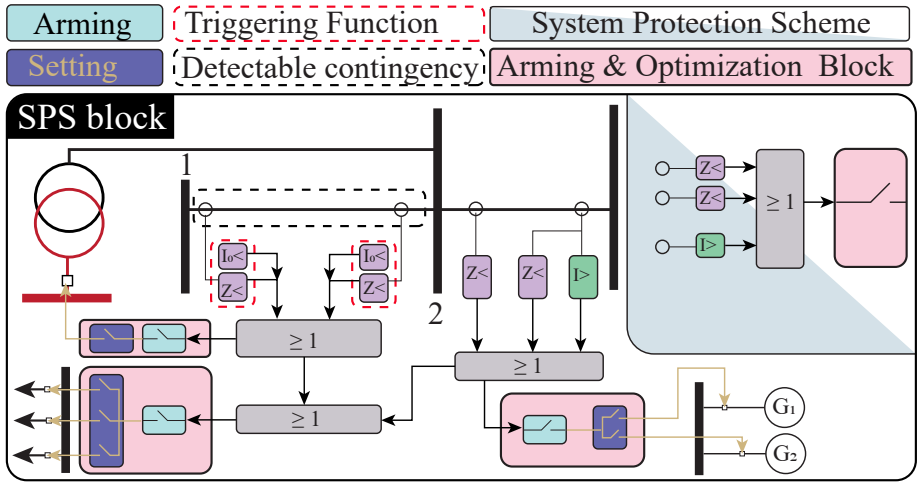

Figure 4.1: Simplified schematic that contains the most relevant concepts and devices considered in this chapter

In this chapter, often the name detectable contingency is used. A detectable contingency can be seen as an event that leads to a trigger function being exceeded. A triggering function is a relay, such as a distance or over-current protection (see Fig. 4.1). Note that the detectable contingency is not necessary where it is detected since an arbitrary contingency may trigger an over-current relay in another place. It is distinguished between event-based and response-based trigger functions (blue respective green relays in Fig. 4.1).

Logic gates such as "OR" and "AND" combine the different trigger functions in an SPS. An SPS can be seen in Fig. 4.1 on the left separated

section. It contains an arming and optimization block (light red) besides trigger functions and logic gates. The arming and optimization block consists of an arming switch that is binary ("True" or "False") and a setting block that determines the amount of mitigation extent that will be called if the arming and trigger conditions are both "True." In reality, there are SPSs where the mitigations extend cannot be changed. In this case, it is only possible to decide whether the SPS should be armed (see the SPS example in Fig. 4.1 that disconnects the transformer). As shown in Fig. 4.1, it is distinguished in this chapter between three different types of control actions. It is shedding loads, rejecting generators, and reconfiguring the grid.

All these measures are used in this chapter exclusively to avoid thermal overload in the static post-contingency state.

4.2 Problem Formulation

As illustrated in Fig. 4.1, one characteristic of the SPSs described in this chapter is its unchangeable physical implementation (i.e., the SPS design). It is realized with logic circuits developed once during an offline planning phase.

SPSs implemented are profitable. As a result, such schemes have increased significantly in recent years. The invariant structure of an SPS described above is usually simple to understand as long as only one particular scheme is considered by itself. However, each scheme increases the overall complexity of the operation, and the coordination of these schemes between each other might be challenging. This is especially the case because such protection schemes can interact negatively with each other.

Besides the unchangeable design, there are indeed changeable parameters that the control room personnel must set. As described in more detail, the personnel in the control room must decide to what extent mitigation should be done and whether it should be armed at all or if it is better to apply preventive measures. In addition to the arming question, it is often also challenging in the control room to decide which already armed SPSs

can now be disarmed. All these decisions are made based on a steady-state contingency analysis and, to a large extent, according to the experience of the control room personnel. To make matters worse, people are under pressure to make the right choice because the wrong arming can have disastrous consequences. However, even if the choice is correct, it is not mathematically proven to be the best choice for the given operating point.

This is why it is essential to have a structured and automatic procedure that addresses the mentioned concerns. The procedure should determine which SPSs must be armed in each operation state and specify the appropriate mitigation extent. Such a procedure relieves the control center staff considerably, and it might be possible to increase the number of SPSs in operation further.

A detailed literature review concerning the research gap can be found in the introduction part of the paper P5.

4.3 Solution Formulation

4.3.1 Requirement

The automation procedure proposed in this chapter must consider the critical points described in section 4.2. First of all, it is essential to consider the current system state. This is why it might be necessary to connect the procedure to a contingency analysis potentially with access to a state estimator. This allows tailoring an optimal solution for a specific contingency scenario, which might reduce unnecessary large margins.

The automation tool proposed must be based on an optimization program because compared to a rule-based tool, this would automatically prove the mathematically best solution. To keep complexity to a minimum, the optimizer should suggest the minimum number of SPSs that must be armed. Nevertheless, it should be possible to detect all dangerous contingencies. However, having a small number of SPSs armed would be insufficient, preventing many uncritical events besides the critical and dangerous contingencies. Arming uncritical but detectable contingencies may lead to the unintentional triggering of control action, which is undesirable and must be

avoided. The procedure should also provide information about which SPSs can now be disarmed. Besides the number of armed SPSs, the transition to the current arming status should be minimized. When correctly armed, the procedure should be able to find appropriate and cost-minimum mitigation extent for the given arming scenario. When choosing the extent of mitigation, it is crucial to consider both physical boundaries and triggering levels of all armed SPSs, mainly due to the adverse effects of multiple SPS interactions. The last requirement clearly states that some power flow and model aspects must be considered.

4.3.2 Problem-Solving Approach

A bi-level optimization procedure is proposed to address all the requirements stated in subsection 4.3.1. How bi-level optimization generally works has been summarized and can be found in the Appendix 8.1. The upper level decides whether and which SPSs should be armed. Concerning Fig. 4.1, the upper level decides which light blue switches must be activated and deactivated. In contrast, the lower-level optimization problem decides how the mitigation extent should be chosen for the scenario the upper-level selects. Concerning Fig. 4.1 decides the lower level which of the switches in the dark blue boxes must be activated.

The necessary condition for the upper-level optimization problem is to detect all contingencies classified as critical (this definition will be specified in more detail later). On the other hand, the necessary condition for the lower level is to select the mitigation action such that the post-contingency state does not violate any set limitations. The solution is sufficient if the upper and lower-level conditions are fulfilled together.

The objective of the upper-level optimization problem is to minimize the number of SPSs to be armed and the possibility of the unintentional triggering of SPSs. The objective of the lower-level problem is the minimization of the mitigation costs.

Compared to the conventional bi-level optimization problem explained in section 8.1, the upper-level in the proposed method here has no information about the optimization problem the follower will solve.

The proposed optimization technique ranks the different objectives according to their relevance. Similar to a lexicographic optimization problem. Consequently, the objectives at the upper level are prioritized over the ones formulated in the lower-level problem. This allows us to solve the problem sequentially.

The problem is solved as follows: First, the upper level tries to find a solution that minimizes its objective function and fulfills all respective constraints. If such a solution is found, the lower level tries to find an optimal mitigation extent to its optimization model and the upper-level solution. If a lower-level solution can be found, the problem is solved. If no solution can be found, the lower level communicates this to the upper level. The previously found arming solution will now be excluded from the solution space by including an additional constraint in the upper-level model. With this updated optimization model, the calculations are repeated.

4.4 Methodology

The main objective of this section is to describe the detailed implementation of the optimization procedure introduced in section 4.3. The implementation is done in blocks. It was decided to use different abstraction layers to describe this structure the best. The main implementation idea can be seen as the top layer and is illustrated in Fig. 4.2. Three blocks are distinguished. The Contingency Analysis Block is the first of them. It is included in the so-called detection module. Its goal is to filter out all detectable and critical contingencies for the current system state (later, the differences will be described in more detail). The block forwards a text file that includes a detailed description of all SPSs that may be triggered and all critical contingencies that would push the system operation point out of its secure operation state. These data are the input for the optimization module, which can be seen as the procedure's core. It consists of two blocks. First, the Optimal Detection Block, and second, the Optimal Setting Block. The Optimal Detection Block aims to implement the upper-level optimization problem, while the Optimal Setting block aims to represent the lower-level

problem. To later solve the bi-level optimization problem, it is essential that the two blocks in the Optimization Module can communicate.

In the following, each block will be explained in detail.

4.4.1 Contingency Analysis Block

The input to this block can be classified as system information and SPS information, which is the following data. The current system state, a static power system model (see Fig. 4.2), system operation limits, and all SPS trigger function thresholds. The objective of the block is to verify if the system operates in a secure operating state. For this reason, all N-1 contingencies are checked.

All events that push the system out of its operating limits or any contingency that an SPS can detect are automatically stored in a list with the corresponding information. The following output describes, as an example, a contingency that fulfills the triggering conditions of an SPS.

```
ca_matrix_SPS_trigger: 1
viol_branch:[7, 8, '1']
viol_branch_flow:0.0
viol_branch_limit_value:None
viol_branch_limit_type:Trip
ca_branch:[7, 8, '1']
viol_object_name: From_X - To_Y
contingency_object_name: From_X - To_Y
```

The output of the Contingency Analysis Block is consequently information regarding contingencies that set eider a triggering function to true or exceed grid limitations.

4.4.2 Optimal Detection Block

The Optimal Detection Block is the first block of the optimization module. It contains the upper-level optimization problem described in section 4.3. The first and, consequently, the most relevant objective is to find the

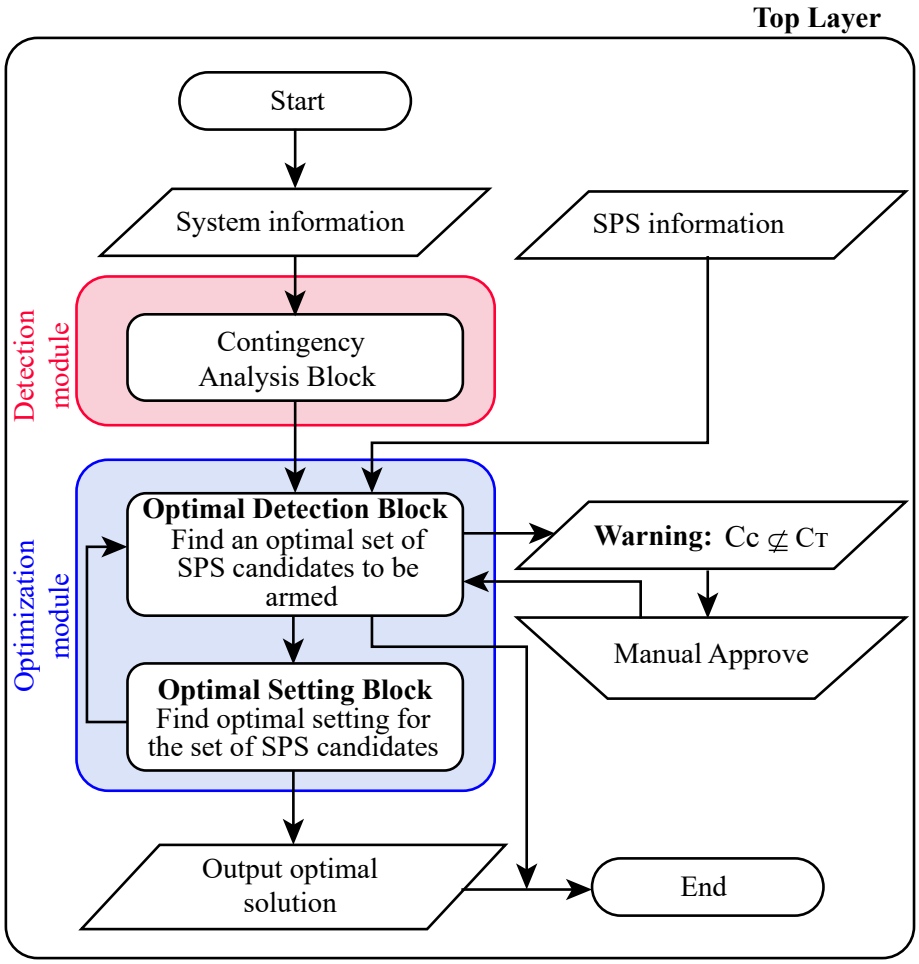

Figure 4.2: Highest abstraction level of the procedure. Note that the outputs and inputs from the SPS arming and Optimally setting block are discussed in detail in the subsection below.

minimal number of SPSs to be armed that detect all critical contingencies and avoid the possibility of false triggering. Later in this thesis, it will be shown that the applied optimization technique is a non-convex problem; therefore, there can be several optima.

The input to the Optimal Detection Block is the contingency and triggering data described in subsection 4.4.1, the SPS design information, and the current arming configuration. The current arming information describes which SPSs are already armed.

In the following subsections, the two blocks, Data Processing and Find Optimal Arming Candidates, will be explained. Together, they represent the Optimal Detection Block as illustrated in Fig. 4.3.

Data Processing

The first step generates the relevant mathematical sets ($\mathcal{T}_E, \mathcal{T}_R, \mathcal{C}_C, \mathcal{C}_T$) and matrices ($M_T, M_C$). The set $\mathcal{T}_E$ contains all event-based trigger functions and $\mathcal{T}_R$ those of the response-based trigger functions. $\mathcal{C}$ can be seen as the universal set of all possible contingencies. Furthermore, a subset $\mathcal{C}_T \subseteq \mathcal{C}$ can be considered. $\mathcal{C}_T = \{c_{T,1}, c_{T,2}, \cdots, c_{T,|\mathcal{C}_T|}\}$ includes all contingencies that are detectable by the triggering functions. In other words, $\mathcal{T} = \mathcal{T}_E \cup \mathcal{T}_R = \{t_1, t_2, \cdots, t_{|\mathcal{T}|}\}$ are all the triggering functions that are necessary to detect all detectable contingencies in the set $\mathcal{C}_T$. Another important subset of $\mathcal{C}$ is $\mathcal{C}_C \subseteq \mathcal{C}$. $\mathcal{C}_C = \{c_{C,1}, c_{C,2}, \cdots, c_{C,|\mathcal{C}_C|}\}$ is the set of all critical contingencies (i.e., all events that exceed at least one system violation). The set $\mathcal{L} = \{l_1, l_2, \cdots, l_{|\mathcal{L}|}\}$ is the set of all system violations that are exceeded due to critical events.

These contingency sets can be analyzed in a Venn diagram as illustrated in Fig. 4.4. $\mathcal{C}_T$ is represented in blue and $\mathcal{C}_C$ is illustrated in red. $\mathcal{C}_C \cap \mathcal{C}_T$ represents all critical contingencies detected by at least one triggering function. $\mathcal{C}_T \setminus \mathcal{C}_C$ are all contingencies that at least one triggering function detects but are not critical. It is highly relevant to avoid arming SPSs that consist of triggering functions linked to such contingencies. Because they would be triggered even if the contingency is not critical, the contingencies in the set $\mathcal{C}_C \setminus \mathcal{C}_T$ are even more severe because these contingencies are

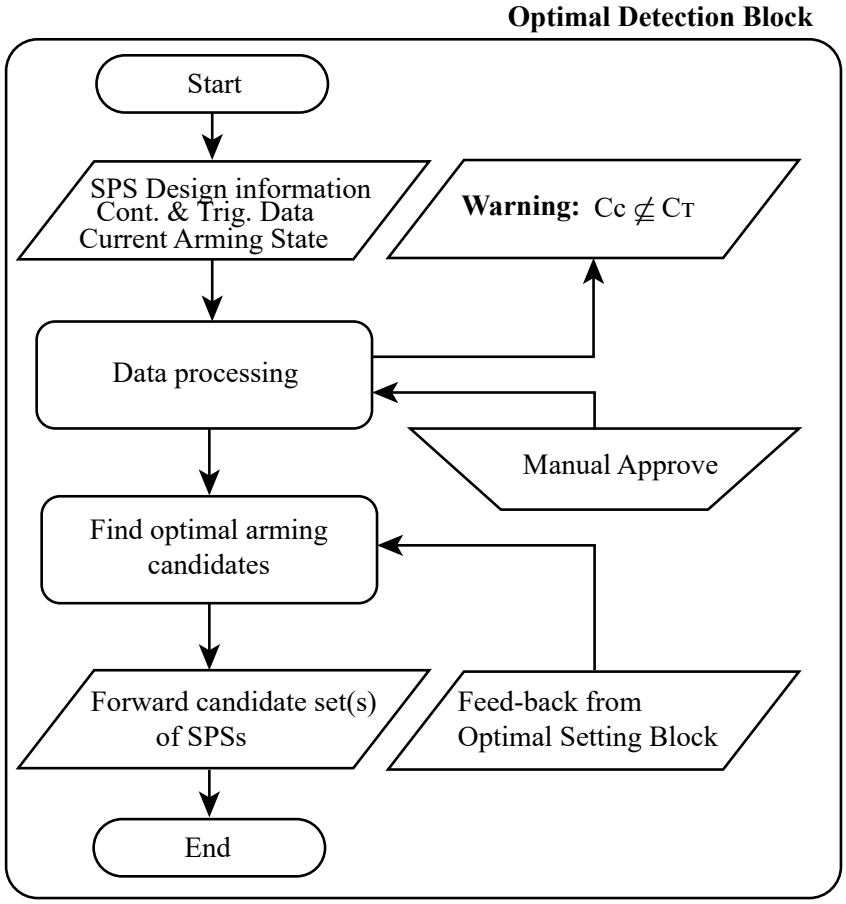

Figure 4.3: Detection block represented as flowchart (second abstraction level)

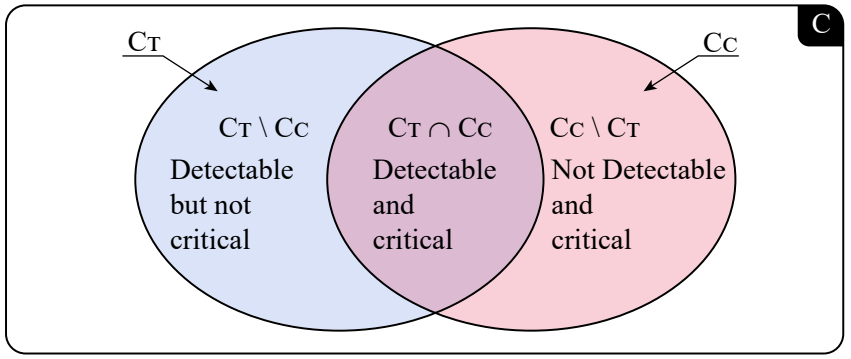

Figure 4.4: Contingency sets $\mathcal{C}_t$ and $\mathcal{C}_c$

critical, and no triggering function would detect them. If such a set of contingencies exists, the operator must be informed about this situation.

If $\mathcal{C}_C \not\subseteq \mathcal{C}_T$, only two measures can be taken. First, the operator changes the system state by rescheduling and repeating the contingency analysis, or second. The operator considers the situation non-critical and consequently clears all those elements of the set $\mathcal{C}_C \setminus \mathcal{C}_T$ manually. This action is illustrated in Fig. 4.2 and Fig. 4.3 by outputting a warning flag and manually clearing the situation. Consequently, it is assumed from now on in this thesis that $\mathcal{C}_C \subseteq \mathcal{C}_T$. Note that rescheduling of generation is a preventive measure that is out of the scope of this thesis.

The so-called contingency matrix M^C is a matrix whose rows are all critical contingencies ($\{c_{C,1}, c_{C,2}, \cdots, |\mathcal{C}_C|\}$) and columns are all system violations ($\{l_1, l_2, \cdots, l_{|\mathcal{L}|}\}$). Similarly, the triggering matrix M^T is a matrix whose rows are the detectable contingencies ($\{c_{T,1}, c_{T,2}, \cdots, c_{|\mathcal{C}_T|}\}$) and whose columns are triggering functions ($\{t_1, t_2, t_3, ..., t_{|\mathcal{T}|}\}$). With the help of the information from the contingency analysis and the SPS specification, the two relations can be defined:

$$\mathcal{R}_C \subseteq (\mathcal{C}_c \times \mathcal{L}) \tag{4.1}$$

$$\mathcal{R}_T \subseteq (\mathcal{C}_T \times \mathcal{T}) \tag{4.2}$$

$\mathcal{R}_\mathcal{T}$ can be seen as an example in Fig. 4.5 (below). The relation $\mathcal{R}_T$ includes only tuples that include the detectable contingency with the corresponding triggering function. The different available SPSs can now be seen as a set that includes certain tuples out of $\mathcal{R}_T$. For example $SPS_5 = \{(C_{T,6}, t_1), (C_{T,4}, t_3), (C_{T,9}, t_8)\}$. Exactly what these tuples look like depends on the specifically defined logic circuit of the SPS. The same can be done for $\mathcal{R}_\mathcal{C}$ but by considering $\mathcal{C}_C$ and $\mathcal{L}$.

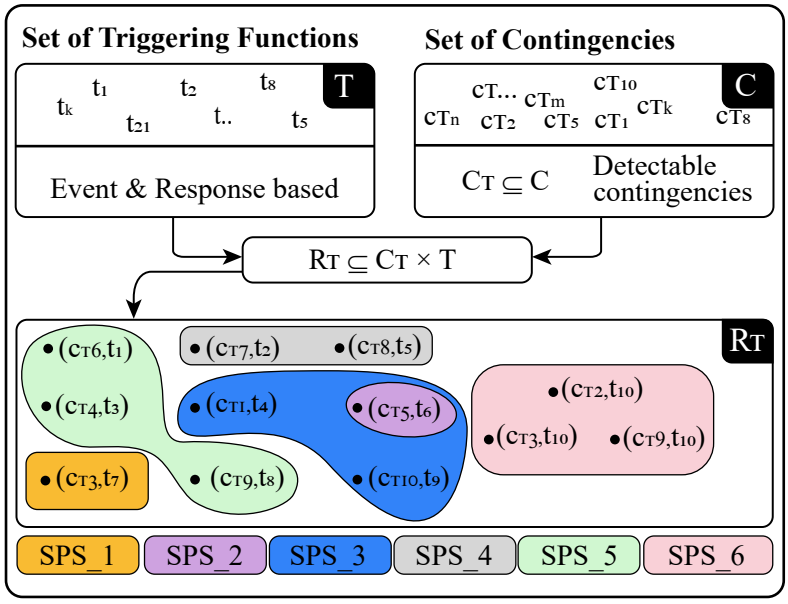

Figure 4.5: SPSs and the Relations

Based on (4.1) and (4.2) the contingency matrix M^C and the triggering

matrix M^T can be defined as written in (4.3) and (4.4):

$$M^T_{i,j} = \begin{cases} 1, & \text{if } (c_{T,i}, t_j) \in \mathcal{R}_T, \\ 0, & \text{else.} \end{cases} \tag{4.3}$$

$$M^C_{i,j} = \begin{cases} 1, & \text{if } (c_{C,i}, l_j) \in \mathcal{R}_C, \\ 0, & \text{else.} \end{cases} \tag{4.4}$$

An example of a contingency matrix and a triggering matrix can be seen in (4.5) respective (4.6).

	l_1	l_2	l_3
$c_{C,1}$	1	1	1
$c_{C,2}$	0	0	1
$c_{C,3}$	1	0	0
$c_{C,4}$	1	1	0

(4.5)

	t_1	t_2	t_3	t_4	t_5	t_6	t_7	t_8	t_9	t_{10}
$c_{T,1}$	0	0	0	1	0	0	0	0	0	0
$c_{T,2}$	0	0	0	0	0	0	0	0	0	1
$c_{T,3}$	0	0	0	0	0	0	1	0	0	1
$c_{T,4}$	0	0	1	0	0	0	0	0	0	0
$c_{T,5}$	0	0	0	0	0	1	0	0	0	0
$c_{T,6}$	1	0	0	0	0	0	0	0	0	0
$c_{T,7}$	0	1	0	0	0	0	0	0	0	0
$c_{T,8}$	0	0	0	0	1	0	0	0	0	1
$c_{T,9}$	0	0	0	0	0	0	0	1	0	0
$c_{T,10}$	0	0	0	0	0	0	0	0	1	0

(4.6)

The triggering matrix represents the relation $\mathcal{R}_T$ based on the definition above. As mentioned before and illustrated in Fig. 4.5 (below), the SPSs can be seen as sets defined by their logic circuits. In the following, each SPS is represented as an element in $\mathcal{D} = \{d_1, d_2, d_3, ..., |\mathcal{D}|\}$. With respect to Fig. 4.5 (below) an example with $|\mathcal{D}| = 6$ is illustrated.

For the later explained optimization, it is helpful to think in the first step to represent each SPS in a separate matrix. These matrices can be merged in a three-dimensional matrix (i.e., in a tensor $M \in \{0,1\}^{|\mathcal{C}_T| \times |\mathcal{T}| \times |\mathcal{D}|}$). The above-described example would look as illustrated in Fig. 4.6.

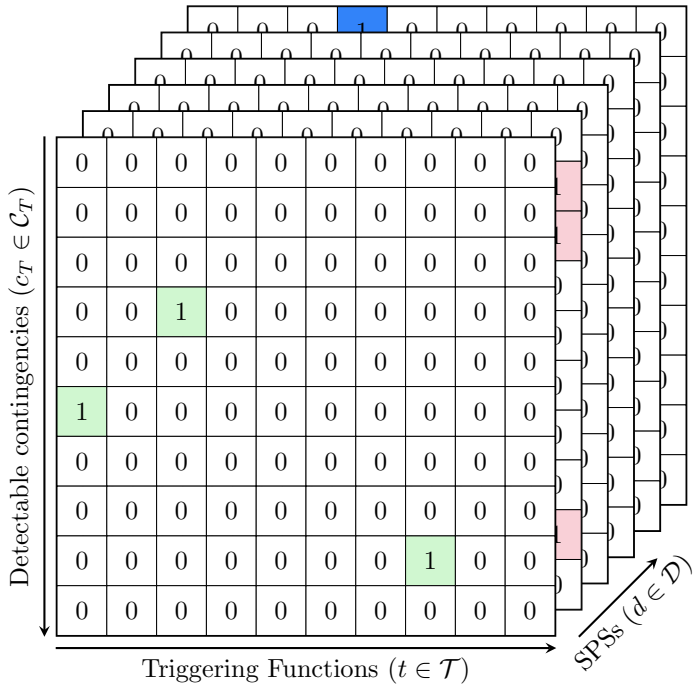

Figure 4.6: Tensor M for the example illustrated in Fig. 4.5)

While the now-defined tensor M includes information about detectable contingencies and the associated SPSs, an additional quantity, including information regarding critical contingencies, is necessary for the optimization procedure. This is why the $V \in \{0,1\}^{|\mathcal{C}_T| \times 1}$ vector is defined. Like M, the rows of V are the detectable contingencies from the set $\mathcal{C}_T$. Moreover, the sequence of the contingencies is the same as in M. Furthermore, for vector V, its rows are always zero if the contingency is classified as non-critical.

Otherwise, the entry is equal to 1. In mathematical notation, V can be defined as:

$$V_i = \begin{cases} 1, & \text{if } c_{T,i} \in (\mathcal{C}_T \cap \mathcal{C}_C) \\ 0, & \text{else} \end{cases} \tag{4.7}$$

The data processing block can be represented as a flowchart as illustrated In Fig. 4.7. It can consequently be summarized as follows. The data processing block inputs information related to the SPS design and contingency analysis. Based on this input, the relevant sets can be created. With this information, the first check regarding the feasibility of the problem is done. If $C_C \not\subseteq C_T$, it implies at least one critical contingency that is not detectable. In this case, the operator must interact with the decision-making tool manually. The final output is either a stop of the procedure or a tensor M and V that can be used in the "Find Optimal Arming Candidates Block" explained in the following subsection.

Find Optimal Arming Candidates

As mentioned above, the essential objective of the Optimal Detection Block is to provide the Optimal Setting Block with a minimal combination of SPSs that would detect all critical contingencies but avoid triggering due to non-critical contingencies. In the case of multiple solutions with the same objective function value, priority is given according to the transition effort concerning the current arming state. In other words, the solution with the most minor arming changes compared to the current arming state is preferred. In addition, it should be ensured that solutions previously declared unfeasible by the Optimal Setting Block are excluded from the optimization process.

In the context of the detectability of contingencies, the columns of M are somewhat irrelevant since they provide information about the exact location and with which kind of triggering function the contingency is detected. Essential for the Optimal Detection Block is whether there is a triggering function at all that can detect the contingency.

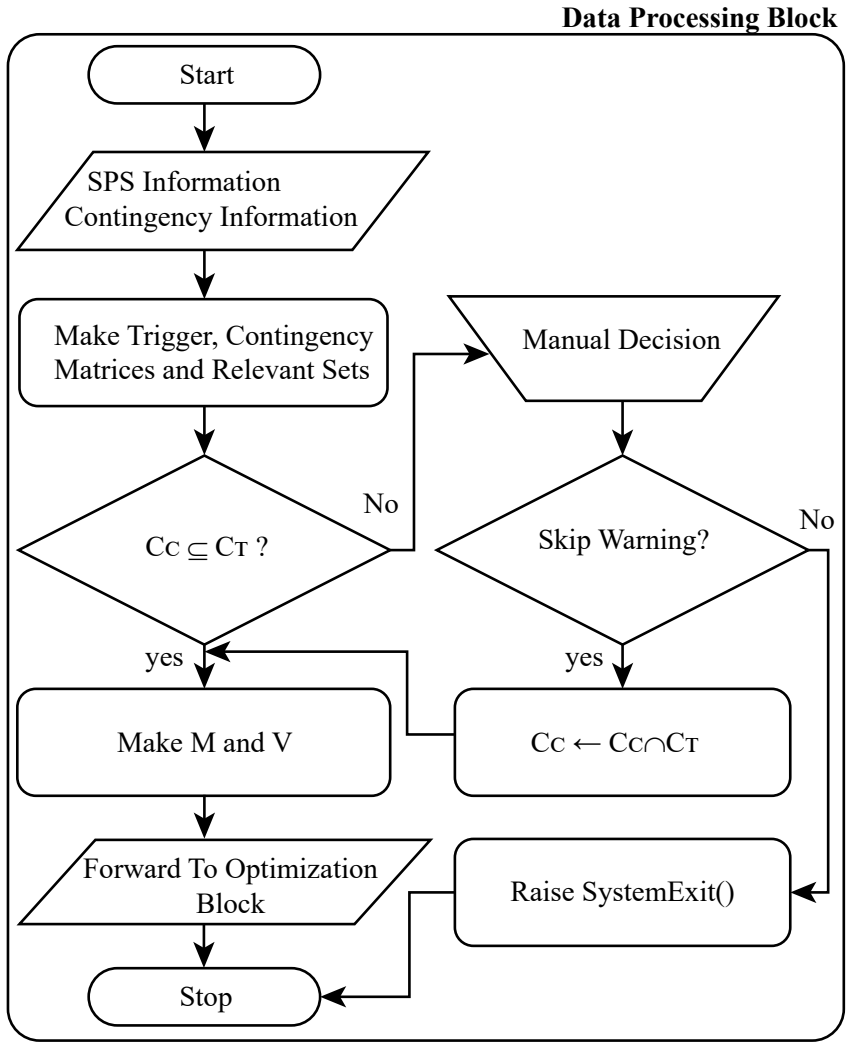

Figure 4.7: Flow chart of the data processing block (third abstraction level)

This is why $M \in \{0,1\}^{|\mathcal{C}_T|\times|\mathcal{T}|\times|\mathcal{D}|}$ can be simplified for the optimization to $Mv \in \mathbb{N}_0^{|\mathcal{C}_T|\times|\mathcal{D}|}$ without losing relevant information. The matrix M_v can be formed as illustrated in the following:

$$M_v = \begin{bmatrix} | & | & | & | \\ \sum_{s=1}^{|\mathbf{T}|} M[:,s,1], & \sum_{s=1}^{|\mathbf{T}|} M[:,s,2], & \cdots, & \sum_{s=1}^{|\mathbf{T}|} M[:,s,|\mathcal{D}|] \\ | & | & | & | \end{bmatrix} \tag{4.8}$$

The optimization problem can be written as stated in (4.9):

$$\min_x \sum_{i=1}^{|\mathcal{D}|} \left(c_0[i] + c_1[i] \sum_{k=1}^{|\mathcal{C}_T|} M_v[k,i]\,(1 - V[k]) \right) x[i]$$

subject to:

$$\begin{aligned} &\text{Cnsts. a)} \quad \sum_{i=1}^{|\mathcal{D}|} M_v[j,i]x[i] \geq V[j] \quad \forall j \in \{1,2,\ldots,|\mathcal{C}_T|\} \\ &\text{Cnsts. b)} \quad \sum_{i|x^*[n,i]=0} x[i] + \sum_{i|x^*[n,i]=1} (1 - x[i]) \geq 1 \quad \forall n \in \{1,2,\ldots,|\mathcal{N}|\} \\ &\text{Cnsts. c)} \quad x \in \{0,1\}^{|\mathcal{D}|} \end{aligned} \tag{4.9}$$

The decision variables of the optimization problem (4.9) are the elements of the vector x. It contains precisely $|\mathcal{D}|$ binary variables (see constraint c)). Each binary variable in x thus represents exactly one SPS where the variable's value implies whether the SPS should be armed or not.

The constraints a) in (4.9) describes how the detectability information of the triggering matrix, respectively the Mv matrix, can be related to the V vector. Note that the entries of the V vector are 1 in those rows that represent a contingency from the set $\mathcal{C}_T \cap \mathcal{C}_C$ (i.e., detectable and critical) and zero otherwise. For this reason, one aims for a linear combination with the column vectors of Mv using x, resulting in a vector in which all elements

are greater than or equal to those of V. These hard constraints ensure that the optimal solution can detect all critical contingencies.

To understand constraints, b) the matrix $x^* \in \{0,1\}^{|\mathcal{N}|\times|\mathcal{D}|}$ must quickly be introduced. x^* Contains all previous solutions declared insufficient by the Optimal Setting Block. Consequently, these solutions must be excluded from the solution space of the optimization problem. With each solution rejected by the Optimal Setting Block, the solution space shrinks, and the matrix dimension x^* increases since the matrix gets new rows. This exclusion of previous solutions is the objective of constraints b). The main idea is to forbid the x vector corresponding to the row vectors stored in x^*. This is achieved with the following constraint $\sum_i |x[i] - x^*[n,i]| \neq 0 \quad \forall n \in \mathcal{N}$ where $\mathcal{N}$ is an index set representing all solutions to be excluded. The restriction can be rewritten linearly, as seen in (4.9).

Minimizing the binary elements activated in x keeps the number of armed SPSs as small as possible. Considering the weights $c_0[i]$ in the objective function makes it possible to prioritize certain SPSs. Besides the number of SPSs to be armed, it is essential to avoid their unintentional triggering. Remember, a contingency is not critical but detectable ($\mathcal{C}_T \setminus \mathcal{C}_C$) if the entry of the respective row in V is zero.

The penalty function used in this optimization procedure is defined as noted in (4.10).

$$f^p_{1,i} = \sum_{k=1}^{|\mathcal{C}_T|} M_v[k,i]\,(1 - V[k])\,x[i] \tag{4.10}$$

$$f^p_{2,i} = \sum_{k=1}^{|\mathcal{C}_T|} \mathcal{H}(M_v[k,i])\,(1 - V[k])\,x[i] \tag{4.11}$$

The term $(1 - V[k])$ is 1 for all contingencies that are detectable but not critical ($\mathcal{C}_T \setminus \mathcal{C}_C$). $M_v[k,i]$ represents how many triggering functions connected to SPS i detect contingency k. $x[i]$ indicates if SPS i is armed or not. In other words, given the considered arming state, the penalty function defined in (4.10) tells about how many possibilities exist for unintentionally activating a triggering function. Alternatively, the penalty function (4.11)

can be used. Unlike (4.10), (4.11) does not count the number of triggering functions but detectable contingencies that would lead to unintentional triggering. This is implemented utilizing the heavy side function $\mathcal{H}$. Typically, the two functions return the same result. In rare situations where two or more triggering functions of the same SPS detect one contingency, the functions deviate from each other.

The flowchart in Fig. 4.8 roughly shows how the optimization model in (4.9) is embedded in the arming tool. As long as the termination condition variable "Happy" is set to "False," the optimizer searches for new optimal combinations of SPSs. After each optimization, the objective function value is checked, and the found solution is excluded from the solutions space. This is repeated as long as a solution has a larger objective function value than the previously found. If this is the case, all solutions found with the same objective function value are sorted for the L_1 Norm ($\sum |\mathrm{Out} - \mathrm{ArmingStat}|$) and stored in a vector called *Out*. Afterward, the *Out* vector is forwarded to the "Optimal Settings Block."

4.4.3 Setting Block

For the optimal candidates of SPSs, the optimal setting block tries to find the cheapest control action that still allows mitigating all critical contingencies. If a solution can be found, the optimal set of SPSs and its mitigation action is ready to be armed and can be adjusted by the control room personnel. If no solution can be found, the Optimal Setting Block communicates this to the Optimal Detection Block, which provides a new combination of SPS candidates.

There were many challenges in this block. Some are briefly mentioned here. Some SPSs use the same possible mitigation action. This coordination had to be integrated into the procedure of the Optimal Setting Block. The optimization procedure does not only consider the physical limits like voltage and current but also the triggering thresholds. So that the post-contingency situation would not trigger SPSs again, these characteristics were realized with an optimal power flow procedure where the quantity and mitigation action is typically discrete. Therefore, the final optimization

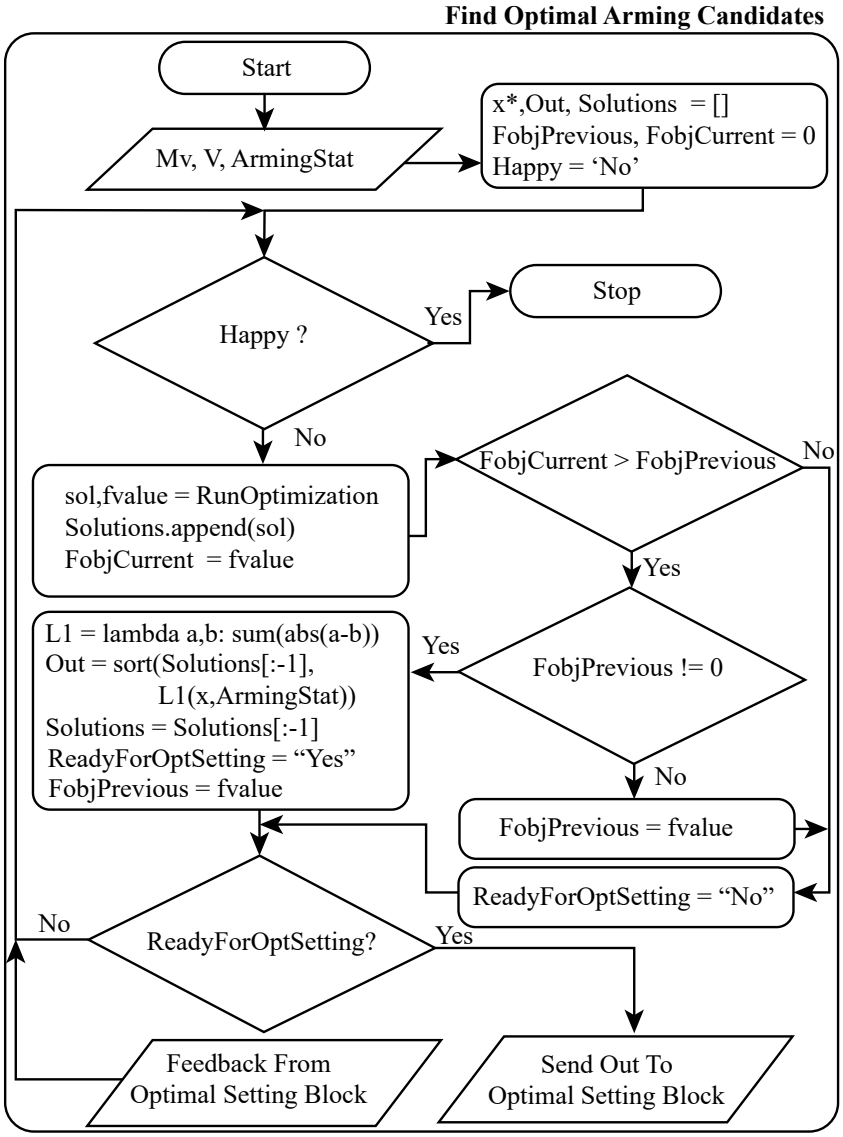

Figure 4.8: Find Optimal Arming Candidates (third abstraction level)

Table 4.1: Different SPSs available and the current arming state for both scenarios

SPS Nr.	Name	Arming Sc. 1	Arming Sc. 2
0	SPS020_021_1	0	1
1	SPS020_021_2	1	0
2	SPS031_032_033	1	1
3	SPS052	0	1
4	SPS052_054_055	1	0
5	SPS051	0	1
6	SPS056_057	1	1
7	SPS011_012	0	1

procedure is mixed integer non-linear, which is fundamentally challenging.

As the Optimal Setting Block is separate from this thesis, a detailed description will not be provided here.

4.5 Study Case

To present the functionality of the Optimal Detection Block, it was chosen to bypass the Optimal Setting Block for this study case. Consequently, the procedure loops automatically through all possible solutions considering the sequence proposed by the Optimal Detection Block. The test model is described in detail in the subsection 4.5.1. Two different scenarios are considered. The first scenario shows the functionality when setting all objective function weights C_0 equally (non-zero) and all C_1 weights to zero (see (4.9)). The second scenario assumes all elements in weight vectors C_0 and C_1 are equal. However, the same SPSs are available in both scenarios, but different initial arming states are assumed. Table 4.1 presents this information in more detail. Furthermore, it should be pointed out that for the considered study case, it does not matter if the penalty function (4.10) or function (4.11) is used since both of them deliver the same result.

4.5.1 Test Model

The model used here was developed specifically for the chapter with various SPSs and their logic circuits and triggering functions. Fig. 4.9 shows the single-line diagram of the used model and all used SPSs.

The model has 40 buses, and three different voltage levels are considered. A blue single-line diagram corresponds to the lowest voltage level, black is high voltage level, and red is the highest. The model considers eight different SPSs (see also Table 4.1) where one SPS allows grid reconfiguration and all others load shedding or generator rejection.

4.6 Results

After the Contingency Analysis Block passes the relevant data, the Optimal Detection Block establishes the relevant matrices and sets. Fig. 4.10 shows the V vector attached to the triggering matrix for the given study case. There are ten detectable contingencies ($\mathcal{C}_T$), where 6 of them are also critical ($\mathcal{C}_T \cap \mathcal{C}_C$). Seven event-based and two response-based triggering functions can detect the given contingencies. It is vital to see that each response-based triggering function can detect multiple contingencies by monitoring a certain device or corridor. An example shows triggering function $(5, 6,' 1',' ReB') \in \mathcal{T}_R$ monitoring the line from bus 5 to bus 6. In contrast, an event-based triggering function detects only the contingency for which it is intended. For example, contingency $(27, 28,' 1') \in \mathcal{C}_T$ is detected by the event-based triggering function $(27, 28,' 1',' EvB') \in \mathcal{T}_E$. However, the logic circuits that connect multiple triggering functions to an SPS cause multiple event-based triggering functions to be armed simultaneously. The purple SPS named ($SPS052\_054\_055$) is an example that shows a logical combination of event-based triggering functions.

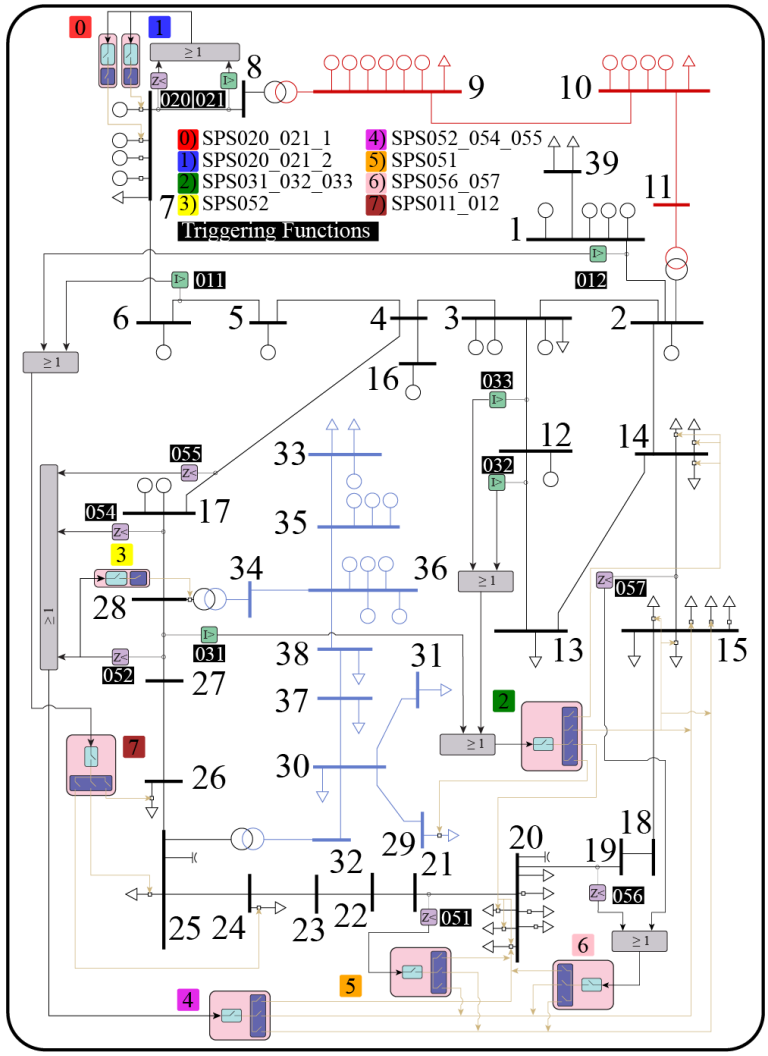

Figure 4.9: Single-line diagram of the considered study case model

	(17, 28, '1', 'EvB')	(7, 8, '1', 'EvB')	(19, 20, '1', 'EvB')	(20, 21, '1', 'EvB')	(27, 28, '1', 'EvB')	(4, 17, '1', 'EvB')	(14, 15, '1', 'EvB')	(12, 13, '1', 'ReB')	(5, 6, '1', 'ReB')	V
(7, 8, '1')	0	1	0	0	0	0	0	0	0	0
(14, 15, '1')	0	0	0	0	0	0	1	0	0	1
(27, 28, '1')	0	0	0	0	1	0	0	0	0	1
(2, 11, '1')	0	0	0	0	0	0	0	0	1	1
(2, 14, '1')	0	0	0	0	0	0	0	1	0	1
(10, 11, '1')	0	0	0	0	0	0	0	0	1	1
(19, 20, '1')	0	0	1	0	0	0	0	0	0	1
(17, 28, '1')	1	0	0	0	0	0	0	0	0	0
(20, 21, '1')	0	0	0	1	0	0	0	0	0	0
(4, 17, '1')	0	0	0	0	0	1	0	0	0	0

Figure 4.10: Triggering Matrix and V vector for the given study case scenarios

Table 4.2: Proposed sequence of solutions for scenario 1

Rank	Set of SPSs	Objective value	L1 distance
1	$\{2,4,6,7\}$	4	2
2	$\{2,3,6,7\}$	4	4
3	$\{1,2,4,6,7\}$	5	1
4	$\{0,2,4,6,7\}$	5	3
5	$\{2,4,5,6,7\}$	5	3
6	$\{2,3,4,6,7\}$	5	3
7	$\{1,2,3,6,7\}$	5	3
8	$\{2,3,5,6,7\}$	5	5
9	$\{0,2,3,6,7\}$	5	5
⋮	⋮	⋮	⋮
	$\{0,1,2,3,4,5,6,7\}$	8	4

4.6.1 Scenario 1: All c0 are Equal to One while all c1 are Equal to Zero

In this case, the arming of SPSs that detect a non-critical situation is not penalized. Consequently, the proposed set of candidate SPSs is minimized first in terms of their number and second in their distance from the current arming state.

Table 4.1 shows the optimal solution sequence. Since it is necessary to detect all critical contingencies, all proposed solutions do so. As shown in Fig. 4.10, the first two solutions are the minimum number of SPSs needed to detect all criticality contingencies. Although both of the best solutions have an objective value of 4, the L1 distance differs. To reach {2,4,6,7}, SPS number 1 must be disarmed, and SPS 7 must be armed. In contrast, to reach {2,3,6,7}, SPS numbers 1 and 4 must be disarmed, and 3,7 must be armed. This is why solution {2,4,6,7} does have less transition with respect to the current arming state and would thus be preferred by the control room personnel.

4.6.2 Scenario 2: C0 and C1 are Equal

Since all weights are now the same and unequal to zero, the optimizer tries to find a trade-off between the minimal number of SPSs and the defined penalty. Note that the penalty function penalizes any arming of SPSs triggered by a non-critical contingency. This would be the case when one of $SPS020\_021\_1$, $SPS020\_021\_2$, $SPS052\_054\_055$ or $SPS051$ is armed. The solution sequence proposed by the optimizer for scenario two is shown in Table 4.3

The best solution found includes 4 SPSs where no non-critical contingency would trigger an SPS. The L1 distance has a value of two because $SPS020\_021\_1$ and $SPS051$ must be disarmed to reach the optimal arming state. Compared to scenario 1, the second best solution already includes 5 SPSs; only the fifth solution contains 4 SPSs again. This can be explained as follows.

As mentioned before, the solution {2,3,6,7} is the best since this is the only solution with 4 SPSs that is not penalized. No other SPS is available that would not automatically result in a penalty. Therefore, all combinations with 5 SPSs automatically have a function value of 6 or more. The second best solution with only 4 SPSs has a function value of 6. This is because the only candidate to be changed in {2,3,6,7} is number 3 with SPS number 4 (i.e.,{2,4,6,7}). Although the combination with SPS number 4 ($SPS052\_054\_055$) can still detect all critical contingencies, it automatically detects also $(4, 17,' 1') \in (\mathcal{C}_T \setminus \mathcal{C}_C)$ and $(17, 28,' 1') \in (\mathcal{C}_T \setminus \mathcal{C}_C)$, which are both not-critical.

Technically, this can be explained by considering Fig. 4.9. The event of interest is the critical contingency (27,28,'1') because it can be detected by either $SPS052$ or $SPS052\_054\_055$. Specifically, triggering function 052 can be used for a grid reconfiguration by opening a breaker between buses 28 and 34 or shedding loads at buses 20 and/or 15. Although the Optimal Setting Block determines the final decision regarding the correct control action, there is already a disadvantage in the arming procedure when choosing $SPS052\_054\_055$. The trip of the line (17,28,'1') or (4,17,'1') does not lead to any critical contingency. One issue that arises when tripping (27,28,'1')

Table 4.3: Proposed Sequence of Solutions for Scenario 2

Rank	Set of SPSs	Objective value	L1 distance
1	$\{2, 3, 6, 7\}$	4	2
2	$\{2, 3, 5, 6, 7\}$	6	1
3	$\{0, 2, 3, 6, 7\}$	6	1
4	$\{1, 2, 3, 6, 7\}$	6	3
5	$\{2, 4, 6, 7\}$	6	4
⋮	⋮	⋮	⋮
	$\{0, 1, 2, 3, 4, 5, 6, 7\}$	13	2

is the significant power flow with its large current in the lower voltage grid (as shown in the blue single-line diagram). The two outages (17,28,'1') and (4,17,'1') also increase the load flow in the lower voltage level, but not nearly as much as the outage (27,28,'1'). This is mainly because contingency (27,28,'1') shifts the pre-contingency load flow between (27,25,'1') to a certain degree to the lower voltage level, which is not the case with the other two contingencies.

4.6.3 Assessment Values

This short section presents some assessment indexes based on this chapter, which can be used during a conventional manual operation to assess how good the current SPS design and arming procedure are and how relevant a tool such as the optimization procedure presented in this chapter may be.

The first indicator is the relation between the critical contingencies that cannot be detected and the total number of critical contingencies (4.12) ($\mathcal{S}$). The goal is to maintain a zero value for every system condition all year round. A significant value indicates a highly loaded system that may be to be upgraded, a poor SPS logic design, or insufficient SPS coverage.

$$\mathcal{S} = \frac{\sum_n |\mathcal{C}_{C,n} \setminus \mathcal{C}_{T,n}|}{\sum_n |\mathcal{C}_{C,n}|} \tag{4.12}$$

The two penalty functions introduced above (4.13) and (4.14) indicate the number of triggering functions that detect non-critical contingencies, respectively, the number of non-critical contingencies. Both for the considered arming state x. This can be summed up over a specific time interval (for example, a year) with the letter n.

$$\sum_{n=1}^{N} \sum_{i=1}^{|\mathcal{D}|} \sum_{k=1}^{|\mathcal{C}_{T,n}|} M_v^n[k,i]\,(1 - V^n[k])\,x^n[i] \tag{4.13}$$

$$\sum_{n=1}^{N} \sum_{i=1}^{|\mathcal{D}|} \sum_{k=1}^{|\mathcal{C}_{T,n}|} \mathcal{H}(M_v^n[k,i])\,(1 - V^n[k])\,x^n[i] \tag{4.14}$$

4.6.4 Summary

The chapter shows a procedure for optimally arming and disarming SPSs, divided into three blocks. First, a contingency analysis block determines which contingencies are critical and detectable. Second, an Optimal Detection Block that finds the optimal SPS candidates to be armed, and third, an Optimal Setting Block that determines the best possible control action for the candidates to mitigate all critical contingencies. Although the entire procedure is quickly introduced, the main focus is on the Optimal Detection Block, which is the main contribution of this chapter.

The Optimal Detection Block distinguishes between detectable and critical contingencies and considers the logic circuits that couple different event- and response-based trigger functions to a single SPS. A binary optimization problem is proposed to find the optimal SPS candidates for arming. The optimization problem minimizes the number of SPSs and the possibility of unintended triggering. Furthermore, the number of transitions is considered so that the proposed solution can be adapted as efficiently as possible to the current arming state in the control room. The Optimal Detection Block can also be seen as a filter for the Optimal Setting Block since it only forwards worthwhile possible SPSs. This reduces the number of variables in the Optimal Setting Block and may be beneficial concerning its

performance.

Two scenarios were presented in a simple but realistic model specifically developed for this chapter. The first scenario showed the solution for the study case when neglecting the penalty term for minimizing the number of possible unintentional triggers. In the second scenario, the penalty term was considered, and a case where the optimizer tries to find a trade-off between allowing potential unintentional triggering and minimizing the number of SPSs to be armed is shown.

The presented tool showed the desired behavior and is especially helpful when the number of possible SPSs is significant and many "OR" blocks connect triggering functions together. In such a situation, this tool could positively support the decision-making process in the control room.

However, some open questions should be addressed in future studies. The most prominent question is how to find the penalty weights properly. In particular, the costs should be taken into account. It would undoubtedly be helpful to know how much the unintentional triggering would cost, how much damage would be done, and how likely this false triggering would be.

4.7 Discussion and Contribution

The chapter's contribution is the development of the "Optimal Detection Block."

Content Contribution for Answering the Research Question: The presented chapter can contribute to answering research questions R1: and R2: as follows:

- R1: *How can control room personnel benefit from modern model-based control algorithms and measurement techniques in the decision-making process of arming SPS?*
  The procedure shown here is helpful because it considers the minimum necessary number of SPSs, thus keeping the complexity as low as possible. Furthermore, in the optimization design, ideas were considered that we received from control-room personnel. For example,

the current arming state should be considered, and the transition from one arming state to the next should be kept small.

- R2: *How do the deterministic, model-based optimization techniques affect the coordination of SPS, the DBM, and SBM? What potential challenges might arise from this approach?* The proposed technique is beneficial for coordination since all the SPS available are considered, not just one single SPS. Furthermore, it is here distinguished between detectable and critical contingencies. Together with the individual triggering functions and the characteristic logic circuits describing the SPS, it is possible to avoid arming contingencies that are not critical. Consequently, this minimizes the possibility of triggering when unnecessary and is beneficial concerning the SBM. Minimizing the number of SPS to be armed may be positive concerning the complexity but is likely to have a negative impact on the DBM. Challenging is the type of the entire optimization problem. It is non-convex and non-linear, which is time-consuming and hard to solve.

Contribution

- RISE initiated the structural representation by contingency and triggering matrix. The extension, for example, all associations to set theory and the structural extension, which is necessary for the binary optimization (Optimal Detection Block), can be counted as a contribution of this thesis.

- An arming procedure is developed that can be implemented as an upper level in a bi-level optimization problem. The procedure selects the set of SPSs with the smallest number and the minimum transition with to the current arming status. Furthermore, it minimizes the possibility of triggering SPSs due to non-critical contingencies.

- Indices are proposed that can be used to evaluate the operator's current arming procedure. It can be considered a metric that allows to decide the weak points regarding the design and operation of SPSs.

- In the context of this chapter, a test model was developed that is provided with a total of 8 different SPSs and their logic gates. It is relatively compact (39 buses) with three different voltage levels and three different types of control actions.

Chapter 5

Optimal and Adaptive Arming of Predictive UFLS for Sudden Grid Islanding

This chapter is based on the publication P4 "Optimal and predictive under-frequency load shedding against critical islanding contingencies." The paper was presented at PowerTech Belgrade in 2023 and provides valuable insights into addressing research questions R1: and R2:.

5.1 Motivation and Objective

Uncontrolled electric islanding is a dangerous contingency that can lead to severe frequency swings due to a sudden mismatch in generation and consumption. The severity of the frequency change depends on the post-contingency power imbalance, the inertia, and the primary reserves.

The current practice is described in subsection 2.6.2 of this thesis. Today, loads are gradually disconnected when the frequency exceeds certain thresholds. The precise amount and location are set in the planning phase based on the current grid topology and expected operation.

A general drawback of the current response-based practice is its non-adaptive implementation. Furthermore, it has a response-based characteristic, i.e., the frequency must decrease until the first loads are shed. This behavior increases the risk of losing further generations [19]. In addition, the process of shedding loads, as explained in subsection 2.6.2, typically requires more loads to be disconnected to keep the frequency in an acceptable range than if the appropriate number of loads were disconnected immediately after a generation interruption is detected.

In the context of sudden islanding, the following challenges are particularly noteworthy. As section 2.4 mentioned, the FCR reserves are selected to cover a reference incidence associated, for example, with the loss of the largest generators in the interconnected grid. Consequently, it is unclear if there are enough spinning reserves to keep the frequency in a particular range after islanding. Another challenge is that the potential loads determined in offline studies and distributed over the interconnected system are sufficient for a specific islanding scenario that may happen.

The sudden formation of an electric island can disorganize all scheduled load-shedding actions because it may influence the number of available loads, spinning reserves, primary response, inertia, and the planned coordination of the unit protection functions.

If an area is detected that would turn into an island due to the loss of a transmission line, it is current practice to increase the generation in the associated area [14]. As a result, the post-contingency power mismatch will be reduced, and load shedding may be sufficient to protect the island from collapse.

However, the decision-making process concerning preventive generation rescheduling is based on steady-state calculations, and the triggered UFLS could be insufficient. Furthermore, if generation re-dispatching is used, it leads to cost since these sources must be activated from the regulation market (i.e., the mFFR market).

This chapter suggests an improved approach to the current method of treating potential islanding described above. The adaptive and event-based procedure considers the dynamic behavior, static aspects, and current system state. It assists the operator in determining whether it is possible

to operate the system in the N-1/2 secure state and even which loads are potential candidates to be armed. The tool also indicates to what extent the event-based UFLS should be armed.

For the implementation of this procedure, the main idea proposed by [63] and subsequently by [69] is followed. The method pre-calculates, repetitive, the minimum amount and location of loads that must be shed for a sudden generation outage, which is achieved by combining a sensitivity-based Optimal Power Flow (OPF) with a simplified dynamical model. The static power flow equations in the OPF are used for approximating the post-contingency steady-state line currents and nodal voltages. The simplified dynamic model is considered for predicting the frequency response over a particular time horizon. The dynamic model used in [63] is second-order. In contrast, [69] extended the idea by including a third-order dynamic model, battery storage, and focusing more on low-inertia aspects. For finding the sensitivities relevant to the OPF, a method proposed in [15] was used. [62] publishes another work in the relevant domain where a model-predictive method was considered for the controlled islanding and the coordination between predictive and conventional UFLS.

The objectives of the paper P4, and consequently this chapter, are the following:

- To present a procedure that assists the operator in determining whether or not the system can be operated in the N-1/2 secure state with respect to a sudden electrical landing.
- As proposed in [63] and [69], the procedure uses a sensitivity-based OPF and a simplified dynamic model to find the right location and amount of UFLS. Two models are compared: a) Similar as in [63] a second-order model (SiGo), but where the work presented here additionally identifies the composite droop. b) A Single-machine-multi-governor (MuGo), where each governor is approximated with a first-order model. In the MuGo model, governor limiters were modeled using binary variables for each time step and each governor.
- To estimate the post-contingency power mismatch, the pre-contingency

line-flow (i.e., infeed to the area) is used as proposed in [19]. In the following, this power flow is called cut flow or flow through the cut and is represented by the variable name ΔP_{cut}

- The objective function of the optimization models considers, besides costs, a function that indicates the line losses.

5.2 Methodology

This section provides a brief overview of the proposed method. A more detailed description of the whole procedure can be found in the related paper P4.

The proposed procedure is shown as a flowchart in Fig. 5.1.

If the contingency analysis detects an event that results in an island, a Root Mean Square (RMS) simulation is performed based on that contingency and the current system state. This simulation aims to generate representative data that can be used later on for the parameter identification of the simplified dynamic model. However, if the RMS simulation does not provide representative results because of an insufficient amount of spinning reserves, the cut flow ΔP_{cut} is calculated and, if necessary, increased by i time a small number $\Delta\varepsilon$. This increase of ΔP_{cut} is done because the initially found cut flow is an estimation that might be too small. Based on the calculated cut flow, a sensitivity-based OPF is run to minimize loads to be shed. This step ensures whether there is a steady-state solution at all. If this is not possible, in other words, if the solution is infeasible, the process is stopped immediately, and the system cannot be operated in the N-1/2 secure state.

Fig. 5.2 shows an illustrative example of such a situation. Let us consider the critical islanding contingency between buses 6 and 7. Furthermore, assuming that the generation of G1 and G2 was higher than the remaining spinning reserves in G3 and G4. In this case, based on the current system state, the droop, the network topology, and the flow through the cut, the pre-optimizer now decides at which point loads should be disconnected to at least be able to supply all loads with the remaining spinning reserves.

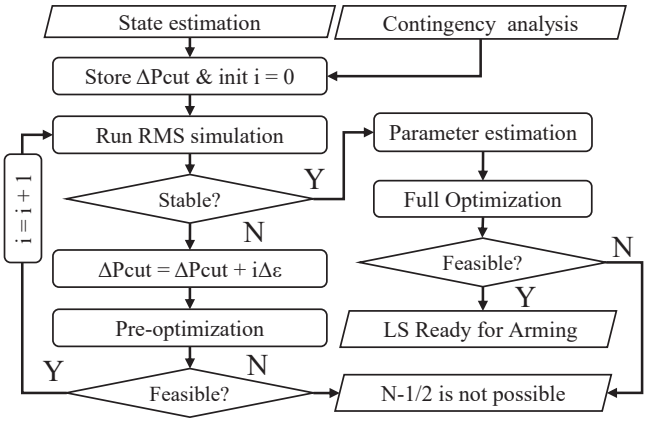

Figure 5.1: Flow chart representing the basic method (from P4)

Since only loads 8 and 9 are available for the UFLS, it depends on the pre-contingency system state whether a solution can be found that critically overloads the corridor between 7 and 8 or not. Precisely, this point is calculated by the pre-optimizer.

However, if a solution is found, the location and size of the UFLS are saved and applied in the RMS simulation. Once a stable solution is found the first time, the parameters of the simplified dynamic model are determined using a least squares method. Using this simplified model and the sensitivity-based OPF, the optimal quantity and position of the UFLS is determined. If this is successful and a solution is found, the system can be operated in N-1/2, else not.

5.3 Test Case and Results

Two different scenarios were looked at using the benchmark IEEE39 bus model, as shown in Fig. 5.3.

It is assumed that the line between bus 26 and 27 is temporarily out

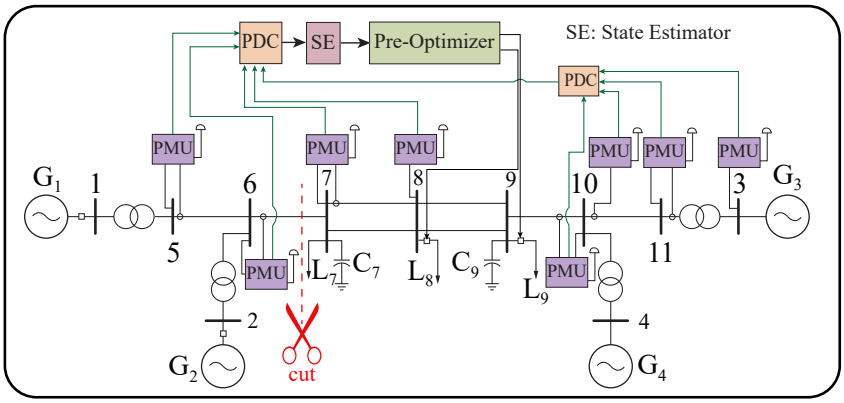

Figure 5.2: Illustrative example of possibly infeasible solution of the pre-optimization

of service, which could be the case because maintenance work is being carried out. A loss of the transmission line between bus 2 and 25 would consequently lead to a critical islanding contingency because it would cause the frequency in the lower (lavender-colorized) island to drop critically.

How exactly the frequency response looks is illustrated in Fig. 5.4.

The y-axis shows the frequency deviation, and the x-axis shows the delta mechanical power. The steady-state droop characteristic of individual generators connected is shown on the right-hand side. The black solid curve on the left-hand side shows the composite droop characteristic in the considered island. The light blue and red background illustrates the permissible frequency range. The solid trajectories on the left-hand side show how the actual Center of Inertia (CoI) frequency changes during the transient phase simulated in PSS®E. The dashed trajectories illustrate the curves of the simplified model represented in the optimizer.

The solid purple trajectory shows the frequency characteristic after losing the line between bus 2 and 25 without triggering any UFLS. When comparing the left and right sides, it becomes clear that several governors have already reached their limit during the first transient phase (see the

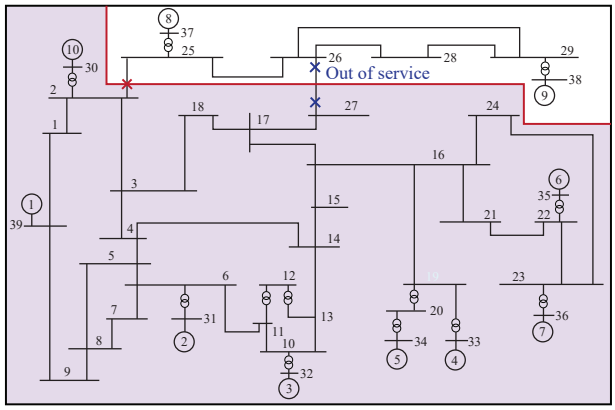

Figure 5.3: Single line representation of the considered test case in the IEEE39 bus system

generators at bus 32, 33, 34, 35, and 36). The result is a frequency trajectory that exceeds the defined limit.

The blue curve shows what the load shedding would look like if the SiGo model parameters were identified based on an RMS model that does not consider limiters. It is obvious that, in this case, too few loads would be shed, which might end up in a rather critical situation since the optimizer would recommend an N-1/2 secure state (i.e., arming of UFLS) even if it is not possible.

Conversely, the red trajectory is based on the load shedding calculated using the SiGo models, whose parameters were determined using the purple frequency trajectory (i.e., an RMS model that considers governor limiters). When comparing the red and blue dashed curves, it can be seen that the red curve now also changes the composite droop used in the dynamic model (see the final values). For the here considered scenarios, this leads to better predicting the transient behavior for the considered contingencies. However, it is essential to note that this identified composite droop is only used for the dynamic model. Binary variables were used to model the limiters in the steady-state OPF equations. It's also worth mentioning that the Post-

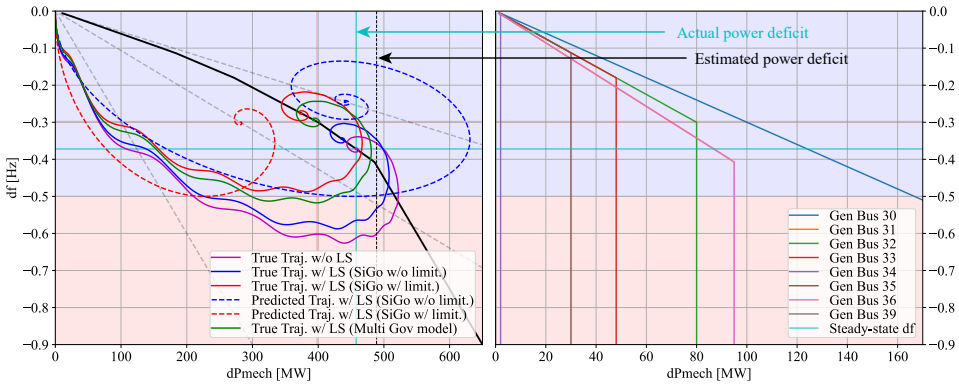

Figure 5.4: Frequency response for the first scenario (sufficient spinning reserves)

contingency steady-state solution found by the OPF (see the light red cross on the left figure) deviates from the actual final value (red solid). The deviation can be explained by comparing the actual and estimated (i.e., flow through the cut ΔP_{cut}), which are represented as vertical straight lines. The difference between them can be explained by the fact that the grid losses differ in pre- and post-contingency states.

A similar result as the red SiGo solution can be found by considering the MuGO model (green trajectory). It is important to note that the optimization process is quite complex because the dynamic model incorporates a variety of binary variables to represent governor limiters.

The frequency response for the second scenario can be seen in Fig. 5.5. When comparing the composite droop curve and the estimated power deficit, it becomes clear that there are too few spinning reserves to simulate a representative frequency response. The RMS simulation confirms this suspicion (see purple trajectory). For this reason, a pre-optimization is now carried out, which yields around 58.8 MW of loads. The light magenta curve shows the simulated trajectory after the proposed load shedding of the pre-optimizer. Although there are now enough spinning reserves, the curve shows that the Frequency-Nadir is still too low. Consequently, based

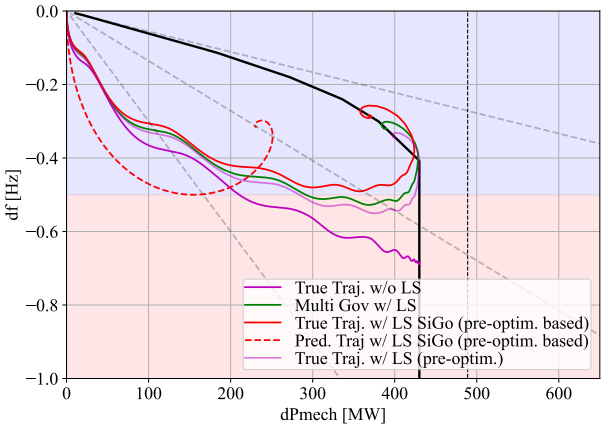

Figure 5.5: Frequency response for the second scenario (insufficient spinning reserves)

on this simulation, the parameters of the simplified model are estimated, and full optimization is performed. The load shedding suggested by the Full-Optimization using the MuGo model shows the green curve and that of the SiGo model the red curve.

5.3.1 Discussion and Contribution

Two different simplified models were tested. The SiGo model showed better performance for the contingency under consideration for two reasons. First, the SiGo model shed more loads than necessary, so the frequency nadir was above the critical frequency limit, providing more safety. The second positive aspect of the SiGo model is that it is much less complex than the MuGo model. For comparison, implementing the considered test case with a prediction horizon of 12 seconds required 850 binary variables.

The cut flow was used as an indicator for the power mismatch, which is the driving force for the frequency change. The example shows that it can be used as an indicator but must be considered carefully since it may deviate.

Content contribution for answering the research question: The presented chapter can contribute to answering research questions R1: and R2: as follows:

- R1: *How can control room personnel benefit from modern model-based control algorithms and measurement techniques in the decision-making process of arming SPS?*
  The presented procedure can assist the control room personnel in determining whether the system can be operated in the N-1/2 secure state concerning possible electric islands. When the procedure concludes that an N-1/2 secure operation is possible, the exact calculated control action can be armed at the determined location. Thus, preventive measures such as generator re-dispatch that need resources from the mFFR market can be avoided, and the system can consequently be operated more effectively and with smaller reserves.

- R2: *How do the deterministic, model-based optimization techniques affect the coordination of SPS, the DBM, and SBM? What potential challenges might arise from this approach?* Since the procedure considers a sensitivity-based OPF, the UFLS is coordinated with the overload protection. Consequently, no other lines should be tripped due to the switching of overload relays. However, one drawback is that the models are based on significant simplifications. Substantial simplifications in the models may give a false impression of being N-1/2 secure, leading to severe problems.

Contribution:
As previously stated, the optimization method outlined in this chapter builds on the concept introduced in [63] and [69]. However, it further emphasizes addressing the difficulties associated with sudden critical islanding. In addition, two simplified models were compared where the effect of reaching the governor limits during the transient phase was considered in more detail. Since the proposed method is explicitly focused on grid islanding, it was decided to split the optimization into pre- and full-optimization modules. Mainly to make sure to generate representative data to identify the

parameters for the simplified model. For calculating the sensitivities used in the OPF, an automatic differentiation method was implemented in Python with the help of a package called JAX [13].

Chapter 6

Optimally Arming of Predictive UFLS Considering Rotor-Angle and Frequency Trajectories

This chapter is based on the publication P2, but has been adjusted in two points. 1) The scenario has been changed to complement the method presented in Chapter 5. 2) The simulation tool programmed in Python was modified so that automatic differentiation can be used to find the trajectory sensitivity. The chapter's content is beneficial for answering the two research questions R1: and R2:

6.1 Motivation and Objective

The previous chapter used a method to incorporate a discretized trajectory of the center-of-inertia frequency into an optimization problem. For this purpose, a highly simplified dynamic model was used whose parameters were identified with a detailed RMS simulation and a least-squares

procedure. Furthermore, the optimization approximated and included the post-contingency steady-state of the algebraic variables.

The question now arises if there is a possibility to include the detailed dynamic model in the optimization directly, which would allow a more sophisticated optimization of the dynamic states and algebraic variables such as voltages.

A more detailed model related to UFLS is motivated by the following phenomena. After a sudden mismatch between electrical and mechanical power, the frequency response can usually be divided into four phases [45]. In the first phase, the difference between mechanical and electrical power is compensated by the kinetic energy reduction, leading to a decrease in frequency. In this phase, the rotors of the different connected generators may oscillate against each other depending on the available damping. The second phase is initiated by using various controllers that slowly begin to provide FCR [39].

Combining the machine speeds into a single quantity (i.e., CoI frequency) can, for these reasons, be an oversimplification, and critical dynamic phenomena such as rotor oscillations may be hidden.

A method that allows the incorporation of a detailed RMS model into an optimization procedure was presented in [66], [68], [65]. The idea is to use trajectory sensitivity to approximate the post-contingency trajectories. Based on the author's knowledge, [66], [68], and later, [65] are the first publications that use trajectory sensitivity theory in the field of model predictive emergency control or system protection schemes. The publications were written in the framework of a Ph.D. thesis [67]. Many authors subsequently used the method in connection with, for example, UFLS.

To the best of our knowledge and understanding (i.e., based on our interpretation and current understanding), the method proposed in [66], [68] and [65] works as follows: [66] and [68] describe a method for real-time stability assessment and emergency control of power systems based on trajectory sensitivity. If a contingency is detected at time t_c, a simulation predicts the system behavior from t_0 to a specific future time. This simulation checks if the trajectories stay in a particular range. If not, the optimal control action triggered at time t_a is calculated with the help of trajectory

sensitivity theory and a more protection-oriented Model Predictive Control (MPC) algorithm where the control action remains the same for the whole horizon. The timeline for the method proposed in [68] and [66] is illustrated in Fig. 6.1, sub-figure a). The open-loop procedure described in [68] and [66] was finally further developed in [65] so that it can be used as a closed-loop MPC controller.

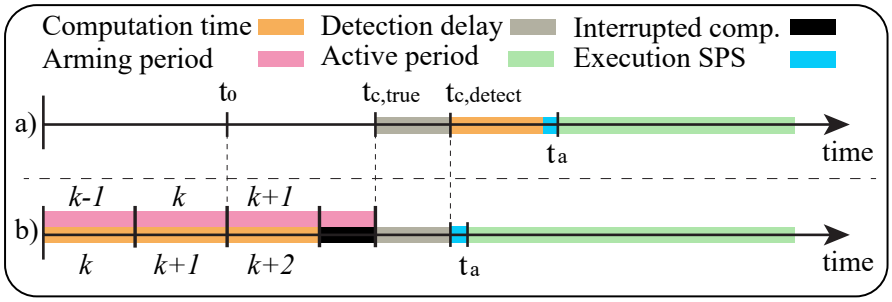

Figure 6.1: a) Relevant time points for the method proposed by [68] and [66]. b) The relevant points in time, which are important for the method described here for optimal arming

.

Today, trajectory-sensitivity theory is known in power systems engineering for various applications. The approximation of trajectories concerning a parameter change is one common application. This method allows the analysis of different parameter changes starting from a nominal scenario without repeating the RMS simulation.

The theory can also be used for preventive, remedial actions, as it was shown by [46]. Trajectory sensitivity and an OPF were used together to reschedule the generators optimally. The rotor angle difference between the generators was used as a metric, which will also be used later in this paper.

The basic idea of trajectory-sensitivity theory is to linearize along a trajectory rather than at a particular equilibrium point, which is why Jacobian matrices must be found at each time step. Computing the Jacobians of differential-algebraic equations can be computationally intensive

and error-prone [24].

So-called Automatic Differentiation (AD) is an accurate and typically more efficient method for finding Jacobian matrices than, for example, numerical finite methods.

To the author's knowledge, [24] is the first publication that considered AD for calculating trajectory sensitivity in the power systems domain.

The author in [24] proposes a new type of AD specifically tailored for power system applications and calls it Partial Decoupled Automatic Differentiation (PD-AD). Tests with models of different scales are shown in which Finite Differentiation (FD), conventional AD, and (PD-AD) are compared in terms of efficiency. The conventional AD performed better than FD, and the proposed new PD-AD outperformed both.

The objectives of this chapter are the following:

- Following the main idea of [66] and [68], an event-based procedure is used to determine the optimal amount and location of UFLS given a known future loss of generation. In addition to the frequency response, the method must consider the voltage trajectories and the difference between the rotor angles. Trajectory sensitivities are calculated using a conventional AD method.

6.2 Methodology

The method presented here is adaptive and event-based as defined in subsection 2.6.5. The main concept is shown in Fig. 6.1 sub-figure b).

It is assumed that a state estimator and a contingency analysis provide the current state and critical contingencies. Furthermore, a detailed dynamic model must be available. Based on this information, a base case scenario for a critical case is simulated, and in parallel, the trajectory sensitivities are calculated with automatic differentiation.

A quadratic optimization problem can be derived that finds the optimal parameter change (i.e., UFLS action) for time 0 such that all approximated algebraic variables and state variables during the prediction horizon remain

within a defined range. If such a solution is found, the SPSs can be armed accordingly.

The optimization problem shown here is marginally different from the one shown in the publication P2. It differs slightly in the chosen optimization variables and some constraints. For this reason, the most important points will be briefly explained here.

The decision variables are in vector $\Delta\lambda = [\Delta P_L, \Delta Q_L]^T$. It contains all possible loads that can be considered for load shedding. The trajectory sensitivities are contained in w_1 and w_2. $w_{1,t}$ is the trajectory sensitivity to the dynamic states at time t concerning the parameter change λ, and $w_{2,t}$ is the same but for the algebraic variables. Results stored in the variables marked with a bar are the simulation results of the base-case scenario.

$$\min_{\Delta\lambda} \quad \Delta\lambda^T K \Delta\lambda \tag{6.1}$$

$$\text{subject to:} \quad \Delta\omega_t = w^{\omega}_{1,t}\Delta\lambda + \Delta\bar{\omega}_t \tag{6.2}$$

$$\Delta\delta_t = w^{\delta}_{1,t}\Delta\lambda + \Delta\bar{\delta}_t \tag{6.3}$$

$$U_t = w^{U}_{2,t}\Delta\lambda + \bar{U}_t \tag{6.4}$$

$$\Delta\omega_{\min} \leq \Delta\omega_t \leq \Delta\omega_{\max} \tag{6.5}$$

$$\Delta\delta^{\min}_{i,j} \leq \Delta\delta^i_t - \Delta\delta^j_t \leq \Delta\delta^{\max}_{i,j} \tag{6.6}$$

$$U_{\min} \leq U_t \leq U_{\max} \tag{6.7}$$

$$\Delta\lambda_{\min} \leq \Delta\lambda \leq \Delta\lambda_{\max} \tag{6.8}$$

$$\tag{6.9}$$

The optimization problem (6.1) - (6.8) finds the cheapest possible $\Delta\lambda$ such that the approximated machine speeds ω, the rotor angle differences $\Delta\delta^i_t - \Delta\delta^j_t$ and the nodal voltages U over the whole prediction horizon stays in a particular range.

Fig. 6.2 shows a graphical representation of the procedure. Compared to Fig. 5.1 from the previous chapter, it is now clear that no further parameter identification is necessary for the present process because the Simulations model is directly included in the optimization.

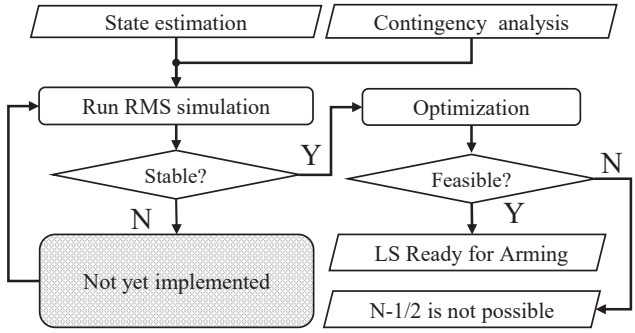

Figure 6.2: Flow chart representing the basic method

6.3 Test Case and Results

The scenario used in this thesis is shown in Fig. 6.3. The critical contingency is the loss of the grid connection at bus number 1. This leads to an island that lets the frequency critically decrease below the defined limit of 49 Hz (see Fig. 6.4). Furthermore, the rotor angles between the machines start swinging against each other (see Fig. 6.5). The most considerable rotor angle difference is between generator numbers 2 and 3, exceeding the ± 45 degrees limit.

In order to address the issue, the optimizer can choose between the two loads on buses 7 and 9 for UFLS, with the option to select continuous numbers. Blue are the trajectories calculated by the optimizer. They are all within the given range. The green trajectories show the simulated system response considering the given control action.

The voltage at node 8 has the highest deviation from its reference value. It is shown in Fig. 6.6. However, the voltages are not critical for the given case because they always stay within the defined limit (even without UFLS).

On the positive side, all trajectories for frequency, rotor angle difference, and voltage are in the defined range (blue and green) after applying the proposed UFLS. Also, the proposed trajectories fit well with the simulated ones, at least initially. It is essential to note that the difference between

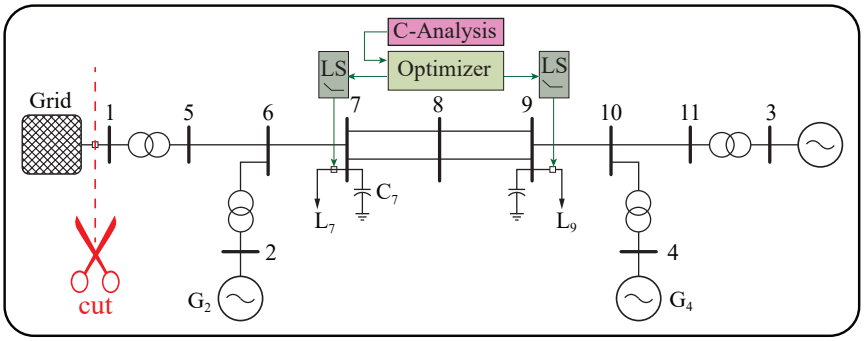

Figure 6.3: Test case adjusted for this chapter

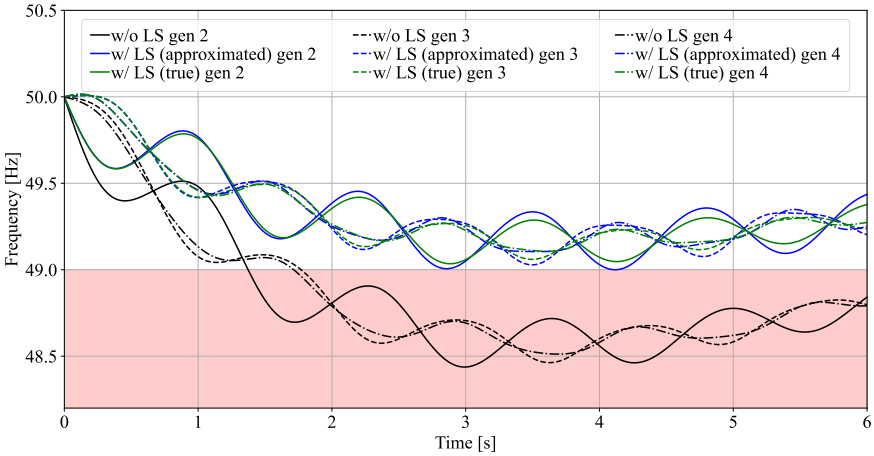

Figure 6.4: Frequency plot

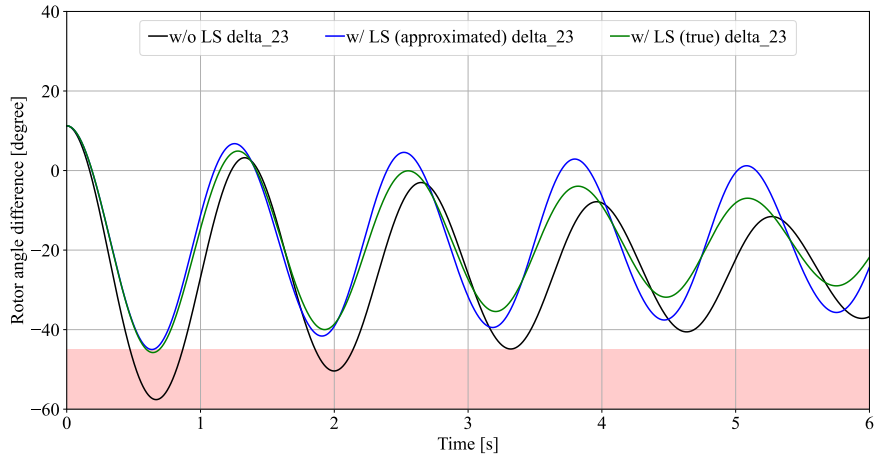

Figure 6.5: Most critical rotor angle difference between machine 2 and machine 3.

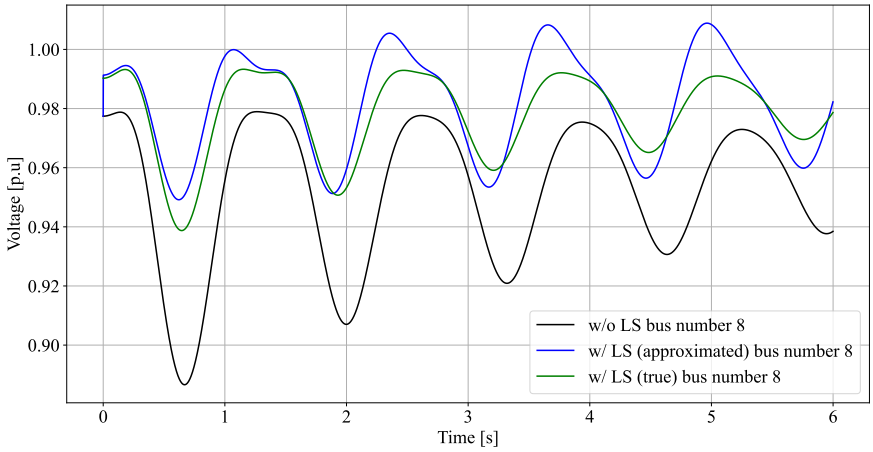

Figure 6.6: Voltage change in the most severe node at bus number 8

the predicted and simulated trajectories becomes larger as time passes. Therefore, it might be possible that there is still an error in the simulation tool tailored for this chapter.

6.3.1 Discussion and Contribution

The presented chapter can contribute to answering research questions R1: and R2: as follows:

- R1: *How can control room personnel benefit from modern model-based control algorithms and measurement techniques in the decision-making process of arming SPS?*
  Since the procedure is a sophistication of the method discussed in the last chapter 5, nothing further can be added here.

- R2: *How do the deterministic, model-based optimization techniques affect the coordination of SPS, the DBM, and SBM? What potential challenges might arise from this approach?* The method presented in this chapter considers a dynamic model and trajectory sensitivity theory, which allows the incorporation of a dynamic model directly into the optimization model. All dynamic states and algebraic variables of the model can be approximated, which means that the degree of freedom for the coordination is high, and the granularity is better than in the approach shown in the last Chapter 5. Specifically, this means that variables such as rotor angle differences can also be considered in the more detailed optimization.

Contribution

The method presented in this chapter follows the main idea proposed in [66] and [68]. The approach proposed deviates in two ways. The first deviation can be seen illustrated in Fig. 6.1. As mentioned in subsection 2.6.5, indicated in Fig. 6.1 sub-figure b), is the proposed method repetitive and is used for arming in an event-based manner. In concrete terms, this means that the optimal control action is pre-calculated for a given contingency. Consequently, the optimal UFLS configuration is armed for the given contingency. This means that at time $t_{c,detect}$, the UFLS can be triggered

directly (see Fig. 6.1 sub-figure b) and the remedial action is active as soon the execution time for the remedial action has elapsed. In contrast, the procedure shown in [66] and [68] calculates the optimization after the contingency has been detected (see Fig. 6.1 sub-figure a)). Both approaches have their advantages and disadvantages. In this Chapter, the proposed method requires no calculation time in the critical phase after the contingency is detected. However, the disadvantage of the method shown here compared to that of [66] and [68] is that it must be calculated repetitively to be able to arm accurately. If the operation point has changed significantly since the last optimization, the calculated remedial action may be insufficient, and that of [66] and [68] may be superior.

For this reason, it is essential for the method proposed here to be calculated as quickly as possible to keep the arming as up-to-date as possible. This point brings us to the second deviation compared to [66] and [68]. A time-intensive procedure in the framework of trajectory sensitivity is to compute the Jacobian matrices. [24] showed that automatic differentiation is very effective for computing trajectory sensitivities. Therefore, the algorithm proposed here for calculating trajectory sensitivities uses an automatic differentiation approach. The simulation tool used in this chapter is a specifically tailored Python-based simulator described in the publication P2. For implementing the automatic differentiation, JAX is used [13].

Chapter 7

Conclusion

This dissertation presents methods to enhance the arming procedure, leading to better coordination and performance of system protection schemes.

A static procedure is described that can be seen as an upper-level of a bi-level optimization problem and finds the smallest number of SPSs to be armed. The other two methods consider, besides static aspects, dynamic quantities. The goal is to improve the performance of event-based underfrequency load shedding using a simplified dynamic model and sensitivity-based optimal power flow or trajectory sensitivity-based methods.

However, all the methods presented have one feature in common. The methods optimize with respect to the current system state for critical future contingencies and repeat this continuously. Therefore, they can be seen as adaptive arming procedures. The presented procedures may support control room personnel in decision-making regarding possible arming configurations and the N-1/2 secure operation.

The method using a static model presented in Chapter 4 may be beneficial concerning security of the schemes because it tries to minimize the number of armed system protection schemes that non-critical contingencies would trigger. The algorithm prioritizes the solutions with minimal arming changes concerning the current arming status, which may benefit the work in the control room. It is worth mentioning that the procedure minimizes

the number of schemes to be armed. This can have a positive effect on the complexity.

The two under-frequency load-shedding methods are adaptive and predictive and consider both frequency and other variables (such as voltages), which may be beneficial concerning coordination. The main idea is to precalculate the optimal arming such that if needed, the only delay is the execution delay of the system protection scheme. Thus, no more computation time is needed during the critical transient phase. This point is particularly interesting in the case of uncertainty regarding inertia, such as islanding scenarios. The methods both positively affect the coordination since they consider wide-area aspects.

Since having the most recent state update for all the proposed methods is essential, a linear state estimation based on phasor measurement units would be preferred. For this reason, this dissertation further deals with the real-time laboratory implementation of phasor measurement units. Three different implementation approaches are considered, all with their advantages and drawbacks. The possibility of an IEC 61850-based integration of phasor measurement units is the most advantageous. It is a sophisticated hardware-in-the-loop method for considering commercial equipment such as intelligent electronic devices or merging units. Expensive equipment such as converters can be avoided, which means that the number of analog outputs is no longer limited, making scaling much simpler.

Future work involves implementing at least one of these proposed arming algorithms in the real-time laboratory. Open questions and challenges exist, especially in the theoretical methods presented here. For example, how detailed is the optimal model? Another question is how often the arming algorithms have to be repeated. Does this have to happen as fast as possible, or can a certain time lag between the optimizations be tolerated? It would also be interesting to consider probabilistic reliability aspects that may be used for classifying the different contingencies.

References

[1] Katrine Gabrielsen Andersen. "Area Based Secondary Frequency Control in the Nordic Power System". NTNU. Master's thesis. Norwegian University of Science and Technology, 2016. URL: https://ntnuopen.ntnu.no/ntnu-xmlui/bitstream/handle/11250/2408871/15093_FULLTEXT.pdf?sequence=1&isAllowed=y (visited on 11/11/2023).

[2] Paul M Anderson, Charles F Henville, Rasheek Rifaat, Brian Johnson, and Sakis Meliopoulos. *Power system protection*. John Wiley & Sons, 2022.

[3] Olubayo Moses Babatunde, Josiah L Munda, and YJER Hamam. "Power system flexibility: A review". In: *Energy Reports* 6 (2020), pp. 101–106.

[4] Daniel Baltensperger, Santiago Sanchez, Salvatore D'Arco, and Kjetil Uhlen. "Assessing hardware in the loop approaches for wide-area monitoring control and protection devices". In: *IEEE Transactions on Power Delivery* (2023), pp. 1–12. DOI: 10.1109/TPWRD.2023.3255414.

[5] Daniel Baltensperger, Kjetil Uhlen, Santiago Sanchez-Acevedo, and Salvatore D'Arco. "Experimental Characterization of Methods for Connecting Real-Time Simulations and Synchrophasors". In: *2021 IEEE Madrid PowerTech*. IEEE. 2021, pp. 1–6.

[6] Christian Bang, Felicia Fock, and Mikael Togeby. "The existing Nordic regulating power market". In: *Ea Energy Analysis, www. ea-energianalyse. dk/reports/1027_the_existing_nordic_regulating_power_market. pdf* (2012).

[7] M. Begovic, D. Novosel, D. Karlsson, C. Henville, and G. Michel. "Wide-Area Protection and Emergency Control". In: *Proceedings of the IEEE* 93.5 (2005), pp. 876–891. DOI: 10.1109/JPROC.2005.847258.

[8] Andrea Benigni, Thomas Strasser, Giovanni De Carne, Marco Liserre, Marco Cupelli, and Antonello Monti. "Real-Time Simulation-Based Testing of Modern Energy Systems: A Review and Discussion". In: *IEEE Industrial Electronics Magazine* 14.2 (2020), pp. 28–39. DOI: 10.1109/MIE.2019.2957996.

[9] Mette Bjørndal, Kurt Jörnsten, and Virginie Pignon. "Congestion management in the Nordic power market—counter purchases and zonal pricing". In: *Journal of Network Industries* 3 (2003), pp. 271–292.

[10] Steven Blair, Nathan Matheson, Richard Munro, and Campbell Booth. "A new platform for validating real-time, large-scale WAMPAC systems". In: *PAC World Conference 2019*. 2019.

[11] Steven M. Blair, Mazheruddin H. Syed, Andrew J. Roscoe, Graeme M. Burt, and Jean-Pierre Braun. "Measurement and Analysis of PMU Reporting Latency for Smart Grid Protection and Control Applications". In: *IEEE Access* 7 (2019), pp. 48689–48698. DOI: 10.1109/ACCESS.2019.2903929.

[12] Audun Botterud. *Long term planning in restructured power systems: dynamic modelling of investments on new power generation under uncertainty*. Fakultet for informasjonsteknologi, matematikk og elektroteknikk, 2003.

[13] James Bradbury, Roy Frostig, Peter Hawkins, Matthew James Johnson, Chris Leary, Dougal Maclaurin, George Necula, Adam Paszke, Jake VanderPlas, Skye Wanderman-Milne, and Qiao Zhang. *JAX:*

composable transformations of Python+NumPy programs. Version 0.3.13. 2018. URL: http://github.com/google/jax.

[14] O. Breidablik, F. Giaver, and I. Glende. "Innovative measures to increase the utilization of Norwegian transmission". In: *2003 IEEE Bologna Power Tech Conference Proceedings,* vol. 1. 2003. DOI: 10.1109/PTC.2003.1304104.

[15] Konstantina Christakou, Jean-Yves LeBoudec, Mario Paolone, and Dan-Cristian Tomozei. "Efficient Computation of Sensitivity Coefficients of Node Voltages and Line Currents in Unbalanced Radial Electrical Distribution Networks". In: *IEEE Transactions on Smart Grid* 4.2 (2013), pp. 741–750. DOI: 10.1109/TSG.2012.2221751.

[16] CIGRE Task Force 38.02.19. *System Protection Schemes in Power networks*. Technical Brochure 187. 2001. URL: https://cigreindia.org/CIGRE%20Lib/Tech.%20Brochure/187%20System%20Protection%20schmes%20in%20power%20system.pdf (visited on 11/11/2023).

[17] Asja Derviškadić, Reza Razzaghi, Quentin Walger, and Mario Paolone. "The white rabbit time synchronization protocol for synchrophasor networks". In: *IEEE transactions on smart grid* 11.1 (2019), pp. 726–738.

[18] Lei Ding, Francisco M. Gonzalez-Longatt, Peter Wall, and Vladimir Terzija. "Two-Step Spectral Clustering Controlled Islanding Algorithm". In: *IEEE Transactions on Power Systems* 28.1 (2013), pp. 75–84. DOI: 10.1109/TPWRS.2012.2197640.

[19] Dinh Thuc Duong and Kjetil Uhlen. "A topology-based scheme for adaptive underfrequency load shedding". In: *2017 IEEE Manchester PowerTech*. IEEE. 2017, pp. 1–6.

[20] ENTSO-e. *Fast Frequency Reserve – Solution to the Nordic inertia challenge*. Accessed: 2023-08-5. 2019. URL: https://www.statnett.no/globalassets/for-aktorer-i-kraftsystemet/utvikling-av-kraftsystemet/nordisk-frekvensstabilitet/ffr-stakeholder-report_13122019.pdf.

[21] ENTSO-e. *P5 – Policy 5: Emergency Operations*. Online. Accessed: 2023-08-14. 2010. URL: https://eepublicdownloads.entsoe.eu/clean-documents/pre2015/publications/entsoe/Operation_Handbook/Policy_5_final.pdf.

[22] Fingrid, Energinet, Svenskakraftnät, Statnett, Kraftnätåland. *Nordic System Operation Agreement (SOA) – Annex Operational Security (OS)*. Tech. rep. 2019. URL: https://www.statnett.no/contentassets/2270ef6fc48e42ae8453833bb86df746/nordic-soa-2019-annex-lfcr.pdf (visited on 07/03/2023).

[23] Lester H Fink and Kjell Carlsen. "Operating under stress and strain". In: *IEEE Spectrum;(United States)* 15.3 (1978).

[24] Guangchao Geng, Venkataramana Ajjarapu, and Quanyuan Jiang. "Application of automatic differentiation in power system trajectory sensitivity analysis". In: *2014 IEEE PES T&D Conference and Exposition*. 2014, pp. 1–5. DOI: 10.1109/TDC.2014.6863266.

[25] Xavier Guillaud, M. Omar Faruque, Alexandre Teninge, Ali Hasan Hariri, Luigi Vanfretti, Mario Paolone, Venkata Dinavahi, Pinaki Mitra, Georg Lauss, Christian Dufour, Paul Forsyth, Anurag K. Srivastava, Kai Strunz, Thomas Strasser, and Ali Davoudi. "Applications of Real-Time Simulation Technologies in Power and Energy Systems". In: *IEEE Power and Energy Technology Systems Journal* 2.3 (2015), pp. 103–115. DOI: 10.1109/JPETS.2015.2445296.

[26] Dinesh Rangana Gurusinghe, Sachintha Kariyawasam, and Dean S. Ouellette. "Performance evaluation of phasor measurement units with sampled value input". In: *15th International Conference on Developments in Power System Protection (DPSP 2020)*. 2020, pp. 1–6. DOI: 10.1049/cp.2020.0052.

[27] Liisa Haarla, Mikko Koskinen, Ritva Hirvonen, and Pierre-Etienne Labeau. *Transmission grid security: a PSA approach*. Springer Science & Business Media, 2011.

[28] E. Hillberg, F. Trengereid, Ø. Breidablik, K. Uhlen, G. Kjølle, S. Løvlund, and J.O. Gjerde. "System Integrity Protection Schemes – Increasing operational security and system capacity". In: *Proc. 44th CIGRE Session*. 2012.

[29] Emil Hillberg. "Perception, Prediction and Prevention of Extraordinary Events in the Power System". In: (2016).

[30] Emil Hillberg, Antony Zegers, Barbara Herndler, Steven Wong, Jean Pompee, Jean-Yves Bourmaud, Sebastian Lehnhoff, Gianluigi Migliavacca, Kjetil Uhlen, Irina Oleinikova, et al. "Flexibility needs in the future power system". In: (2019). URL: https://ntnuopen.ntnu.no/ntnu-xmlui/bitstream/handle/11250/2595775/ISGAN_DiscussionPaper_Flexibility_Needs_In_Future_Power_Systems_2019_v01.pdf?sequence=1 (visited on 11/11/2023).

[31] Pär Holmberg and Ewa Lazarczyk. "Comparison of congestion management techniques: Nodal, zonal and discriminatory pricing". In: *The Energy Journal* 36.2 (2015).

[32] Graeme Hutchison, Øyvind Breidablik, Harri Kuisti, Ilkka Luukkonen, Magnus Nielsen, Flemming Brinch Nielsen, Johan Setréus, Lars Gjedsted Sørensen, and Jukka Turunen. *Frequency Based Emergency Disconnection Policy Review for the Nordic Region Report*. Tech. rep. Nordic Analysis Group (NAG), June 2017. URL: https://www.statnett.no/globalassets/for-aktorer-i-kraftsystemet/utvikling-av-kraftsystemet/nordisk-frekvensstabilitet/frequency-based-emergency-disconnection-policy-review-for-the-nordic-region-v1.0.pdf.

[33] "IEEE Guide for Phasor Data Concentrator Requirements for Power System Protection, Control, andMonitoring". In: *IEEE Std C37.244-2013* (2013), pp. 1–65. DOI: 10.1109/IEEESTD.2013.6514039.

[34] "IEEE Standard for Synchrophasor Data Transfer for Power Systems". In: *IEEE Std C37.118.2-2011 (Revision of IEEE Std C37.118-2005)* (2011), pp. 1–53. DOI: 10.1109/IEEESTD.2011.6111222.

[35] "IEEE Standard for Synchrophasor Measurements for Power Systems". In: *IEEE Std C37.118.1-2011 (Revision of IEEE Std C37.118-2005)* (2011), pp. 1–61. DOI: 10.1109/IEEESTD.2011.6111219.

[36] International Energy Agency. *World Energy Outlook 2022*. https://www.iea.org/reports/world-energy-outlook-2022. Accessed: 2023-07-19. License: CC BY 4.0 (report); CC BY NC SA 4.0 (Annex A). Paris, 2022.

[37] Vyacheslav V Kalashnikov, Stephan Dempe, Gerardo A Pérez-Valdés, Nataliya I Kalashnykova, and José-Fernando Camacho-Vallejo. "Bilevel programming and applications". In: *Mathematical Problems in Engineering* 2015 (2015).

[38] Abolfazl Khodadadi, Lars Herre, Priyanka Shinde, Robert Eriksson, Lennart Söder, and Mikael Amelin. "Nordic Balancing Markets: Overview of Market Rules". In: *2020 17th International Conference on the European Energy Market (EEM)*. 2020, pp. 1–6. DOI: 10.1109/EEM49802.2020.9221992.

[39] Uhlen Kjetil. *Frequency stability and control (part 2)*. Lecture notes for the course TET4180 - Power System Stability and Control. Norwegian University of Science and Technology. 2020.

[40] Matthias Knauer. "Bilevel-Optimalsteuerung mittels hybrider Lösungsmethoden am Beispiel eines deckengeführten Regalbediengerätes in einem Hochregallager". PhD thesis. Universität Bremen, 2009. URL: https://media.suub.uni-bremen.de/bitstream/elib/2674/1/00011478.pdf (visited on 11/11/2023).

[41] H. Kuisti, M.Lahtinen, M.Nilsson, K.Eketorp, E.Ørum, D.Whitley, A. Slotsvik, and A.Jansson. *NAG - FREQUENCY QUALITY REPORT*. Accessed: 2023-08-4. ENTSO-e, 2015. URL: https://www.statnett.no/globalassets/for-aktorer-i-kraftsystemet/utvikling-av-kraftsystemet/nordisk-frekvensstabilitet/frequency-quality-phase-1-v2.0.pdf.

[42] P. Kundur. *Power System Stability and Control*. New York: McGraw-Hill, 1994.

[43] Tomas E Dy Liacco. "The adaptive reliability control system". In: *IEEE Transactions on Power Apparatus and Systems* 5 (1967), pp. 517–531.

[44] Rannveig Løken, Frode Trengereid, and Johan Inderberg Vestrum. *OP039 Use of system protection in Statnett*. Tech. rep. Statnett SF, 2016. URL: https://cimug.ucaiug.org/CIMGroups/ENTSO-E_IOP/2016/Shared%20Documents/paperIOP/OP039%20Statnett%20SIPS.pdf.

[45] Jan Machowski, Zbigniew Lubosny, Janusz W Bialek, and James R Bumby. *Power system dynamics: stability and control*. John Wiley & Sons, 2020.

[46] Tony B Nguyen and MA Pai. "Dynamic security-constrained rescheduling of power systems using trajectory sensitivities". In: *IEEE Transactions on Power Systems* 18.2 (2003), pp. 848–854.

[47] Irina Oleinikova, Antonio Iliceto, and Emil Hillberg. *Flexibility for Resilience: How can flexibility support power grids resilience?* 2022. URL: https://www.diva-portal.org/smash/get/diva2:1663266/FULLTEXT01.pdf (visited on 11/11/2023).

[48] Mathaios Panteli, Peter A Crossley, and John Fitch. "Quantifying the reliability level of system integrity protection schemes". In: *IET Generation, Transmission & Distribution* 8.4 (2014), pp. 753–764.

[49] Pierre Pinson. *Module 2 - Electricity spot markets*. Online Course, 31761 Renewables in Energy Markets, University, DTU. Accessed: 2023-08-1. URL: https://pierrepinson.com/index.php/teaching/module-2-electricity-spot-markets-e-g-day-ahead/.

[50] Pierre Pinson. *Module 3 – Intra-day and balancing markets*. Online Course, 31761 Renewables in Energy Markets, University, DTU. Accessed: 2023-08-2. URL: https://pierrepinson.com/index.php/teaching/module-3-intra-day-and-balancing-markets/.

[51] Pierre Pinson. *Module 4 – Ancillary services*. Online Course, 31761 Renewables in Energy Markets, University, DTU. Accessed: 2023-08-4. URL: https://pierrepinson.com/index.php/teaching/module-4-ancillary-services/.

[52] Joana Rasmussen. *System Protection Schemes in Eastern Denmark*. Technical University of Denmark, Department of Electrical Engineering, 2006. URL: https://backend.orbit.dtu.dk/ws/portalfiles/portal/5069248/oersted-dtu2518.pdf (visited on 11/11/2023).

[53] Yann Rebours and Daniel Kirschen. "A survey of definitions and specifications of reserve services". In: *Report, University of Manchester* (2005), pp. 1–38. URL: https://labs.ece.uw.edu/real/Library/Reports/Survey_of_Reserve_Services.pdf (visited on 11/11/2023).

[54] Christian Rehtanz and Joachim Bertsch. "Wide area measurement and protection system for emergency voltage stability control". In: *2002 IEEE Power Engineering Society Winter Meeting. Conference Proceedings (Cat. No. 02CH37309)*. Vol. 2. IEEE. 2002, pp. 842–847.

[55] Santiago Sanchez-Acevedo, Daniel Baltensperger, and Salvatore D'Arco. "Accuracy Analysis of a Dynamic State Estimator with a Hardware in the Loop Approach". In: *2023 IEEE Belgrade PowerTech*. 2023, pp. 01–06. DOI: 10.1109/PowerTech55446.2023.10202908.

[56] Adolf J Schwab. *Elektroenergiesysteme: Erzeugung, Übertragung und Verteilung elektrischer Energie*. Springer-Verlag, 2015.

[57] Stefan Stanković, Emil Hillberg, and Susanne Ackeby. "System Integrity Protection Schemes: Naming Conventions and the Need for Standardization". In: *Energies* 15.11 (2022), p. 3920.

[58] Statnett. *Rapport fra systemansvarlig: Om kraftsystemet i Norge 2022, Offentlig*. Tech. rep. 13/02251-24. Statnett, 2022. URL: https://www.statnett.no/for-aktorer-i-kraftbransjen/systemansvaret/arsrapporter-fra-systemansvarlig/ (visited on 11/14/2023).

[59] Statnett, Fingrid, Energinet, and Svenska Krafnät. *Nordic Grid Development Plan 2019*. `https://www.fingrid.fi/globalassets/dokumentit/fi/tiedotteet/lehdistotiedotteet/stet0126_nordic_grid_dp_2019.pdf`. Accessed: 2023-07-07. 2019.

[60] Kjetil Uhlen. *Frequency stability and control (part 1)*. Lecture notes for the course TET4180 - Power System Stability and Control. Norwegian University of Science and Technology. 2020.

[61] Kjetil Uhlen. *Power System Components*. Lecture notes for the course TET4180 - Power System Stability and Control. Norwegian University of Science and Technology. 2020.

[62] Maria Vrakopoulou and Göran Andersson. "An Adaptive Load Shedding Technique for Controlled Islanding". In: *17th Power Systems Computation Conference, Stockholm*. Citeseer. 2011, pp. 22–26.

[63] Quentin Walger, Yihui Zuo, Asja Derviškadić, Guglielmo Frigo, and Mario Paolone. "OPF-based under frequency load shedding predicting the dynamic frequency trajectory". In: *Electric Power Systems Research* 189 (2020), p. 106748.

[64] Geir Warland. *Flexible transfer limits in an open power market-Congestion versus risk of interruption*. Tech. rep. Norges teknisk-naturvitenskapelige universitet, 1999.

[65] M. Zima and G. Andersson. "Model Predictive Control Employing Trajectory Sensitivities for Power Systems Applications". In: *Proceedings of the 44th IEEE Conference on Decision and Control*. 2005, pp. 4452–4456. DOI: `10.1109/CDC.2005.1582863`.

[66] M. Zima and G. Andersson. "Stability assessment and emergency control method using trajectory sensitivities". In: *2003 IEEE Bologna Power Tech Conference Proceedings,* vol. 2. 7 pp. Vol.2-. 2003. DOI: `10.1109/PTC.2003.1304313`.

[67] Marek Zima. "Contributions to security of electric power systems". PhD thesis. ETH Zurich, 2006.

[68] Marek Zima, Petr Korba, and Göran Andersson. "Power systems voltage emergency control approach using trajectory sensitivities". In: *Proceedings of 2003 IEEE Conference on Control Applications, 2003. CCA 2003.* Vol. 1. IEEE. 2003, pp. 189–194.

[69] Yihui Zuo, Asja Derviškadić, and Mario Paolone. "OPF-driven Under Frequency Load Shedding in Low-Inertia Power Grids Hosting Large-scale Battery Energy Storage Systems". In: *2021 IEEE Madrid PowerTech*. 2021, pp. 1–6. DOI: 10.1109/PowerTech46648.2021.9494951.

Chapter 8

Appendix

8.1 Bi-Level Optimization

A classical bilevel optimization can be seen as a hierarchical problem or a game in which two players make decisions on their levels [37]. The upper level represents the so-called leader, and the lower level is the follower. The leader tries as a first move to select $x \in \mathbb{R}^n$ such that the upper-level objective function $F(x, y)$ is minimized. Similarly, the follower chooses its variable $y \in \mathbb{R}^m$ based on the leader's previous decision to minimize the lower objective function [40]. Both objective functions are scalar and map the two vectors x and y to a real-valued number ($f, F : R^n \times R^m \to R$). The two different optimization problems are, in general, both constrained. The lower level $g(x, y)$ and the upper level $G(x, y)$ are functions that map x and y to a new vector ($g : R^n \times R^m \to R^p$) respectively ($G : R^n \times R^m \to R^q$). The bilevel optimization problem can be expressed in the following (8.1).

$$
\begin{aligned}
\underset{x}{\text{minimize}} \quad & F(x,y) \\
\text{subject to} \quad & G(x,y) \leq 0 \\
& x \in X \\
& (x,y) \in \mathbf{gph}\Psi(x) \\
\text{where} \quad & \\
& \varphi(x) = \underset{y}{\text{minimize}} \quad f(x,y) \\
& \text{subject to} \quad g(x,y) \leq 0 \\
& y \in T \subseteq R^m
\end{aligned}
\tag{8.1}
$$

In bi-level optimization, the decision of both levels influences each other [40]. This is intuitively clear for the follower since he makes his choice based on the first move taken by the leader. Typically, the leader also has information about how the follower will behave with respect to his choice. This is noted in (8.1) with $(x,y) \in \mathbf{gph}\Psi(x)$ which can be seen as the coupling between the second level and the first level. This will quickly be explained here by following the notation and descriptions proposed by [37]. Considering first the feasible set mapping stated in (8.2). Generates a set of y that all fulfill the second-level constraints for a given decision x of the leader. The lower-level solution set mapping is written in (8.3). The function returns a set of all y that minimize $f(x,y)$.

$$Y(x) := \{y : g(x,y) \leq 0\} \tag{8.2}$$

$$\Psi(x) := \{y \in Y(x) \cap T : f(x,y) \leq \varphi(x)\} \tag{8.3}$$

The graph (gph) that includes all tuples from y to a certain x is written in (8.4).

$$\mathbf{gph}\Psi := \{(x,y) \in \mathbb{R}^n \times \mathbb{R}^m : y \in \Psi(x)\} \tag{8.4}$$

The problem becomes more challenging when the $\Psi(x)$ does not provide a unique solution. This can lead to multiple different values of F(x,y).

This ambiguity is often solved with an optimistic or pessimistic approach. In the optimistic case, it is assumed that the follower cooperates with the leader and returns only the y that is optimal for the leader's goal. In the pessimistic approach, the leader can no longer assume that the follower will cooperate. Consequently, it is assumed that the follower returns the worst possible y for the leader[40].

Publications

Paper I

Experimental Characterization of Methods for Connecting Real-Time Simulations and Synchrophasors

Daniel Baltensperger, Kjetil Uhlen
Department of Electric Power Engineering
Norwegian University of Science and Technology
Trondheim, Norway
daniel.s.baltensperger@ntnu.no

Santiago Sanchez-Acevedo, Salvatore D'Arco
Department of Energy Systems
SINTEF Energy Research
Trondheim, Norway
santiago.sanchez@sintef.no

2021 IEEE Madrid PowerTech | 978-1-6654-3597-0/21/$31.00 ©2021 IEEE | DOI: 10.1109/PowerTech46648.2021.9494884

***Abstract*—Wide area monitoring, protection and control systems will likely be implemented in future transmission control rooms and will be essential to ensure the correct operation of the power systems. These solutions will heavily rely on the application of Phasor Measurement Units and synchrophasors. Thus, it is critical that any algorithm implementation is extensively tested in advance covering any possible operative scenario. Hardware in the Loop testing can be a very effective approach to test algorithm implementations in a realistic but virtual and fully controllable environment. This implies the necessity of combining synchrophasors, and PMU hardware with real-time simulations. This paper examines three alternative approaches for combining synchrophasors with a real-time simulation platform. Furthermore, an experimental setup where these approaches have been implemented and tested is described.**

***Index Terms*—Wide area monitoring, power systems control and protection, synchrophasors, PMU, Hardware in the Loop.**

I. Introduction

The electric power system is a critical infrastructure with a high relevance for the present society. Transmission system operators (TSO) have to tackle the challenging task of operating the system more efficiently while considering technical, economical and geographical restrictions [1]. However, a first trend is the increased levels of generation from renewable sources as wind and solar whose power production is less controllable than hydro and thermal power plants. This is accompanied with a reduction of system inertia and will lead to more difficulties in balancing the power demand and in the frequency regulation. Moreover, the increasing demand of electric energy will also push the power systems to operate closer to their limits. These effects combined are expected to increases the likelihood of instabilities and to render more complicated the operation of future power systems [2]. Thus, TSOs will need to rely on better control and protection systems in next generation control rooms.

Due to the technical developments in communication technology and measurement synchronization, phasor measurement units (PMUs) are becoming more affordable and widespread in the power systems. A PMU estimates amplitude, phase, frequency and rate of change of frequency from measured analog voltages and currents. Each of these estimated phasors is time stamped to a highly precise primary source of time and is referred as synchrophasor. Moreover, the update frequency from PMU measurements is around 2 orders of magnitude higher than in SCADA-EMS monitoring. The higher update frequency and a wide geographical coverage with synchronized measurements allow to obtain an accurate view of the power system and its dynamics via the synchrophasors. The maturity of PMU technologies has been essential to enable the development of concepts related to wide area monitoring, protection and control systems (WAMPACS). The WAMPACS rely on real-time PMU data streams to identify the status of the system and implement preventive or corrective actions. These approaches can provide advanced features that would not be feasible with solutions based on SCADA-EMS.

The application of synchrophasors for power systems has been a very active field for research and development and the technical literature offers a wide range of examples of algorithms for monitoring and protection. These algorithms could allow to operate the power system closer to its limits and, thus, increase the transfer capacity without reduction of security. Furthermore, they can be used for early recognition of instabilities or for optimal load shedding schemes [3]. However, due to the extreme reliability requirements for power systems, it is crucial to be able to extensively test any algorithm implementation before the deployment in a real system. In this context, Hardware in the Loop (HiL) testing approaches can be very valuable to replicate operative conditions for WAMPACS and for PMU hardware and test these in a realistic and highly controllable virtual laboratory environment. HiL integrates the control or monitoring hardware with a real-time emulation of the coupled physical system. This is of

This work was supported by the project SynchroPhasor based Automatic Real-time Control (SPARC), funded by the ENERGIX Program of the Research Council of Norway, under Project 280967, and the industry partners, Statnett, Fingrid, Energinet, Svenska Kraftnät, Landsnet and GE.

978-1-6654-3597-0/21/$31.00 ©2021 IEEE

great benefit since it also allows testing many conditions that could be rare or not feasible in a real power system. In a perspective of WAMPACS the HiL requires the integration of synchrophasors with a real-time simulator. Thus, it is relevant to identify the possibilities for HiL implementation and to characterize their benefits and limitations.

A first method of integrating a large number of PMUs into a HiL setup is with the use of synthetic PMUs generated in the real-time simulator itself. The challenge in this approach is to guarantee that the PMUs behave as real PMUs in terms of measurements characteristics and concerning the communication. [12] presented how the design and deployment of a c37.118 compliant p-class PMU can be included in to the OPAL-RT eMEGAsim real-time simulator. This was done by using a e-IpMSDFT synchrophasor estimation algorithm. The relevance for real-time HiL platforms used for proof-of-concept is emphasized in [10], where a real-time state estimation application based on synchrophasor technology was presented and assessed. For state estimation this concept is of special relevance because the true system state in the real field is typically unknown. In [11] three different use cases of PMUs and WAMPACS test applications in HIL with a real-time simulator are summarized. The first application is a test suite for PMU compliance. It allows to automate the compliance tests defined in the C37.118 tests in HYPERSIM. The second application allows to asses a wide area damping controller and to compare it with a commercial PSS. The third application is for testing cyber-security regarding a time synchronization spoofing attack on synchrophasor based WAMPACS applications. In [13] a laboratory setup for WAMPACS as well as different applications developed within a research project are presented. The laboratory setup includes a real-time simulator with possibility to amplify analog signals as well as a the opportunity to use sampled values according to the IEC 61850 protocol. Furthermore, different IEDs with PMU functionality are included. In [15] the Norwegian National Smart Grid Laboratory (NSGL) was presented together with two WAMS applications. The first application is an algorithm which allows to assess voltage stability and the second application can be used for online detection of power oscillations.

This paper has the objective to present and assess three alternative possibilities to combine synchrophasors with a real-time simulation environment in order to perform HiL testing of WAMPACS implementations. Furthermore, the paper provides an example of an experimental setup where these alternative solutions have been implemented and tested. Finally, these three alternative approaches are characterized in order to identify their relative performance and to highlight their advantages and limitations.

II. Synchrophasor fundamentals

The objective of this section is to provide an overview about fundamental components in the application of synchrophasors in power systems that will be necessary for the experimental characterization presented in this paper.

A. Phasor measurement unit (PMU)

A typical PMU architecture consists of a timing module, a DAQ module, a Synchrophasor estimation algorithm and a module for data streaming. The timing module provides time synchronization via different synchronization protocols (see II-D). The DAQ module consists of an anti-aliasing filter and an analog to digital converter module [7]. The objective of the estimation module is to estimate the magnitude, phase, frequency and rate of change of frequency of the fundamental tone based on the given current and voltage signals. In the streaming module the measurements are streamed according to a certain standard (see.II-C) in the telecom network [16]. All phases of the estimated synchrophasors are relative to a trigonometric cosine function with nominal frequency synchronized to the Coordinated Universal time.

B. Phasor data concentrator (PDC)

A PDC can be seen as a node point in the communication network, where synchrophasor data from different PMUs or other PDCs are processed and streamed to the next PDC or application [14]. The most relevant objective for a PDC in the perspective of this paper is to sort the incoming synchrophasors according to their time stamp and filter out data with a notable delay [8]. The functionality is implemented with a buffer and a specific time out. The time out is the time the PDC waits for synchrophasors with a certain time stamp. If the buffer is full or the time set has elapsed the PDC will forward the data [8]. Consequently, the less timeout the faster the PDC will forward the data. On the other hand a small timeout leads to a higher probability of packet loss [8].

C. Standards and communication protocols

In 1995 the first standard for transmission of synchrophasors in real-time was developed under the name IEEE 1344. The basic concepts of synchrophasors its measurement and communication was introduced [6]. In 2005 the first C37.118 standard was introduced, which addressed tests and accuracy requirements for steady state conditions. In 2011 the standard was split in two parts. The first part (IEEE 37.118.1) considers performance requirements for steady state and dynamic conditions the second part (IEEE 37.118.2) includes the the communication regulations for synchrophasor transmission. The C37.242-2013 is another standard about synchrophasor technologies. It includes the testing and calibration procedure for synchrophasor hardware [9].
Another concept introduced by the IEC 61850 standard is the so-called distributed PMU. The core idea is to distribute the individual functions defined in section II-A in different devices in the substation. Typically merging units synchronised with a precise time protocol (PTP) digitize the voltage and current signal after the transducers and timestamp these samples. The sampled values are sent to an IED with PMU functionality [7].

D. Time synchronization and clocks

Clocks for electronic devices are based on crystal oscillators that ticks at a nominal frequency. Every crystal is slightly

different and varies over time and temperature. To guarantee a common time stamp it is important to synchronize the different PMUs to the UTC time. A time error of $1\mu s$ for example leads to a phase error of 0.022 degrees in a 60 Hz system and 0.018 degrees in a 50 Hz system. According to the IEEE Std. C37.118.1 the TVR has to be below 1%. For 1% TVE the maximum phase deviation is 0.573° if no error in the magnitude is assumed [5]. This leads to a maximum tolerable time error of $\pm 31.8\mu s$ for a 50 Hz system ($\Delta\varphi_{max}/(2\pi f_0)$).

III. Approaches for integrating synchrophasors in real-time simulations

In this paper three different approaches for including PMUs in a real-time platform are considered and illustrated as different paths in Fig. 1. The three approaches use a phasor data concentrator (PDC) that can stream the phasors of the PMUs to multiple destinations inside and possibly outside the communication network of the NSGL. Hence, it is possible to use external controllers integrated with the WAMPACS solutions running in this setup.

A. Synthetic Synchrophasor approach

The aim of this method is to stream phasor signals from the real-time simulator to a PDC using first the C37.118 server service in the real-time simulator. Hence, the PDC can gather and stream back all the phasors to the same real-time simulator that using at the same time the C37.118 client service. This path can be conveniently applied to inject a massive number of PMUs and phasors in the network. Therefore, a large power system can be simulated in real-time and WAMPAC strategies can be validated. A disadvantage is that there are no considerable time delays regarding the phasor estimation algorithm except if the estimation algorithm is included in the real-time simulator as for example presented in [12], but then the computational complexity increases.

B. Sampled values and Physical IED approach

In this approach the real-time simulator has a merging unit functionality and publishes SVs with time stamps, which are finally sent to an IED. The IED computes the synchrophasors and send them via PDC back to the real-time simulator. This approach is also known as HiL test. The advantage is that it is possible to validate the WAMPAC methods with real devices based on the use of digital measurements i.e. IEC 61850-9-2 SVs. A drawback is that the platform price increases with the number of devices. Besides, the approach has limitation of PMUs as a function of the capabilities of the IEDs connected.

C. Power-Hardware-In-The-Loop approach

In this approach the three phase analog sinusoidal voltage and current signals are generated, amplified and finally measured with a real PMU. The phase voltages and currents are obtained with the Park transforms of the magnitude and phase angle of the positive sequence phasor obtained from the real-time simulator. The estimated synchrophasors are sent via PDC back to the real-time simulator. An advantage is that this is a very realistic path, since it contains a large number of effects that are recorded in a real application. It is possible to observe phase shifts because of instrumentation voltage transformers, and delays regarding network communication, synchrophasor estimation algorithm and PDC functionality. There are multiple drawbacks within this solution. First, the equipment used in this path is more expensive. Second, the amount of different output signals is limited by the setup itself. Furthermore connections can be complex and lead to errors and it can be more dangerous to operate since physical quantities are measured. Moreover, this approach can introduce unwanted delays due to the phasor to analog conversion.

IV. Laboratory Setup

This section provides a description of the laboratory setup at the NSGL in Trondheim for testing WAMPACS implementations and applications of Synchrophasors. The NSGL is designed to conduct experimental activities on power system components as IEDs, power electronics converters and electrical machines. A real-time simulation platform allows hardware in the loop (HiL) experiments on IEDs with support of industrial communication protocols. Testing with the power-HiL (PHiL) approach is also feasible due to a controlled power amplifier (200 kVA from Egston Power and 5 kHz frequency bandwith). An overview of the laboratory setup used for synchrophasor assessment is illustrated in Fig. 2. The following list describes the components applied in the setup for implementing and characterizing the three approaches for combining Synchrophasors and PMU hardware in real-time simulations.

a) Real-time simulator: The OPAL-RT includes an internal OREGANO hardware board for IRIG-B synchronization. The platform supports industrial communication protocols C37.118 client and server, and IEC 61850 sampled values (SVs). Furthermore, the OPAL-RT provides optic fiber ports for fast control of external devices. OPAL-RT has a dynamic phasor simulator tool called ePHASORSIM that can be used to simulate dynamic power systems and compute the phasors. This tool can be integrated in all the approaches mentioned above.

b) System clocks: The grandmaster clock is a SEL 2488 clock with IRIG-B output and network synchronization based on PTP for the client devices in the communication network. A second clock is a SEL 2407 Satellite-Synchronized Clock with IRIG-B synchronization output ports used with the OPAL-RT.

c) PDC software: A SEL-5073 PDC software installed in a Host-Computer.

d) Phasor measurement units: The system counts with three IED/MU/PMUs. A Siemens MU 6MU85 with PMU function and able to synchronize with IRIG-B or PTP. A IED Siemens 7SJ85, capable of PMU functionalities and SVs subscriptions. This IED is able to synchronize with IRIG-B or PTP. Finally, a SEL 401 merging unit (MU) capable of PMU functionalities and able to synchronize with IRIG-B or PTP.

e) Software: The systems has a host computer with wireshark. The system uses configuration software for the PMUs.

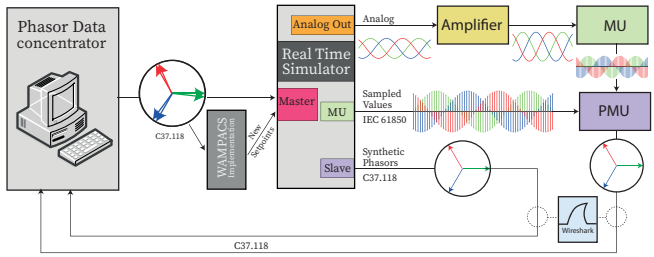

Fig. 1. Test platform with three phasor validation paths.

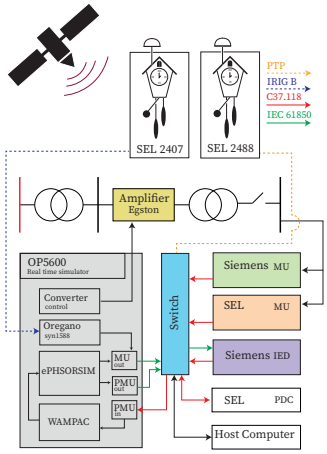

Fig. 2. Schematic illustration of the test platform.

f) Power amplifier: A 200 kVA controlled power amplifier with 5 kHz bandwith acting as a grid emulator.

g) Signal conditioning: The voltage is measured with three Noratel instrumentation voltage transformers Y-Y connected. These transformers have an accuracy class of 0,2%, with a transformer ratio of 400/110.

A. Configuration of the setup for real-time and HiL

The setup for real-time simulation is composed of the OPAL-RT which can be used with the C37.118 client and server protocols. Hence, it is possible to stream PMU's phasor to a PDC with the slave protocol and obtain them back into the OPAL-RT with the client protocol. This is the basic starting test to validate synchrophasor applications (experimental results will be presented in the next section). Once the real-time simulation has been verified the next step is to analyze the HiL experimental setup integrating the IED with PMU function.

B. Configuration of the setup for Power Hardware in the Loop

In the power-hardware-in-the-loop path, a SEL-401 MU with PMU functionality is installed and synchronized with PTP. The measurement is analog for the three phase sinusoidal voltages after the power amplifier. The PMU data is

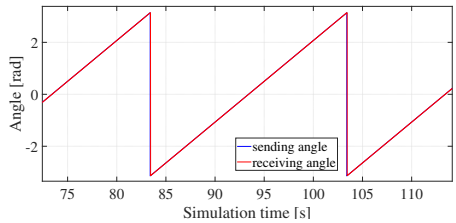

Fig. 3. Real-time simulation for single phasor with constant magnitude and variable angle.

concentrated in the PDC computer and sent it to the OPAL-RT. For all following experiments only voltage measurements were considered. Instrumentation voltage transformers were used. The transformers are connected to the merging units with floating neutral. This because in the laboratory environment symmetrical conditions are assumed. Hence, this installation follows the manufactured recommendations.

V. Experimental Results

This section shows the relevant experimental results obtained for the three approaches presented above.

A. Real-time simulation

In a first step a real-time simulation was performed. A phasor was transmitted with constant magnitude and constantly rotating angle. The rotating phasor was sent from the OPAL-RT via PDC back to the OPAL-RT. Figure 4 illustrates the experiment. The blue phasor leaves the simulator while the red phasor was received in OPAL-RT.

The network communication and PDC delay is estimated by comparing the current time with the time stamp of the received phasor (see Fig. 5). Another method to calculate the delay assumes a constant off-nominal frequency of 0.05 Hz i.e. angle variation slope and calculates the delay based on Fig. 4. The resulting delay is varying between 0.5 and 1.7 milliseconds. Which is visualized in a histogram in Fig. 6.

B. Hardware-in-the-loop

In this section a Siemens IED was included in the loop. It creates sychrophasors based on sampled values published

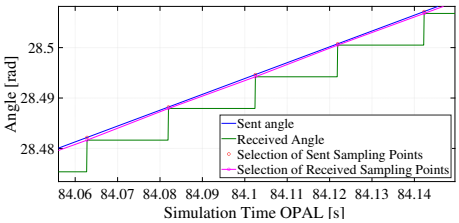

Fig. 4. Zoomed sent and received angles. The signals time shift represent the time delay.

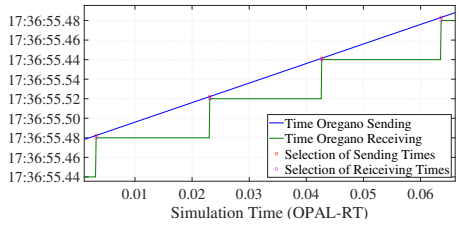

Fig. 5. Time stamp vs Simulation Time.

by the OPAL-RT. This section addresses the relevance to time quality (RTQ) of the phasor packet deliver to the PDC. The RTQ is part of the C37.118.2 and is defined as the maximum time error at all times [14]. As hexadecimal number 0 stands for normal operation and F (15 in decimal) for the worst case (Fault-clock failure, time not reliable) [14]. In this example a constant sinusoidal signal with nominal frequency and constant phase angle is sent to the IED as sampled values. The problem of a loop in the communication network is analyzed. The loop creates repeated layer-2 packets that will produce wrong calculations in the IEDs. Therefore, PTP, SVs packets and phasor calculations will be affected. Note that both PTP and SV use the local area network. Figure 7 shows the coherence between time quality and calculated phase angle in the IED. Figure 7 bottom shows the time quality translated for the given packets and Fig. 7 top curve presents the angle read for the same phasor packets. The signals were extracted with Wireshark software between the Siemens IED's PMU and the

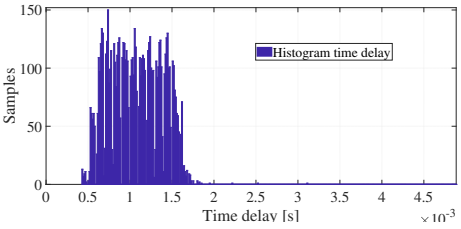

Fig. 6. Histogram for the calculated delay between sending and received angles in the OPAL-RT.

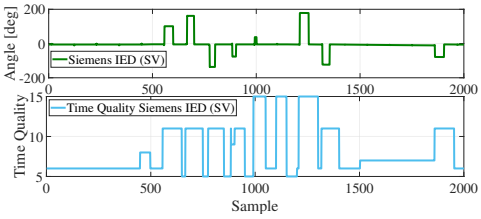

Fig. 7. Influence of time quality to phase angle.

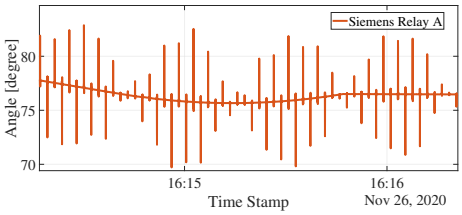

Fig. 8. Phase angle of Siemens IED PMU.

PDC as illustrated in Fig. 2.

The voltage phase plotted over the time can be seen in figure 8. It is illustrated that this particular loop led to a kind of spikes in the phase measurement.

C. Power-Hardware-in-the-loop

The PHiL part includes all three introduced approaches. Figure 9 shows the different angles plotted over time. The synthetic phasor defined in the OPAL-RT is drawn in blue. The synthetic PMU has voltage phase 0 degrees and it is streamed with this fixed value. The green line visualizes the angle for the PHiL voltage measured at the secondary side of the instrumentation transformer. This device is synchronized with PTP. The red line illustrates the phase angle of a synchrophasor which is calculated with the IED subscribed to SVs published with the OPAL-RT. The loop in the communication network discussed in the previous section is removed and the measurement spikes are consequently vanished.

Finally, Fig. 10 shows a test case with PHiL in which the tool ePHASORSIM has been used to generate the reference

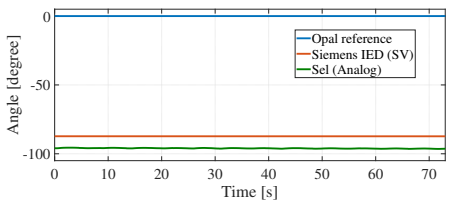

Fig. 9. Constant angle phasors for PHiL experiment. Reference phase angle (blue), IED phase angle (green) and phasor angle of the PMU measuring physical voltage (red).

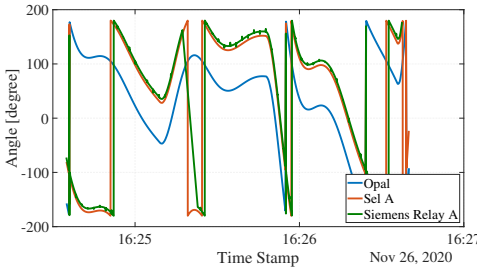

Fig. 10. Nordic 44 phase angle at a selected bus

phasor in the OPAL-RT. A dynamic power system model of the Nordic 44 power system was simulated. A phasor reference was generated using the voltage of a selected bus in the model. In the simulation, the step changes of a load excite the dynamics of the dynamic power system. Hence, the phase angles at the buses of the power system vary respect the slack bus. Figure 10 presents the variation of the angle at the selected bus.

VI. Conclusions

This paper presented three approaches for integrating synchrophasors or PMU hardware with a real time simulation platform. The objective is to be able to create a platform for validating implementations of wide area monitoring protection and control systems (WAMPACS) with a Hardware in the Loop (HiL) methodology. The first approach is based on a direct streaming of synthetic synchrophasors from the real-time simulator. This requires minimum additional hardware and is very scalable. Indeed, the limitations on the number of synchrophasors is mainly associated to the license restrictions and to the capacity of the communication connections. However, this suffers from a lowest degree of fidelity since no PMU hardware is included and effects such as delays should be added artificially. In a second approach the real time simulator behaves as a virtual merging unit and streams sampled values to a device acting as a PMU. This configuration ensures a higher degree of realism because the synchrophasors are generated by an actual PMU device and effects associated to delay can correctly captured. The scalability is also rather sufficient since the limitation is in the number of PMUs and in the number of synchrophasors that can handle. In the third approach the real time simulator generates references for an analog amplifier that reproduce the quantities as real voltage and currents. This can ensure the highest level of realism but could be limiting to a very few synchrophasors and involve also more costly and complex to operate hardware. In general, the three approaches should not be intended as mutual exclusive but could be also partly combined together. An example of the implementation of these three approaches on a laboratory platform has been provided in the paper with a first characterization. The experimental results indicate that all investigated solutions are feasible and that a sampled value approach is a good alternative to a power-hardware in the loop or synthetic PMU solution.

References

[1] A. B. Leirbukt, J. O. Gjerde, P. Korba, K. Uhlen, L. K. Vormedal and L. Warland, "Wide Area Monitoring Experiences in Norway," 2006 IEEE PES Power Systems Conference and Exposition, Atlanta, GA, 2006, pp. 353-360, doi: 10.1109/PSCE.2006.296331.

[2] M. Larsson, P. Korba, M. Zima, Implementationand applications of wide-area monitoring systems, in:2007 IEEE Power Engineering Society General Meet-ing, 2007, pp. 1–6.

[3] M. Zima, M. Larsson, P. Korba, C. Rehtanz, G. Andersson, Design aspects for wide-area monitoring and control systems, Proceedings of the IEEE 93 (5)(2005) 980–996.

[4] Ieee standard for synchrophasor measurements for power systems, IEEE Std C37.118.1-2011 (Revisionof IEEE Std C37.118-2005) (2011) 1–61.

[5] R. S. Singh, H. Hooshyar and L. Vanfretti, "Assessment of time synchronization requirements for Phasor Measurement Units," 2015 IEEE Eindhoven PowerTech, Eindhoven, 2015, pp. 1-6, doi: 10.1109/PTC.2015.7232728.

[6] K. E. Martin, "Synchrophasor Standards Development - IEEE C37.118 & IEC 61850," 2011 44th Hawaii International Conference on System Sciences, Kauai, HI, USA, 2011, pp. 1-8, doi: 10.1109/HICSS.2011.393.

[7] A. Monti, C. Muscas, and F. Ponci, "Phasor measurement units and wide area monitoring systems". San Diego, CA: Academic Press, 2016.

[8] Zhu, K., Chenine, M., Nordström, L., Holmström, S., & Ericsson, G. (2013). An Empirical Study of Synchrophasor Communication Delay in a Utility TCP/IP Network, International Journal of Emerging Electric Power Systems, 14(4), 341-350. doi: https://doi.org/10.1515/ijeeps-2013-0062

[9] S. Li, L. Zhang, J. Paquin, J. Bélanger and L. Vanfretti, "Hardware-in-the-Loop Use Cases for Synchrophasor Applications," 2019 International Conference on Smart Grid Synchronized Measurements and Analytics (SGSMA), College Station, TX, USA, 2019, pp. 1-8, doi: 10.1109/SGSMA.2019.8784526.

[10] M.Paolone, M.Pignati, P.Romano, S.Sarri, L.Zanni, R.Cherkaoui, "A hardware-in-the-loop test platform for the real-time state estimation of active distribution networks using phasor measurement units', Proc. of the 2013 Cigré SC6 Colloquium, Cigré-Conseil International des Grands Réseaux Électriques, Oct. 2013, Yokohama, Japan.

[11] S. Li, L. Zhang, J. Paquin, J. Bélanger and L. Vanfretti, "Hardware-in-the-Loop Use Cases for Synchrophasor Applications," 2019 International Conference on Smart Grid Synchronized Measurements and Analytics (SGSMA), College Station, TX, USA, 2019, pp. 1-8, doi: 10.1109/SGSMA.2019.8784526.

[12] P. Romano, M. Pignati and M. Paolone, "Integration of an IEEE Std. C37.118 compliant PMU into a real-time simulator," 2015 IEEE Eindhoven PowerTech, Eindhoven, 2015, pp. 1-6, doi: 10.1109/PTC.2015.7232794.

[13] M. S. Almas, M. Baudette, L. Vanfretti, S. Løvlund and J. O. Gjerde, "Synchrophasor network, laboratory and software applications developed in the STRONg2rid project," 2014 IEEE PES General Meeting Conference & Exposition, National Harbor, MD, 2014, pp. 1-5, doi: 10.1109/PESGM.2014.6938835

[14] "IEEE Standard for Synchrophasor Data Transfer for Power Systems," in IEEE Std C37.118.2-2011 (Revision of IEEE Std C37.118-2005) , vol., no., pp.1-53, 28 Dec. 2011, doi: 10.1109/IEEESTD.2011.6111222.

[15] T. D. Duong, S. D'Arco and J. O. Tande, "Architecture and laboratory implementation of a testing platform for Wide Area Monitoring Systems," IECON 2019 - 45th Annual Conference of the IEEE Industrial Electronics Society, Lisbon, Portugal, 2019, pp. 6419-6424.

[16] M. Hoefling et al., "Integration of IEEE C37.118 and publish/subscribe communication," 2015 IEEE International Conference on Communications (ICC), London, 2015, pp. 764-769, doi: 10.1109/ICC.2015.7248414.

Paper II

2022 IEEE PES Innovative Smart Grid Technologies Conference Europe (ISGT-Europe) | 978-1-6654-8032-1/22/$31.00 ©2022 IEEE | DOI: 10.1109/ISGT-Europe54678.2022.9960423

Optimal Coordination of Multiple System Protection Schemes against Critical Overload Conditions

Daniel Baltensperger[1], Kjetil Uhlen
Department of Electric Power Engineering
Norwegian University of Science and Technology
Trondheim, Norway
[1]daniel.s.baltensperger@ntnu.no

***Abstract*—System protection schemes (SPS) are increasingly used as a means to raise transmission capacity as well as improve power system security and thereby postpone costly grid investments. Event-based SPS are typically rule-based and tailored for a specific problem. This makes it increasingly difficult to operate the installed schemes so that they do not negatively influence each other. This paper shows a centrally operated (i.e wide-area protection) event-based SPS that considers multiple grid constraints. The procedure coordinates existing remedial action schemes and converter-based sources like wind power plants. The simulation method is explained in detail and the protection procedure is illustrated with an example of a line trip. The method can be beneficial for using the grid more efficiently (with smaller reserves) and a higher amount of non-dispatchable sources.**

***Index Terms*—System Protection Schemes, Remedial Action Schemes, Wide-Area Protection**

I. Introduction

A scenario named "Clima Neutral Nordics" was created by the Nordic TSOs and shows one of multiple potential future development paths. It assumes an increase of electrical energy from 400 TWh per year up to 655 TWh by 2040. Additionally, it is assumed that renewable generation (i.e. Wind, Hydro, Photovoltaic) is more than doubled from 85 GW to 189 GW. As a result, there is a need for grid reinforcement, which leads to significant investments to increase the grid capacities in several corridors [1].

SPS can help to increase the reliability of supply as well as raise transmission capacity and the trading capacity [2]. Consequently, such protection schemes have the potential to postpone or even reduce the amount of costly grid reinforcement [3]. These positive characteristics can also be seen in the increasing trend of operating system protection schemes.

In this paper the term SPS and Remedial Action Schemes (RAS) are used according to the CIGRE definition :"A System Protection Scheme or Remedial Action Scheme is designed to detect abnormal system conditions and take predetermined, corrective action (other than the isolation of faulted elements) to preserve system integrity and provide acceptable system performance [4]". Examples of control action are: Generator rejection, HVDC fast power change, controlled opening of interconnections, load shedding etc. [4]

From a technical point of view, critical corridors can be operated more effectively (i.e., closer to the system limit and its components) with an SPS by relaxing the N-1 criteria in a controlled manner to a so-called $N - 1/2$ secure state. This corresponds to an operation that achieves an N-1 safe state through arming an SPS [3]. The literature distinguishes between response-based SPS with feedback behavior (e.g., conventional under-frequency load shedding) and so-called event-based SPS (feed-forward) where the control action is pre-calculated before a specific contingency appears. These event-based SPS are typically faster, and they are designed in offline studies by the grid-planing personnel [5].

In Norway, the conventional SPS design is typically rule-based and most often tailored for a specific event that would lead to a voltage limit violation or overload situation. However, the term overload in this context includes not only thermal overload but also the exceeding of stability limits. SPS are often manually armed in the first step by the transmission system operator and, in the second step, automatically triggered if the appropriate contingency appears.

Optimal Power Flow (OPF) can be used to tackle the challenges mentioned above with event-based SPSs. Literature [6] for example, propose a static online approach that uses a Thevenin equivalent method for a fast contingency screening as well as the determination of aperiodic angle instability limits. The optimal control actions (i.e., load shedding and rescheduling generator active power and voltage set-points) are pre-calculated in an OPF. A convexified OPF connected to a PMU-based state-estimator was published in [7]. The optimizer pre-calculates the under-frequency load shedding remedial action for a known future contingency (event-based) subject to all nodal voltages and line currents are within limits. Additionally, a predicted discretized frequency trajectory (based on a second-order dynamic model) is considered in the OPF as a physical constraint.

Trajectory sensitivity theory is a known technique used in dynamic security assessment. The theory allows estimating based on a full RMS simulation how a reference case trajectory

This work was supported by the project SynchroPhasor based Automatic Real-time Control (SPARC), funded by the ENERGIX Program of the Research Council of Norway, under Project 280967, and the industry partners, Statnett, Fingrid, Energinet, Svenska Kraftnät, Landsnet and GE.

(dynamic states as well as algebraic variables) would change if one or multiple arbitrarily selectable parameters were to change. This property makes it a suitable tool for SPS. In [8] and [9] for example, a generator rescheduling techniques to avoid transient rotor-angle instabilities is proposed. The methods are included in a stability constrained OPF and consider the rotor angle trajectory sensitivity with respect to the generation active power output. The author of [10] and [11] introduced trajectory sensitivity theory for real-time emergency control with Model Predictive Control (MPC). A more protection-oriented version of MPC is proposed where a set of control actions are calculated and remain the same over the whole horizon. In [10] an example was presented where it was shown how the theory could improve the coordination between tap-changer, changing generator set-points and load-shedding. Another MPC formulation based on trajectory sensitivity for voltage control was proposed in [12] where a voltage stability margin was additionally considered to optimally switch shunt capacitors.

A. Objective of the paper

The above-described characteristics of today's SPS and the increasing trend force the TSOs to think about new, more automated, and sophisticated approaches to operating SPS. This is mainly to achieve better coordination between the different SPSs, the control, and the unit protection.

This paper describes an event-based automatic SPS approach that pre-calculates the appropriate remedial action for a known critical future contingency. It is based on centralized optimizer which finds optimal control action and consequently guaranties a cost-optimal and well coordinated behaviour. The paper follows the main idea proposed in [10] and [11] and shows how this can be used to coordinate the curtailment of renewable generation and other existing event-based SPSs. The method considers voltage, phase and thermal overloads as limitations in the optimization process.

II. Methodology

This section's objective is to introduce the theoretical concepts used in this paper quickly. First, the used dynamical and algebraic models are described, followed by a short introduction to the relevant aspects of trajectory sensitivity theory and how a QP formulation can be used to coordinate the different remedial actions optimally.

A. Algebraic model

In this subsection the algebraic model $G(x, y, \lambda)$ is introduced. $\mathcal{N}$ is in the following nomenclature a set including all buses, $\mathcal{L} \subset \mathcal{N}$ is a set of all load buses and $\mathcal{G} \subset \mathcal{N}$, $\mathcal{C} \subset \mathcal{N}$ represents set of generator buses and converter nodes (e.g where wind power plants) are connected. $\mathcal{T}$ is a set including all transmission lines which build a potential bottleneck, and Ω_i is a set including all nodes connected to bus i. y is a vector representing all considered algebraic variables and is defined in equation 1. Y is in the following the admittance matrix and Y_i^B is used to calculate the line current in branch number i.

$$y = [[P_e], [Q_e], [V], [\Delta\delta], [I_d], [I_{i,j}]] \tag{1}$$

The different algebraic equations used in following simulation process can consequently be written as:

$$\underline{S}_{Gen,i} = (P_{e,i} + \mathrm{j}Q_{e,i}) \quad \forall i \in \mathcal{G} \tag{2}$$

$$\underline{S}_{Gen,i} = (\Delta P_{w,i} + \mathrm{j}\Delta Q_{w,i}) \quad \forall i \in \mathcal{C} \tag{3}$$

$$\underline{S}_{Gen,i} = 0 \quad \forall i \in \mathcal{L} \tag{4}$$

$$\underline{S}_{Gen,i} - \underline{S}_{load,i} = \underline{V}_i \sum_{j \in \Omega_i} \underline{Y}^*_{i,j} \underline{V}^*_j \quad \forall i \in \mathcal{N} \tag{5}$$

$$I_{d,i} = -\frac{\mathrm{Im}(\underline{S}_{e,i})}{|\underline{E}'_{q,i}|} \quad \forall i \in \mathcal{G} \tag{6}$$

$$|I_i| = \left|\underline{Y}_i^B \underline{V}\right| \quad \forall i \in \mathcal{T} \tag{7}$$

Equation 2 to 4 define the injected electric power for generator buses, load buses and buses where a converter is connected. The initial set-point of the wind-power is modeled as a negative constant power load. $\Delta P_{w,i}$ and $\Delta Q_{w,i}$ is the change of the wind power output which is a state from the dynamical model. Equation 5 represents a conventional power flow problem. Equation 6 is used to calculate the d-axis component of the generator terminal current and equation 7 is used to verify the branch current in the different bottlenecks. At this point, it should be mentioned that the generator quantity Xd' is included in the admittance matrix, and the electrical power behind the generator impedance Xd' is calculated directly via a load flow calculation.

B. Dynamic model

This subsection describes the dynamical model $f(x, y, \lambda)$ in its state space representation 8 to 14 quickly. The synchronous generators are described by a third-order machine model as it is written in 8 to 10. The converters with its inputs $P_{c,i}^{set}$ and $Q_{c,i}^{set}$ are described in equation 13 and 14, automatic voltage regulator (AVR) and governors are modeled as a first order systems, the later two include additionally a proportional feed back control loop as described in 11 and 12.

$$\Delta\dot{\delta}_i = 2\pi 50 \left(\Delta\omega_i - \Delta\omega_4\right) \tag{8}$$

$$\Delta\dot{\omega}_i = (2H_i)^{-1} \left(P^0_{m,i} + \Delta P_{m,i} - P_{e,i} - D\Delta\omega_i\right) \tag{9}$$

$$\dot{E}'_q = (T'_{d0,i})^{-1} \left(E^0_{f,i} + \Delta E_{f,i} - E'_q + I_d \left(X_d - X'_d\right)\right) \tag{10}$$

$$\Delta\dot{P}_{m,i} = -(T_{s,i})^{-1} \left(\Delta P_{m,i} + K_g \Delta\omega\right) \tag{11}$$

$$\Delta\dot{E}_{f,i} = -(T_{e,i})^{-1} \left(\Delta E_{f,i} + K_e \left(E'_{q,i} - E^{ref}_{q,i}\right)\right) \tag{12}$$

$$\Delta\dot{P}_{w,i} = -(T_{w,i})^{-1} \left(\Delta P_{w,i} - \Delta P^{set}_{c,i}\right) \tag{13}$$

$$\Delta\dot{Q}_{w,i} = -(T_{w,i})^{-1} \left(\Delta Q_{w,i} - \Delta Q^{set}_{c,i}\right) \tag{14}$$

Equation 8 to 12 is done for all generators in $\mathcal{G}$ and 13 and 14 describes the dynamics of the different converters in $\mathcal{C}$.

C. Trajectory Sensitivity

This section summarizes the used linearization technique. The objective is to provide the reader with the essential concept. More detailed and in-depth explanations can be found in [13] and [14]. The non-linear dynamic behavior of a power system can be described by a differential-algebraic discrete (DAD) model. A particular simplification that is used in this paper is the formulation of the system as a model consisting of a set of non-linear algebraic as well as differential equations (DAE). However, in both cases, the trajectory sensitivity can provide valuable information about the behavior of the dynamic states x and the algebraic states y for small changes in an arbitrary system parameter λ (e.g. load, line impedance, etc.). Under these assumptions, the system model can be formulated as:

$$\dot{x} = f(x, y, \lambda) \tag{15}$$

$$0 = G(x, y, \lambda) \tag{16}$$

Where $x \in \mathbb{R}^p$, $y \in \mathbb{R}^q$ and $\lambda \in \mathbb{R}^m$ a vector including all parameters under consideration. The trajectory sensitivities for a parameter change are defined as:

$$w_1 := \frac{\partial x}{\partial \lambda} \in \mathbb{R}^{p \times m}, \quad w_2 := \frac{\partial y}{\partial \lambda} \in \mathbb{R}^{q \times m} \tag{17}$$

$$\tag{18}$$

By applying chain rule follows from (15) and (16) directly:

$$\dot{w_1} = \frac{\partial f}{\partial x} w_1 + \frac{\partial f}{\partial y} w_2 + \frac{\partial f}{\partial \lambda} \tag{19}$$

$$0 = \frac{\partial G}{\partial x} w_1 + \frac{\partial G}{\partial y} w_2 + \frac{\partial G}{\partial \lambda} \tag{20}$$

When knowing a reference base case, let us say a specific contingency, the trajectory sensitivities can be computed with an additional marginal expansion in parallel to the RMS simulation. This because w_1 are just a set of $(p \times m)$ additional ordinary linear differential equations (ODEs) and w_2 is an additional set of $(q \times m)$ linear equations which can be computed easily. How the sensitivities are calculated in parallel to the base case simulation will be explained in more detail in section II-D. However, when w_1, w_2 and the reference case state $(\bar{x}, \bar{y})$ for each time step $t \in T$ are known, the trajectories for a small parameter change $\Delta\lambda = \lambda - \lambda_0$ can be approximated by: $x \approx w_1 \Delta\lambda + \bar{x}$ and $y \approx w_2 \Delta\lambda + \bar{y}$

D. Simulation procedure

In this section, the simulation procedure implemented in Python is quickly introduced. Figure 1 is a graphical representation of the procedure. In the first step, a typical power flow is solved to initialize the dynamic state vector x and the vector with all algebraic variables y. After initialization, the algebraic equations are solved in each time step. These equations provide a renewed y vector and the sensitivity matrix w_2, which includes sensitivities regarding the algebraic variables. The input for these algebraic equations is a subset of the dynamic state vector x as well as the trajectory sensitivity matrix w_1. The differential equations consider the newly

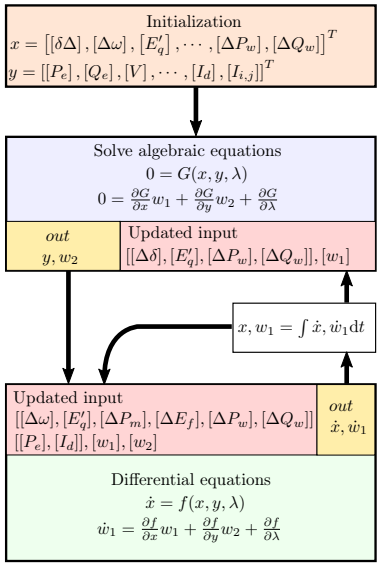

Fig. 1. Graphical illustration of the simulation procedure

calculated y vector as well as a subset of the dynamic state vector x and both trajectory sensitivity matrices w_1 and w_2. This set of first-order differential equations is integrated for the next time stamp and again used as an input for the algebraic equations and the differential equations for the next time step. It should be mentioned again that the two trajectory sensitivities matrices w_1 and w_2 are calculated in parallel to the simulation. Consequently, the Jacobian matrices are recalculated in each step.

E. Formulation of the optimization problem

The objective is to find the cost-optimal load shedding at bus j and the optimal reference set-point change (curtailment) in the converter at bus k. The costs for the different control actions are defined in the diagonal matrix K. The various control actions (delta variables) which are subject to be optimized are included in the vector written in equation 21. All physical limitations (except line currents) are considered dynamically over the whole prediction horizon of T. Since for thermal overloads, most often only the steady-state current is of interest, just the last time step in the prediction horizon is taken into account for these quantities. All constraints are described linearly since they rely on the sensitivity and the base case.The optimization considers a discretized, equidistant sampled time horizon from t_0 to t_{end}. T is a set including all time steps (i.e. n time steps from t_0 to t_{end}). It is important to notice that the control variables are set constant from the beginning until the end of the horizon this follows the approach described in [10]. The dynamic state and the algebraic variables, on the other hand, are included in the

optimization over the whole horizon such that they describe the future trajectories of the system.

Equation 22 cover the described optimisation problem

$$\Delta\lambda = [\Delta P_{L,j}, \Delta Q_{L,j}, \Delta P^{set}_{c,k}, \Delta Q^{set}_{c,k}]^T. \tag{21}$$

$$\begin{aligned}
\min \quad & \Delta\lambda^T K \Delta\lambda \\
\text{s.t.} \quad & \Delta\omega_t = w^{\omega}_{1,t}\Delta\lambda + \Delta\bar{\omega}_t \\
& U_t = w^{U}_{2,t}\Delta\lambda + \bar{U}_t \\
& \Delta\delta_t = w^{\delta}_{2,t}\Delta\lambda + \Delta\bar{\delta}_t \\
& I_{i,j} = w^{I}_{2,t}\Delta\lambda + \bar{I}_{i,j,t} \\
& \Delta\omega_{min} \leq \Delta\omega_t \leq \Delta\omega_{max} \\
& \Delta\delta^{min}_{i,j} \leq \Delta\delta_i - \Delta\delta_j \leq \Delta\delta^{max}_{i,j} \\
& I_{min} \leq I_{i,j,t} \leq I_{max} \\
& U_{min} \leq U_t \leq U_{max} \\
& \Delta Q_{L,j} = \Delta P_{L,j} \tan(\alpha)
\end{aligned} \tag{22}$$

III. Results

In this section first the base case scenario from which the reference trajectories can be established is introduced. Afterward, the solution of the optimizer is shown.

A. Base case scenario

The example scenario is implemented in the Kundur-two area model [15]. The set-points of the generators are adjusted such that 335.14 MW of active power flows from bus 7 to 9.

The contingency under investigation is a trip of one of the parallel lines in the corridor between bus 8 and 9. This leads to local oscillations between the generators at bus 3 and 4 and inter-area oscillations between the single machine in the left area against the two machines in the area on the right side. These oscillations result in phase angel differences which may exceeds a pre-determines security margin of 45 degrees. Figure 2 shows these electro-mechanical oscillations.

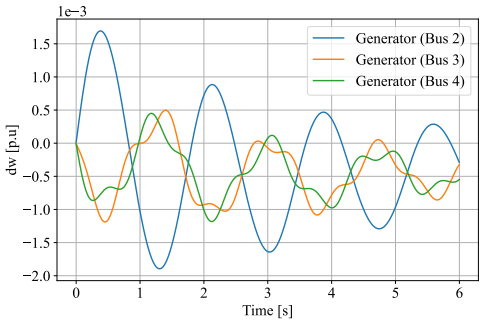

Fig. 2. Electro-mechanical oscillations

The transient behaviour of the voltage magnitude can be seen in figure 3. While all thermal limits are met, the voltage falls twice well below the pre-determined voltage limit of 0.9 p.u.

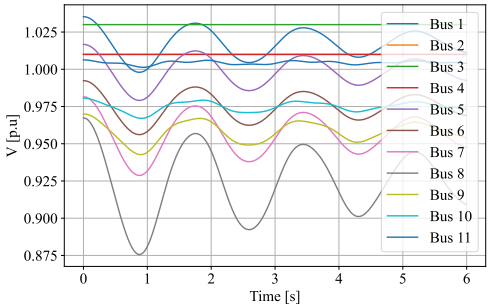

Fig. 3. Transient voltage behaviour

B. Optimal control action

This section discusses the results of the optimisation problem that determines the optimal control action for the above introduced critical contingency. The protection systems to be coordinated are a wind turbine on bus number 1 whose power can be curtailed and a load on bus 9 that can be shed with respect to a constant cos phi (see figure 4)

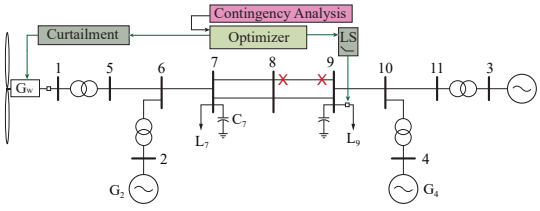

Fig. 4. Schematic representation of the protection scheme

In this example, it is assumed that both protection systems are equally expensive. However, it should be noted that this can be freely determined and, for example, market-related values can be used. Table I shows the assumed costs and the determined optimal control action.

TABLE I
(No) control action considering all physical constraints. (RV) control action for the voltage relaxed scenario (see figure 6)

	$\Delta P_{L,9}$	$\Delta Q_{L,9}$	ΔP^{set}_{w}	ΔQ^{set}_{w}
cost	0.1	0	0.1	0.1
Action (No) [p.u]	-1.204e-2	-0.903e-2	-1.609e-2	0.447e-2
Action (RV) [p.u]	-0.379e-2	-0.284e-2	-0.561e-2	0.078e-2

Figure 5 shows the critical trajectories for the small example network. The upper figure shows the voltage angle difference between bus 7 and 9. This is considered here as a stability criterion. Note that rotor angles could also be considered directly without major modifications, as it was proposed for example in [9]. In blue, the voltage angle difference without applied remedial action (i.e base case) is plotted. The angle difference

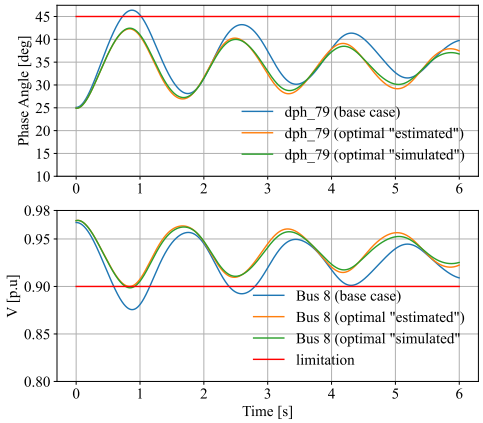

Fig. 5. Critical trajectories (without remedial action, with remedial action "estimated" and "simulated")

clearly exceeds the predefined limit (red). The orange curve thus shows the optimiser's estimated solution. It represents the approximated curve based on trajectory sensitivities. The green curve shows the optimal trajectory, which was simulated again with changed parameter values. It is therefore considered here as the true simulated curve. Since the amount of control action is minimised via the cost function, one would expect the optimiser to select the control variables in such a way that the maximum voltage angle difference is exactly 45 degrees. This is not the case and is due to the fact that in this situation the voltage could not be kept in the limit. Figure 6 shows an example of what the scenario would look like if the voltage constraints would be relaxed. The numeric values of the control action for the voltage relaxed example is noted in the last row of table I. The critical voltage magnitude at node 8 is plotted in the figure 5 below. The legend is the same as in the figure 5 above. It can be seen now that the optimiser chooses the control variables so that the estimated trajectory exactly touches but does not exceed the minimum voltage limit. This means that both critical points can be met.

IV. Conclusion and Outlook

The paper shows a centrally operated (i.e., wide-area protection) event-based SPS that considers multiple grid constraints. Compared to the traditional rule-based approach is, the presented method more adaptive and guarantees a cost-optimal control action. It follows the the main idea that is presented in [10] and is used here to coordinate converter-based energy sources and load-shedding optimally. Additionally, the simulation procedure is explained detailed, and a scenario where a line trip in a critical corridor is analyzed and discussed. The results show that the estimated trajectories used in the optimization just marginally deviate from the true simulated trajectories. In a future work, the focus will be on

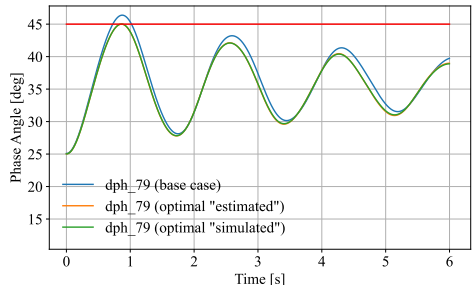

Fig. 6. Phase difference with relaxed voltage constraints

improving the calculation speed and making the Python code more flexible for different grid models.

References

[1] Statnett, "Nordic grid development perspective 2021," 2022. [Online]. Available: https://www.statnett.no/globalassets/for-aktorer-i-kraftsystemet/planer-og-analyser/nordic-grid-development-perspective-2021.pdf

[2] Rannveig Løken, Frode Trengereid, Johan Inderberg Vestrum, "Op039 use of system protection in statnett," https://cimug.ucaiug.org/CIMGroups/ENTSO-E_IOP/2016/Shared%20Documents/paperIOP/OP039%20Statnett%20SIPS.pdf, 2016.

[3] E. Hillberg, F. Trengereid, Ø. Breidablik, K. Uhlen, G. Kjølle, S. Løvlund, and J. Gjerde, "Systemintegrity protection schemes—increasing operational security and systemcapacity," in *In Proceedings of the 44th CIGRE Session, Paris, France*, 2012.

[4] Cigre, *SYSTEM PROTECTION SCHEMES IN POWER NETWORKS*. Task Force: 38.02.19, Technical Brochure: 187, 2001.

[5] J. Rasmussen, *System Protection Schemes in Eastern Denmark*. Technical University of Denmark, Department of Electrical Engineering, 2006.

[6] A. S. Pedersen, M. Blanke, J. G. Møller, and H. Jóhannsson, "On-line generation and arming of system protection schemes," in *2016 Electric Power Quality and Supply Reliability (PQ)*. IEEE, 2016, pp. 277–282.

[7] Q. Walger, Y. Zuo, A. Derviškadić, G. Frigo, and M. Paolone, "Opf-based under frequency load shedding predicting the dynamic frequency trajectory," *Electric Power Systems Research*, vol. 189, p. 106748, 2020.

[8] L. Tang and J. D. McCalley, "An efficient transient stability constrained optimal power flow using trajectory sensitivity," in *2012 North American Power Symposium (NAPS)*, 2012, pp. 1–6.

[9] T. Nguyen and M. Pai, "Dynamic security-constrained rescheduling of power systems using trajectory sensitivities," *IEEE Transactions on Power Systems*, vol. 18, no. 2, pp. 848–854, 2003.

[10] M. Zima and G. Andersson, "Stability assessment and emergency control method using trajectory sensitivities," in *2003 IEEE Bologna Power Tech Conference Proceedings,*, vol. 2, 2003, pp. 7 pp. Vol.2–.

[11] ——, "Model predictive control employing trajectory sensitivities for power systems applications," in *Proceedings of the 44th IEEE Conference on Decision and Control*. IEEE, 2005, pp. 4452–4456.

[12] L. Jin, R. Kumar, and N. Elia, "Model predictive control-based real-time power system protection schemes," *IEEE Transactions on Power Systems*, vol. 25, no. 2, pp. 988–998, 2010.

[13] I. Hiskens and M. Pai, "Trajectory sensitivity analysis of hybrid systems," *IEEE Transactions on Circuits and Systems I: Fundamental Theory and Applications*, vol. 47, no. 2, pp. 204–220, 2000.

[14] M. Laufenberg and M. Pai, "A new approach to dynamic security assessment using trajectory sensitivities," in *Proceedings of the 20th International Conference on Power Industry Computer Applications*, 1997, pp. 272–277.

[15] P. Kundur and N. Balu, *Power System Stability and Control*, ser. EPRI power system engineering series. McGraw-Hill, 1994.

Paper III

Assessing Hardware in the Loop Approaches for Wide-Area Monitoring Control and Protection Devices

Daniel Baltensperger, Santiago Sanchez, Salvatore D'Arco, and Kjetil Uhlen, *Member, IEEE*

***Abstract*—Wide-area monitoring, protection, and control (WAMPAC) systems are expected to support the transmission system operators in maintaining stability and security of supply in the future power systems. The WAMPAC solutions heavily rely on deployment and use of phasor measurement units (PMU) and related communication technologies. Laboratory testing in a realistic environment utilizing hardware in the loop (HIL) approaches can be successfully used to evaluate WAMPAC functionalities algorithms and to accelerate proofs of concept. However, different implementations of the HIL testing can be adopted and their inherent characteristics affect both the accuracy of the results and the overall testing capabilities. The objective of this article is to provide a comparative assessment of three HIL approaches for laboratory testing of WAMPAC systems and devices. These testing approaches have been implemented in a laboratory configuration and applied to characterize WAMPAC devices. Moreover, methodologies to quantify the error introduced by these testing approaches in static and dynamic conditions are presented and applied to this laboratory configuration.**

***Index Terms*—Synchrophasor, PMUs, wide area control and protection, real-time simulation.**

I. Introduction

THE electric power system is highly important for today's modern society and belongs consequently to the so-called critical infrastructure. The increasing amount of renewable energy sources, liberalization of the market, and a generally increasing demand introduce new challenges to be tackled by the transmission system operators (TSOs) [1]. TSOs are committed to operate their system more efficiently (e.g. increase transfer capacity) such that geographical, economic and technical requirements still can be fulfilled [2].

In modern interconnected systems, an emergency can be spread quickly in the whole area. Centralized well-coordinated protection and control strategies such as these provided by wide-area monitoring, protection, and control (WAMPAC) systems have the potential to arm or even automatically trigger the optimal control action in critical situations. These strategies heavily rely on modern communication and sensing technology. Typically, GPS synchronized phasor measurement units (PMUs) are considered for generating a wide-area snapshot of the instantaneous current and voltage phasors as well as of the system frequency and rate of change of frequency (ROCOF). These devices are becoming increasingly affordable and are considered extremely accurate [3]. Due to its fast update (e.g., 50 samples per second), this technology can also provide valuable insights on the transient behavior (e.g., electro-mechanical oscillations).

The extreme reliability requirements for control and protection in power transmission systems necessitate an extensive testing phase before deployment in the field. HIL testing can be seen as a step between the off-line simulation, planning process, and final application of new schemes, as well as it can be used for proof of concept. A HIL testing configuration consists of a digital real-time simulator (RTS) as well as hardware components such as controllers (e.g., automatic voltage regulator, intelligent electronic devices (IEDs)), actuators and amplifiers. Moreover, this testing approach can be essential for testing rare events that cannot be easily produced or experienced in the real field application.

HIL testing approaches are rather well established for testing protection relays because realistic conditions can be reproduced by simulating in real time a power system model, thus, providing information about the closed loop behavior [4]. Moreover, it is easy to change the conditions by varying fault location, duration and type or the parameters of the power system. For example, [5] shows, beside a stand-alone test, a HIL test case for an overcurrent protection relay. More recently HIL testing approaches have been also extended to WAMPAC devices and systems. An example is pointed out in [6] where the authors generated up to 2000 different scenarios for testing system protection schemes between Colombia and Ecuador. Another HIL test setup for WAMPAC is described in [7] and [8]. In the latter, the authors

Manuscript received 3 May 2022; revised 31 August 2022 and 5 December 2022; accepted 19 February 2023. Date of publication 10 March 2023; date of current version 25 July 2023. This work was supported by SynchroPhasor based Automatic Real-time Control (SPARC) project, funded by the ENERGIX Program of the Research Council of Norway, under Grant 280967, and in part by the industry partners, Statnett, Fingrid, Energinet, Svenska Kraftnät, Landsnet and GE. Paper no. TPWRD-00645-2022. *(Corresponding author: Daniel Baltensperger.)*

Daniel Baltensperger and Kjetil Uhlen are with the Department of Electrical Engineering, Norwegian University of Science, Technology, 7013 Trondheim, Norway (e-mail: daniel.s.baltensperger@ntnu.no; kjetil.uhlen@ntnu.no).

Santiago Sanchez and Salvatore D'Arco are with the Department of Energy Systems, Sintef Energy Research, 7034 Trondheim, Norway (e-mail: santiago.sanchez@sintef.no; salvatore.darco@sintef.no).

Color versions of one or more figures in this article are available at https://doi.org/10.1109/TPWRD.2023.3255414.

Digital Object Identifier 10.1109/TPWRD.2023.3255414

presents a testbed that includes two commercial IEDs in the loop, which acts as over-current relays to protect two lines in a real-time simulated model. The platform is used for evaluating cyber-attacks which is a vital topic also considered by [9].

One challenge of WAMPAC systems is their complexity, and consequently, there are many potential sources of failure. [10] shows a new approach for reliability analysis of WAMPAC systems and describes that the sources of failures can be divided into four groups (measurement input, wide area communication, actuator, and analytic execution) and each of these subdivided again (e.g. measurement instruments, PMU, local communication). To evaluate and demonstrate this structure, HIL can be used. [11] divides the evaluation process into three steps (type-testing, application-testing, and end-to-end testing) and the authors show the dependency of length and type of windowing function to an end application such as fault location determination.

The influence of an amplifier in the loop and the effect of different reporting rates to the simulator are described in [12]. The importance of time delays is considered in [13], where two distribution functions are established with an empirical approach that describes time delays for unprocessed PMU data and sorted PMU data. Delays appearing in a real-time state estimation setup are considered in [14] where the authors use the possibility to time-stamp the data at different places in the real-time WAMPAC setup in order to assess the total time delay and how much time each individual process took. Time synchronization is critical in the phasor estimation process since time uncertainty leads directly to a phase angle error. The work in [15] describes the influence of a loss of time synchronization to three different WAMPAC applications (i.e. phase angle monitoring, anti-islanding [16] and power oscillation damper). In [7] a procedure for evaluating a PMU and PDC setup is presented. An RTDS simulator is used to perform static and dynamic tests with an external PMU as well as synthetic PMUs generated in the RTDS. A SEL-451 device acts as a PMU and an Omicron CMS-156 is used as an amplifier. A SEL-2407 is used for IRIG-B time synchronization.

All these referred publications assume synthetic synchrophasors generated by the RTS itself, by hard-wired connected devices or by a combination of both. With the increasing availability of the IEC 61850 standard, a third new digital approach for PMU integration in the RTS setup can be considered where IEDs subscribe sampled values (SV) to estimate synchrophasors. Typical errors introduced in a conventional hard-wired real-time setup can originate from measurement transformers, analog to digital conversion, filtering, noise, scaling factors, and other delays. The errors in sampled values based synchrophasors are expected to be smaller since not all of the listed error sources are present. According to the author's knowledge, [17] is the first publication that includes IEC 61850 sampled values in a real-time setup together with synchrophasors for the performance evaluation of three commercial PMUs. The first PMU is a conventional hard-wired device, the second PMU subscribes sampled values, and the third PMU is able to process both types of inputs in parallel. Dynamic and steady-state tests are conducted assuming a synthetic synchrophasor generated in the RTS as a reference. In such a configuration, the main difficulty is still distinguishing where the errors appear (signal generation, phasor estimation algorithm, communication, and synchronization).

A. Contribution and Objective of the Paper

The objective of this article is to provide a comparative assessment of three HIL approaches for WAMPAC testing including synthetic synchrophasors, IEDs subscribing sample values and hard-wired IEDs extending the work presented in [18]. This article contributes to the state of the art with the following new topics:

- To highlight the relative advantages and drawbacks of approaches for integrating WAMPAC devices and PMU measurements in a real-time HIL setup for testing WAMPAC applications. This includes the relatively less covered configuration where IEDs subscribe to sample values produced by the RTS according to the IEC 61850 standard.
- To provide an example of a complete implementation in a laboratory environment including IEDs providing PMU functionalities and MUs for conversion of analog signals into synchrophasors. All devices connected (i.e. RTS, high precision signal generator (ReTeSe), IEDs, and MUs) are time-synchronized to a grandmaster GPS clock via IEEE 1588 precision time protocol (PTP) with power profile or with IRIG-B.
- To describe inaccuracies that can appear when using these HIL testing approaches and to show a sequence of tests that can be applied to characterize and quantify the inaccuracies introduced. This includes both tests in steady state and dynamic conditions. The high precision signal generator can generate sampled values as well as analog outputs allowing to determine whether the source of error is from the measurement setup or from the RTS and the amplifier in the loop.
- To illustrate the differences when using the synchrophasors with their UTC timestamp or with the simulation time provided by the RTS.

The paper is structured as follows: in Section II the basics about synchrophasor technology, attached functionalities, as well as a metric for evaluating the accuracy are introduced. Section III explains the different options of how PMUs can be used in a HIL testing setup based on an example from the Norwegian National Smart Grid Laboratory (NSGL). The main part IV provides information regarding the methodology for characterizing the HIL approaches and the results from the tests conducted. The final Section VI summarizes the paper and emphasizes the relevant outcomes from IV.

II. PMU Accuracy Metrics

A setup including synchrophasor technology typically consists of one or more PMUs, a Phasor Data Concentrator (PDC) and a clock. The PMU estimates phase, magnitude, frequency and ROCOF of given input samples measured over a certain window. A time-stamp and consequently a clock is needed in each PMU to be able to compare different synchrophasors measured

at different locations. These clocks are time synchronized to a primary source of time which can be, for example, a GPS signal. To disseminate the time in a covered building, precision time protocol (PTP) or IRIG-B can be used. The PDC finally sorts the incoming synchrophasors according to their time-stamp and filter out data with a notable delay [13]. The IEEE standard C37.118 [19] defines three different metrics to evaluate the accuracy of a PMU. The first is the total vector error (TVE) merging the inaccuracy of phase and amplitude in one quantity, see (1). The Frequency error (FE) shown in (2) describes the deviation between the true and the estimated frequencies. The ROCOF measurement error (RFE) in (3) defines the deviation between the true ROCOF and the estimated value. In (1) $\hat{X}$ refers to the sequence of estimates and X is the sequence of reference values (in this article the inputs of the RTS or ReTeSe). The subscripts r and i stand for real and imaginary part of the phasor.

$$TVE = \sqrt{\frac{\left(\hat{X}_r - X_r\right)^2 + \left(\hat{X}_i - X_i\right)^2}{\left(X_r\right)^2 + \left(X_i\right)^2}} \tag{1}$$

$$FE = \left\| f_{true} - f_{measured} \right\| \tag{2}$$

$$RFE = \left\| \left(\frac{\mathrm{d}f}{\mathrm{d}t}\right)_{true} - \left(\frac{\mathrm{d}f}{\mathrm{d}t}\right)_{measured} \right\| \tag{3}$$

Depending on the application, merging phase and magnitude error in a single quantity as it is proposed for the TVE can be a disadvantage, since it is no longer possible to distinguish between them in the analysis phase. Therefore, in this article the TVE is presented together with the phase and magnitude error separately. We define the phase and magnitude error as following:

$$E_{ang} = \hat{\varphi}_{x,1} - \varphi_x \tag{4}$$

$$E_{mag} = \frac{|\hat{X}| - |X|}{|X|} \tag{5}$$

where φ indicates the phase of the considered quantity.

In this article only positive sequence components are considered despite negative and zero sequence can be critical to assess fault conditions in wide area systems. This is mainly because a positive sequence phasor model is executed in the real-time simulator and because the three wire system adopted in the laboratory setup does not allow the flow of zero-sequence currents. However, from a technical point of view, the considerations developed in the paper can be generalized to the case where negative and zero sequence are also included in the simulation model and in the physical circuit.

The delay in the PMU itself is strongly related to the windowing and filtering, which depends on the reporting rate (in this article 50 frames per second) and the used PMU class [20]. The standard [19] defines the so-called PMU reporting latency as: "the maximum time interval between the data report time as indicated by the data time stamp, and the time when the data becomes available at the PMU output (denoted by the first transition of the first bit of the output message at the communication interface point)". The PDC latency is the time

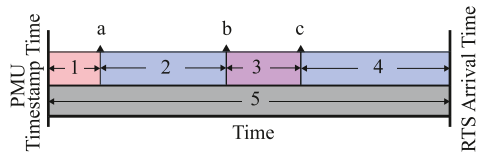

Fig. 1. The different latency in the WAMAPC setup (adjusted from [21]): 1: PMU reporting latency, 2: Network latency, 3: PDC latency, 4: Network latency, 5: Synchrophasor data latency, a: Message leave PMU, b: The first message arrives PDC, c: Message leaves PDC.

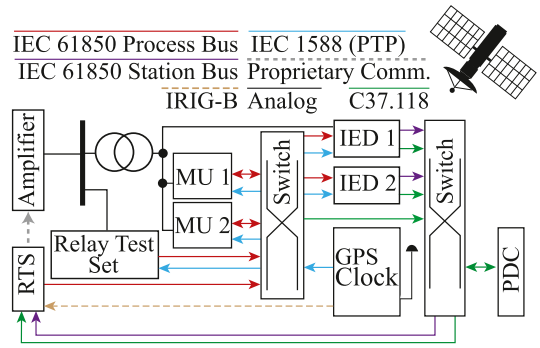

Fig. 2. IEC 61850 substation based hybrid test platform.

the first message enters the PDC, and the complete set of measurements is forwarded [21]. All delays between the PMU and PDC as well as the time between the different PDCs to each other are counted as network latency. The overall latency is the sum of all the mentioned latencies and is consequently called synchrophasor data latency [21]. The different delays are illustrated in Fig. 1. According to [20], it is important to evaluate each system case-by-case since actual values can be different. The overall time can have a large range between 20 ms up to 10 s or more [20].

III. Different Approaches of Integrating PMUs in a HIL Setup

In this article, a real-time setup is used that allows the integration of synchrophasor technologies with three different approaches. All PMUs are located in a common local area network (LAN) together with a PDC, ReTeSe and RTS as shown in Fig. 2. The PDC forwarded the different PMU streams to the RTS or, at a later stage, to an external controller where WAMPAC algorithms are implemented. The three different methods are briefly presented below, and the setup with all possible configurations is shown in Fig. 3.

A. Configuration With Synthetic Synchrophasors

In this configuration, the real-time simulator is used firstly to generate the phasors and secondly as a server for synchrophasors. The PDC acts as a client that sends the PMU stream back to the real-time simulator. This method is characterized by its simplicity and a large number of phasors in a WAMPAC scenario

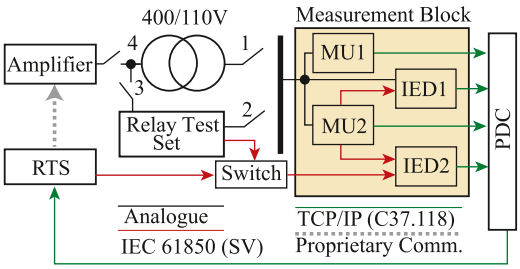

Fig. 3. Test setup with all configuration options for signal sources.

can be generated and processed without increasing investment costs. Since no hardware is in the loop when considering this approach, the question arises as to whether this method also realistically reflects the behavior of the PMUs. This configuration could be slightly more representative by including a phasor estimation algorithm as in [22] for example. In this article, the addition of a phasor estimation algorithm is not considered.

B. Configuration With Analog Signals and Power Amplifier

This approach can be considered the most realistic as it considers three-phase analog sinusoidal signals generated by the RTS to represent voltages and currents in the simulated model. These analog signals quantities are first amplified and then measured by either a hard-wired commercial IED or MU. Delays related to the TCP/IP network, PDC, or the estimation algorithms of the PMUs and uncertainties introduced by the transducers are evident in this approach. It is worth mentioning here that the VTs and CTs used in this laboratory setup can not be compared with those in a real-world high voltage substation since the laboratory is limited in the output analog voltages and currents. However, the real-world VTs and CTs can be modeled inside the RTS if necessary. A disadvantage is the limited number of analog outputs for the RTS, the more complicated wiring, the higher costs and constraints introduced by the presence of a power amplifier for each of the signals. Since the loop operates with higher voltages, safety is also an important issue to consider.

C. Configuration With IEC 61850 Sampled Values

IEDs can subscribe to sampled values by two different approaches. The connections are shown in Fig. 2 and Fig. 3.The first approach subscribes sampled values from RTS or ReTeSe which are both connected to the LAN. This approach does not introduce errors associated to the analog to digital conversion [17]. The second approach uses a commercial MU for digitizing the analog measured voltages and currents. The latter follows the same sequence as it can be seen in modern digital substations. In both approaches, the IED acts as a distributed PMU and estimates the quantities described in Section II based on SVs stream. These approaches can both be classified as hardware in the loop configurations since in both cases at least one hardware device is in the loop e.g. IED, MU or both. Since the RTS publishes sampled values (acting as a merging unit) and the IEDs subscribe to these data, this method can be seen as a cost-effective alternative to the amplifier in the loop scenario because it still allows validating WAMPAC solutions with real commercial devices. In this approach effects due to the estimation algorithm and processing time can be taken into account. However, a disadvantage is the limited amount of synchrophasors that can be generated per device.

D. Hybrid Loop: Sampled Values, Synthetic and Analog Measurements

This approach combines the three loops described above. A part of the physical quantities i.e. voltage and current of the real-time simulated power system will be streamed with synthetic synchrophasors, some ac signals can be streamed with sampled values directly to an IED under test and some nodes of the grid will use an amplifier in the loop approach. This application requires an understanding of the limitations for each separate test approach.

IV. Test Setup, Configuration and Assessment

The main objective of this section is to evaluate the behavior of the different approaches introduced in Section III and to gain insights regarding the inaccuracies introduced by the measurement devices, VTs, signal generator with its amplifier and any other additional laboratory equipment.

The assessment is done according to a three steps procedure by activating the switches shown in Fig. 3 while the measurement block remains the same. The first test is a steady state test where the reference values in the ReTeSe (i.e. magnitude and phase) are changed to understand the inaccuracies introduced by the different measurement devices under various operation points. In a second step, the ReTeSe is still used as a signal generator but a VT is included in the loop to experimentally observe its introduced uncertainties. The used instrument transformer is a class 0.2% device for measuring a nominal voltage of 400 V on the primary and 110 V on the secondary side. In the third step the ReTeSe is disconnected from the setup and the RTS is used with an external amplifier in the loop. This test allows to analyse the steady-state deviations introduced by the real-time simulator, the large amplifier, the surrounding equipment as well as the dynamic behavior of the setup. A reference for all various tests is defined to determine and evaluate the inaccuracies. Depending on the test scenario, the expected true reference value is either the set value of the ReTeSe or the synthetic synchrophasor generated in the RTS.

As explained above two different approaches for generating analog signals are used in this article. First, generate the signals in the ReTeSe and use the RTS just for collecting data, or second, use the RTS together with a large separate amplifier in the loop.

The used ReTeSe is an Omicron CMC 356 device able to generate up to 300 V phase to ground with a high degree of accuracy (i.e. Error $< 0.03\%$ reading + 0.01% range typical and Error $< 0.08\%$ reading + 0.02% range guaranteed) [23].

The RTS is an OPAL-RT 5600 with 12 cores (i686 operating at 3467 MHz). Additionally, a Xilinx Kintex 7 FPGA FPGA unit is embedded that allows propagating the clock signal to the processor's core. The internal clock is a Oregano hardware board

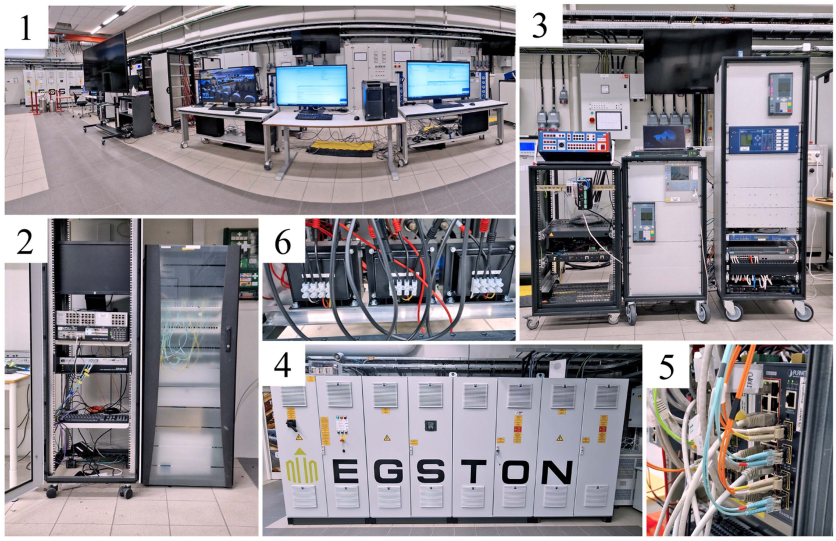

Fig. 4. Photography of the laboratory setup, (1) PDC and Host computers, (2) RTS: OPAL-RT, (3) ReTeSe Omicron, IEDs and MUs, SEL GPS and PTP clock, (4) Power amplifier EGSTON, (5) network communication switches Planet and (6) instrumentation transformers.

time synchronized with IRIG-B to the GPS clock. Analog signals generated by the RTS are amplified by a high-bandwidth (i.e. 15 kHz) power amplifier manufactured by Egston Power with a maximal output power of 200 kVA at 400 V [24]. The sinusoidal analog signals are automatically generated via an inverse Park transformation from a phasor quantity coming from the real-time simulation or set manually. The amplifier introduces a 5 μs for the communication link and its dynamic behavior can be approximated with a first-order low pass filter with a 15 kHz cut-off frequency [25].

For publishing sampled values both signal generators can be used. In the tests presented in this article one of the two ports of IED 2 was used to obtain sampled values from either RTS or ReTeSe. (depending on the scenario see also Fig. 3).

MUs and IEDs from three different manufacturer have been included and Fig. 4 shows the entire laboratory setup and all the used equipment. The additional equipment used in the laboratory setup consists of:

- a PDC with reference SEL5073.
- IED SIEMENS 7SJ85 and ABB RET670
- MU SIEMENS 6MU85IED and SEL 401
- instrumentation transformers from NORATEL
- industrial network communication switches Planet and ARUBA 3810M
- grandmaster clock SEL 2488.

The sampling rates for the different devices are as following. The MUs and IEDs sample the analog quantities at 16 and 8 kHz. Sample values are used with 4000 samples per second and 50 synchrophasors are generated per second according to the standard (C37.118). The simulation in RTS is performed with a step size of 50 microseconds.

In this article, all devices except one MU (SEL 401) run in M class mode according to standard C37.118-2011 [19]. The other

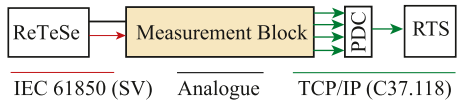

Fig. 5. Test configuration ReTeSe source without transformer.

device (SEL 401) uses a C37.118-2005 [26] standard which distinguishes between 0 and 1 and not M and P. However, a digital filter with a cutoff frequency of approximately 1/4 of the message rate (50 per second) is selected in this device. According to the manufacturer, [27], this results in a slower time domain response but it delivers synchrophasors that are free of aliasing signals. It should also be noted that the devices tested are not dedicated PMU devices but rather IEDs with integrated PMU functionalities. These devices generate C37.118 standardized synchrophasors with 50 frames per second and are functionally equivalent to dedicated PMUs with negligible differences for the scope of this article. More information about the implementation of PMU functionalities in IEC 61850 IEDs can be found in [28].

In the next subsections the different uncertainties will, be evaluated with the procedure stated at the beginning of this section.

A. Evaluation of Laboratory Setup Without Measurement Transformer (ReTeSe Source)

In this scenario, the ReTeSe acts as a signal generator, and the phasors generated by the different devices are evaluated without an instrument transformer. The basic configuration is illustrated in Fig. 5. The RTS acts in this case just for collecting measurement data. Which later can be used for evaluating the results.

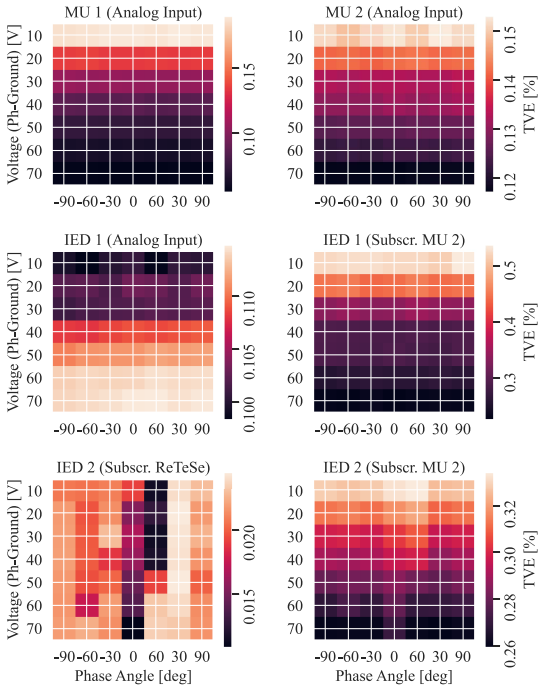

Fig. 6. TVE in per-cent for different magnitudes and phases.

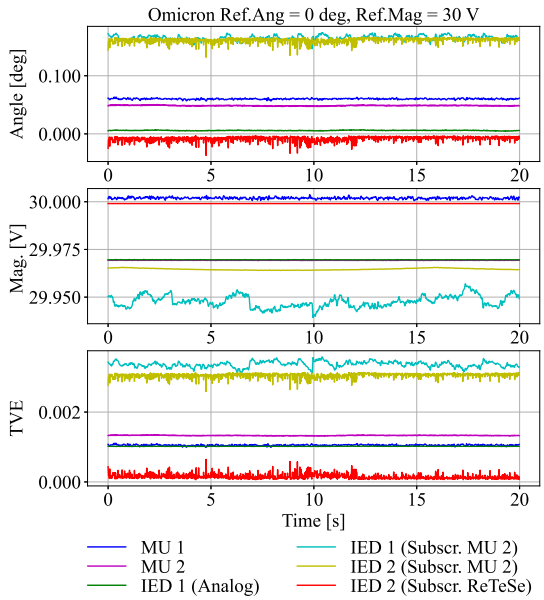

Fig. 7. Positive sequence magnitude, phase and TVE (without VT) for a selected operation point plotted over time.

TABLE I
EVALUATION OF PHASE DRIFT

Device	slope [deg/sec]	bias [deg]
MU 1	1.9618e-06	6.0138e-02
MU 2	-1.8760e-05	4.8857e-02
IED 1 (Analog)	-6.3202e-06	5.9415e-03
IED 1 (Subscribe to MU 2)	1.2584e-04	1.6381e-01
IED 2 (Subscribe to Realay Test Set)	1.8646e-04	-1.0369e-02
IED 2 (Subscribe to MU 2)	1.6315e-04	1.5939e-01

The objective of this procedure is to examining the inaccuracies introduced by the IEDs and MUs. Fig. 6 shows similarly as in [29] the mean total vector error in per-cent for each device in different operation points (phase and magnitude). MU1 and MU2 show a smaller TVE at higher voltages which indicates a relatively constant absolute error. Since IED 1 and IED 2 both subscribe to MU 2, similar behavior can be seen from them. IED 1 additionally estimates the phasors based on the analog input. For these measurements, the TVE accuracy behaves the opposite. The synchrophasors estimated in IED 2 based on sampled values subscribed directly from the signal generator present the smallest TVE. It can also be seen that there is neither a correlation regarding magnitude nor angle. The phase, magnitude and total vector error plotted over time is illustrated in Fig. 7. The best phase estimation is done by the IED which measures analog signals.

The instantaneous phase is defined according to the standard C37.118 [19] as the phase difference between a cosine function with zero-degree phase shift and nominal frequency aligned to the UTC. Consequently, it is assumed in the following that an inaccuracy in the synchronization leads to inaccuracy of the phase, i.e., drift. The drift of the measurements is analyzed in this article with the help of a linear regression method based on least square minimization. The method returns the two parameter bias and slope. The slope is assumed here as an indicator for the drift, since we consider data with a constant reference angle. Table I shows slope and bias parameters describing the linear approximation of the phase based on measurements illustrated in Fig. 7. From Table I it can be seen that the drift is relatively small, and it is assumed that the remaining deviation from zero is due to measurement errors that are not fully Gaussian distributed (see Fig. 10).

It was found in this experiment that for this real-time setup the phase or magnitude is partially better estimated individually by devices measuring the analog voltage. Finally, the TVE is always worse than the device that get sampled values directly from the ReTeSe.

B. Evaluation of Laboratory Setup With Measurement Transformer (ReTeSe Source)

In this section, the influence of the instrument transformer is evaluated. The simplified illustrated configuration can be seen in Fig. 8. To implement the scenario in the laboratory the switches 3 and 1 are closed (see Fig. 3).

Table II as well as Figs. 9 and 10 shows that this laboratory configuration adds an additional phase lead of around 0.1 °. Fig. 10 shows also the distribution and it can be seen that not all measurements are Gaussian distributed. It is important to mention that the ReTeSe was set around 80 V phase to ground

TABLE II
ERROR STATISTIC FOR SIGNALS GENERATED BY THE RELAY TEST SET

	MU 1	MU 2	IED 1 (Analog)	IED 1 (Subscr. MU 2)	IED 2 (Subscr. Realay Test Set)	IED 2 (Subscr. MU 2)
mean Ph. error [deg]	7.7282e-02	5.7308e-02	1.3466e-02	2.0987e-01	-1.1525e-02	1.6749e-01
mean Ph. error with VT [deg]	1.7510e-01	1.5576e-01	1.1364e-01	3.0027e-01	-1.1677e-02	2.6531e-01
std Ph. error [deg]	1.5520e-03	8.4485e-04	5.9884e-04	6.2853e-03	4.8168e-03	4.8384e-03
std Ph. error with VT [deg]	1.3752e-03	9.4590e-04	6.5997e-04	1.1586e-02	4.4716e-03	4.5006e-03
mean Mag. error [%]	-2.4645e-03	-1.0002e-01	-9.9467e-02	-2.5447e-01	-3.2391e-03	-1.1496e-01
mean Mag. error with VT [%]	2.5253e-02	-7.3333e-02	-7.4713e-02	-2.1471e-01	-3.1928e-03	-8.8493e-02
std Mag. error [%]	2.4706e-03	2.2452e-04	2.2610e-04	1.5736e-02	3.4615e-06	1.4818e-03
std Ph. error with VT [%]	2.1413e-03	2.5117e-04	2.3672e-04	1.5940e-02	2.9429e-06	1.4458e-03

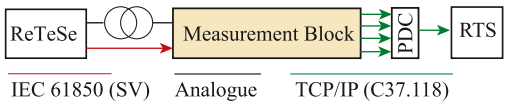

Fig. 8. Configuration ReTeSe with transformer.

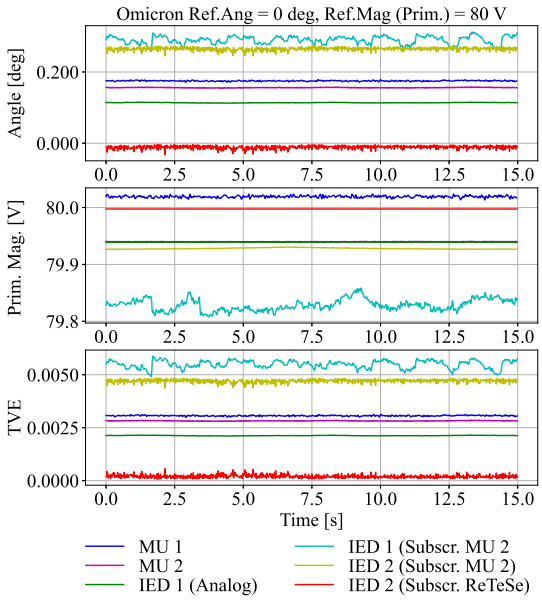

Fig. 9. Positive sequence magnitude, phase and TVE (with VT) for an selected operation point plotted over time.

(138.56 V phase to phase), which leads to an operation point far off from the nominal operating point of the VT. Consequently, the accuracy specification announced by the manufacturer cannot be expected.

A comparison of the accuracies with and without transformer can be seen in Table II.

C. Evaluation of Laboratory Setup With Measurement Transformer (RTS Source)

In this section, the amplifier in the loop scenario is considered. Compared to the other scenarios, dynamic tests can be realized too. The scenario can be adjusted by closing switches 1 and 4 while opening switches 2 and 3 in illustration 3. A simplified representation of the scenario is illustrated in Fig. 11. Note in this scenario the RTS is used as source and for data storage.

Fig. 12 shows the angle, magnitude, and TVE over time. It can be seen that all phases estimated based on analog inputs have an error around 3 degrees. IED 2, which subscribes with one channel sampled values directly from the RTS shows a much more precise phase. The magnitude error is between 0.02% and 0.15% for all measurements. Due to the significant phase error, the TVE is around 6% for all devices estimating phasors from the analog path (amplifier). Based on the knowledge gained from the tests discussed in IV-A and IV-B it can be concluded that these errors are introduced either by the RTS or the amplifier but not in the VT nor in the IEDs and MUs. Furthermore, the RTS publishes also sampled values and the phasors based on those signals are correct in precision for the given test. This explains the inaccuracies expected on relation to the amplifier for this laboratory setup. Note, the specific value of the angle presented is related to the amplifiers available in the presented laboratory and cannot be extended to all laboratories from a quantitative point of view.

Two different dynamic tests are applied in this article. The first test is a magnitude step change of the reference value from 90% to 100% of the nominal value in the RTS, which is 400 V phase to phase. The second test is a ramping voltage phase (i.e., an off-nominal frequency of 0.05 Hz). During this test, the voltage is kept constant at its nominal value. As described before, the voltage phase has an inaccuracy when doing static tests in this configuration. We assume this static deviation remains the same while the phase is ramped. This assumption consequently allows to compensate the error and thus to analyze, for example, delays related to the dynamic test separately.

The main objective is to identify the overall latency and to show the importance of considering the UTC time stamp in a WAMPAC test system. Note, the PDC in the loop receives all phasors from the different units and forwards each PMU stream with a separate identification number (ID) and internet protocol address (IP) to the RTS.

All data is captured with a sampling time of one millisecond and stored in the RTS. Beside the different receiving phasors from the various IEDs and MUs also a synthetic phasor, the reference signal and the simulation time of the RTS is captured. The synthetic phasor is directly generated in the RTS and was described in Section III-A. Figs. 13 and 14 show the phase and magnitude of both tests plotted versus the precise simulation

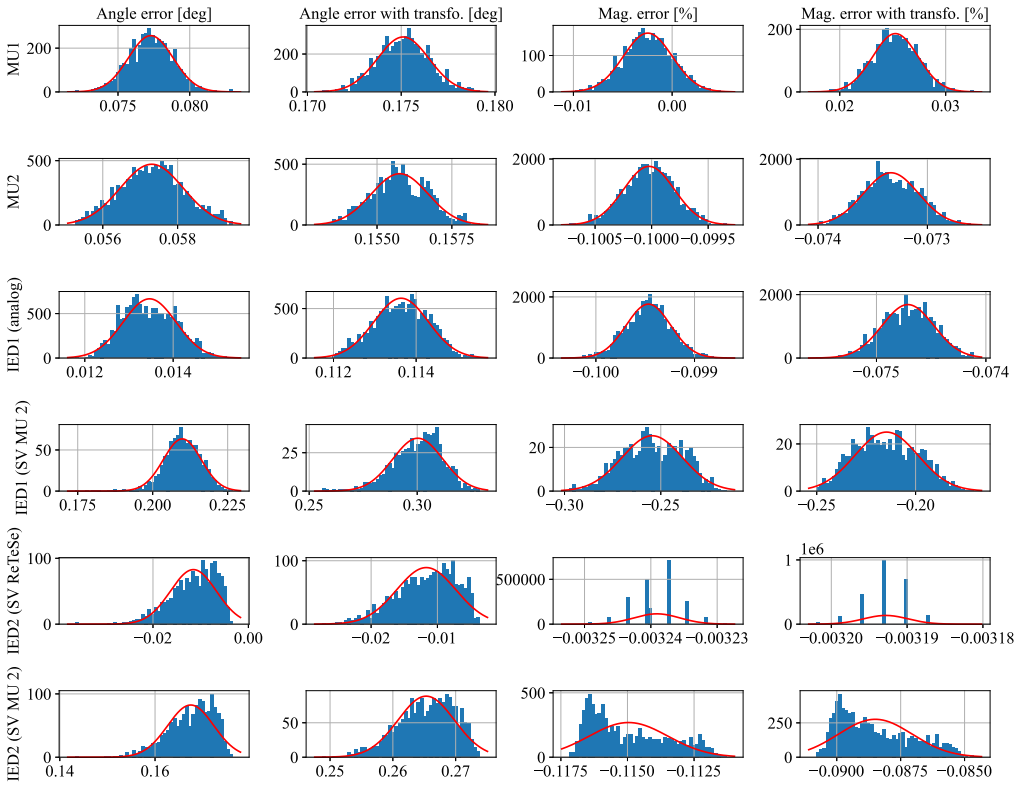

Fig. 10. Error distribution of all IEDs and MUs connected (signals generated by the relay test set).

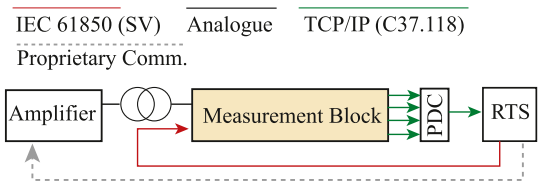

Fig. 11. Configuration of RTS as signal generator and data storage.

time, generated in the RTS self. In both tests, it is shown how the phasors arrive at different times. The overall latency can be seen by comparing the reference signals with the receiving phasors plotted over the simulation time.

Figs. 15 and 16 show the same measurement quantities but are now plotted over the phasors UTC time stamp. This follows the main synchrophasor concept, and indeed it can be seen that no significant delays do exist anymore. All devices except the synthetic phasor follow more or less the same dynamic behavior.

Today the coordinated universal time (UTC) time stamp is rather large number of seconds. For the sake of clarity the time axis of Figs. 15 and 16 is shifted with the UTC time stamp at the moment the experiment was done. Consequently, both plots start at time zero. The test with the different plotting approaches show clearly the relevance of considering the UTC time stamp when working with synchrophasors in a real-time setup. Otherwise, different delays could be experienced which could have a negative impact on the WAMPAC application.

It should be noted that the reference phasor is stored directly in the RTS and that the reporting rate of the reference PMU is higher than that of the received phasors. Hence, the receiving phasors have a lower resolution than the reference phasors for plotting them together.

V. Discussion

Directly subscribing IEC 61850 sampled values from a RTS is a promising variant of how devices generating synchrophasors can be integrated in a real-time setup. Real commercial IEDs or MUs can estimate phasors based on subscribed data without the need of analog signals. This can reduce costs since expensive hardwired equipment such as amplifiers and transformers are no longer needed for implementing a HIL with PMUs. The approach can also be easily scaled since the available output terminals in hardwired equipment can be a limiting factor. However, it should be considered that some devices may not

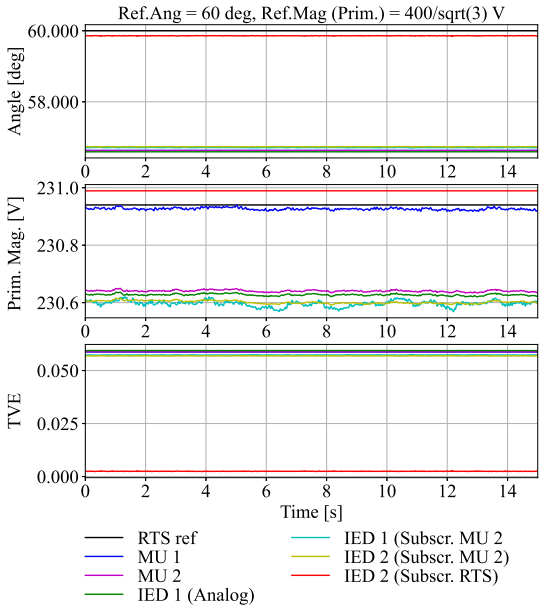

Fig. 12. Positive sequence magnitude, phase and TVE (with VT) for an selected operation point plotted over time (signals generated by RTS).

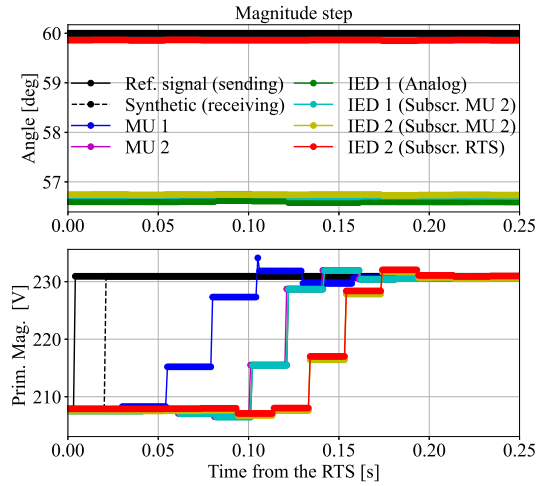

Fig. 13. Positive sequence magnitude and phase for a magnitude step change of 10%. Phase and magnitude versus the simulation time in the RTS.

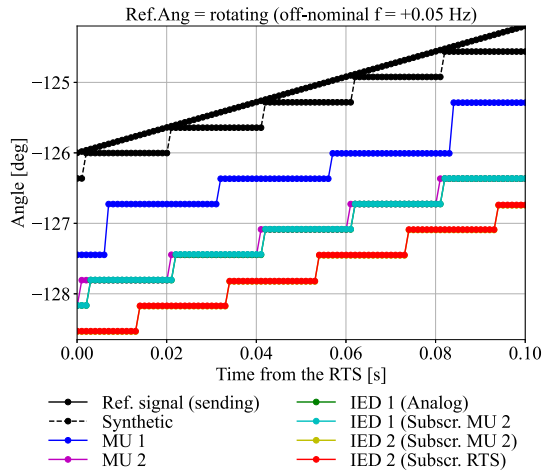

Fig. 14. Positive sequence off-nominal frequency plotted versus simulation time in the RTS.

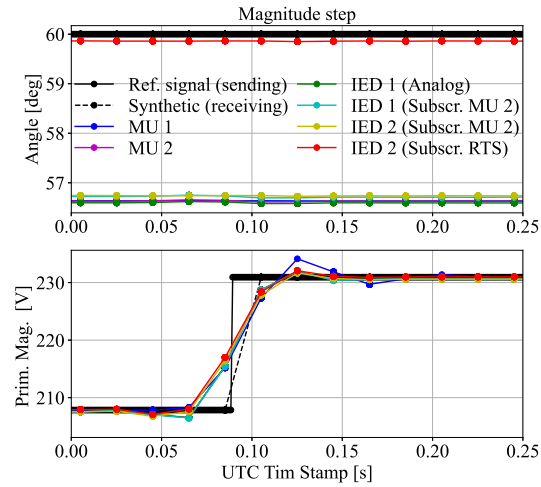

Fig. 15. Positive sequence magnitude and phase for a magnitude step change of 10 %. Phase and magnitude versus its according UTC time stamp (Note: The plotted time stamp is shifted around UTC time 1661628567.014856815 seconds).

support this approach and that any error or inaccuracy introduced in the physical measurement is not included.

Before testing any WAMPAC algorithms in a real-time laboratory configuration, it can be very beneficial to evaluated the setup with the proposed three steps method to identify the presence of inaccuracies and the devices responsible for it. The sequence of static tests performed with a ReTeSe and RTS can be helpful in efficiently finding the sources of errors in a WAMPAC test system. In the results presented, all considered IEDs and MUs behaved correctly and in the range the standard requires. Static errors up to 6% TVE were experienced when using a PHIL configuration with all the surrounding laboratory equipment.The static tests showed also that directly subscribing to sampled values from ReTeSe or RTS reduces the TVE. This should be taken into account, especially in a hybrid setup. Of course, these tests require another source (ReTeSe) that publishes IEC 61850 values as well as analog voltages representing an added cost. However, with this method, it could be quickly determined that the main source of error is between the RTS and the input of the VT and not in the RTS, VT, the MUs or in the IEDs used.

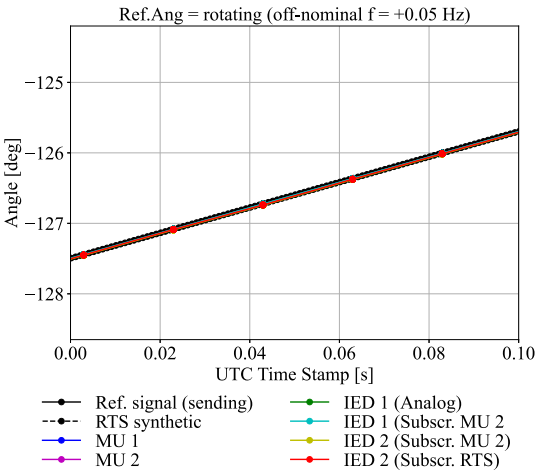

Fig. 16. Positive sequence off-nominal frequency plotted versus its according UTC time stamp (Note: The plotted time stamp is shifted around UTC time 1661628677.917056799 seconds).

WAMPAC test setups should be checked regarding the synchrophasor data latency. In this article, this was done by plotting the receiving phasors as well as the reference signal against the simulation time. The dynamic tests showed that in the presented laboratory setup the overall latency is relatively large. It should be emphasized that the measurements are synchronized well and the time stamp is correct. However, the phasor data received at the RTS is more than 150 ms. The overall latency can be plotted since the IRIG-B time synchronized internal clock in the RTS provides the simulation with an accurate time. Consequently, two different plots can be generated for each dynamic test. When plotting the phasors against the simulation time (see Figs. 13, 14) an estimation of the synchrophasor data latency is visible. The second approach is plotting the phasors against their UTC timestamp (see Figs. 15, 16). Which shows that the phasors are correctly time stamped. Note that the reference signal is directly stored in the real-time simulator and does consequently have a higher sampling rate than 50 samples per second.

The results demonstrate that UTC stamps of the individual phasors should be preferred for validating WAMPAC techniques. It was shown that when plotting the respective magnitudes and phases against their appropriate UTC timestamp, all results appear correct. However, when the phasors are plotted against the RTS simulation time, non negligible delays are introduced and these could affect WAMPAC functionalities.

VI. Conclusion

This article presented three approaches for testing WAMPAC devices and algorithms in a laboratory environment with real-time capabilities. Moreover, errors and delays that are inherently introduced have been described together with methods to quantitatively characterize them.

In the first approach, a hardwired power amplifier receives references from the real time simulator and produces voltages applied to devices generating the synchrophasors. Errors are expected from instrument transformer, amplifier, digital to analog conversion as well as other unknown error sources in the loop. In the second approach, synthetic synchrophasors are generated directly in the real-time simulator without including actual physical PMUs or IEDs with PMU functionalities. Finally in the third approach, the real time simulator transfers sample values according to the IEC 61850 to WAMPAC devices that will then produce the synchrophasors. It is not the objective of this article to prioritize one of the various approaches, since each configuration has its advantages and drawbacks. The focus is on the comparative assessment and the verification of different uncertainties that can be seen in such a setup.

Three steps were presented that help detecting static errors and two dynamic tests based on a step in magnitude and a rotating phase test. These tests quantify the errors introduced in the testing setup that should be eventually accounted when evaluating the experimental results.

References

[1] S. C. Müller, A. Kubis, S. Brato, U. Häger, C. Rehtanz, and J. Götze, "New applications for wide-area monitoring, protection and control," in *Proc. IEEE 3rd PES Innov. Smart Grid Technol. Europe*, 2012, pp. 1–8.

[2] A. Leirbukt, J. Gjerde, P. Korba, K. Uhlen, L. Vormedal, and L. Warland, "Wide area monitoring experiences in Norway," in *Proc. IEEE PES Power Syst. Conf. Expo.*, 2006, pp. 353–360.

[3] V. Terzijaet al., "Wide-area monitoring, protection, and control of future electric power networks," *Proc. IEEE*, vol. 99, no. 1, pp. 80–93, Jan. 2011.

[4] P. McLaren, R. Kuffel, R. Wierckx, J. Giesbrecht, and L. Arendt, "A real time digital simulator for testing relays," *IEEE Trans. Power Del.*, vol. 7, no. 1, pp. 207–213, Jan. 1992.

[5] M. S. Almas and L. Vanfretti, "Methodologies for power protection relay testing: From conventional to real-time hardware-in-the-loop (HIL) simulation approaches," in *Proc. Int. Conf. Power Syst. Transients*, 2013.

[6] F. Quintero-Zuluagaet al., "Hardware in the loop design and testing of a PMU-based special protection scheme: Case study of Colombia- Ecuador interconnection," in *Proc. IEEE PES Transmiss. Distrib. Conf. Exhib. - Latin Amer.*, 2020, pp. 1–6.

[7] K. Diakos, Q. Wu, and A. H. Nielsen, "Phasor measurement unit and phasor data concentrator test with real time digital simulator," in *Proc. IEEE PES Asia-Pacific Power Energy Eng. Conf.*, 2014, pp. 1–5.

[8] S. Poudel, Z. Ni, and N. Malla, "Real-time cyber physical system testbed for power system security and control," *Int. J. Elect. Power Energy Syst.*, vol. 90, pp. 124–133, 2017. [Online]. Available: https://www.sciencedirect.com/science/article/pii/S0142061516312911

[9] R. Khan, K. McLaughlin, J. H. D. Laverty, H. David, and S. Sezer, "Demonstrating cyber-physical attacks and defense for synchrophasor technology in smart grid," in *Proc. 16th Annu. Conf. Privacy, Secur. Trust*, 2018, pp. 1–10.

[10] Y. Zhang, M. Larsson, B. Pal, and N. F. Thornhill, "Simulation approach to reliability analysis of WAMPAC system," in *Proc. IEEE Power Energy Soc. Innov. Smart Grid Technol. Conf.*, 2015, pp. 1–5.

[11] T. Becejac and P. Dehghanian, "PMU multilevel end-to-end testing to assess synchrophasor measurements during faults," *IEEE Power Energy Technol. Syst. J.*, vol. 6, no. 1, pp. 71–80, Mar. 2019.

[12] S. Li, L. Zhang, J.-N. Paquin, J. Bélanger, and L. Vanfretti, "Hardware-in-the-loop use cases for synchrophasor applications," in *Proc. Int. Conf. Smart Grid Synchronized Meas. Analytics*, 2019, pp. 1–8.

[13] K. Zhu, M. Chenine, L. Nordström, S. Holmström, and G. Ericsson, "An empirical study of synchrophasor communication delay in a utility TCP/IP network," *Int. J. Emerg. Electric Power Syst.*, vol. 14, no. 4, pp. 341–350, 2013.

[14] S. Sarri, M. Pignati, P. Romano, L. Zanni, and M. Paolone, "A hardware-in-the-loop test platform for the performance assessment of a pmu-based real-time state estimator for active distribution networks," in *Proc. IEEE Eindhoven PowerTech*, 2015, pp. 1–6.

[15] M. Almas and L. Vanfretti, "Impact of time-synchronization signal loss on PMU-based WAMPAC applications," in *Proc. IEEE Power Energy Soc. Gen. Meeting*, 2016, pp. 1–5.
[16] M. S. Almas and L. Vanfretti, "RT-HIL implementation of hybrid synchrophasor and GOOSE-based passive islanding schemes," in *Proc. IEEE Power Energy Soc. Gen. Meeting*, 2016, p. 1, doi: 10.1109/PESGM.2016.7741310.
[17] D. Gurusinghe, S. Kariyawasam, and D. Ouellette, "Performance evaluation of phasor measurement units with sampled value input," in *Proc. 15th Int. Conf. Develop. Power Syst. Protection*, 2020, pp. 1–6.
[18] D. Baltensperger, K. Uhlen, S. Sanchez-Acevedo, and S. D'Arco, "Experimental characterization of methods for connecting real-time simulations and synchrophasors," in *Proc. IEEE Madrid PowerTech*, 2021, pp. 1–6.
[19] *IEEE Standard for Synchrophasor Measurements for Power Systems*, IEEE Standard C37.118.1-2011 (Revision of IEEE Standard C37.118-2005), 2011.
[20] *IEEE Standard for Synchrophasor Data Transfer for Power Systems*, IEEE Standard C37.118.2-2011 (Revision of IEEE Standard C37.118-2005), 2011.
[21] *IEEE Guide for Phasor Data Concentrator Requirements for Power System Protection, Control, Andmonitoring*, IEEE Standard C37.244-2013, 2013.
[22] P. Romano, M. Pignati, and M. Paolone, "Integration of an IEEE Std. c37.118 compliant PMU into a real-time simulator," in *Proc. IEEE Eindhoven PowerTech*, 2015, pp. 1–6.
[23] Omicron, "The universal relay test set and commissioning tool," Tech. Brochure CMC 356, 2021.
[24] T. D. Duong, S. D'Arco, and J. O. Tande, "Architecture and laboratory implementation of a testing platform for wide area monitoring systems," in *Proc. IEEE 45th Annu. Conf. Ind. Electron. Soc.*, 2019, pp. 6419–6424.
[25] S. Sanchez, S. D'Arco, A. Holdyk, and E. Tedeschi, "An approach for small scale power hardware in the loop emulation of hvdc cables," in *Proc. 13th Int. Conf. Ecological Veh. Renewable Energies*, 2018, pp. 1–8.
[26] *IEEE Standard for Synchrophasors for Power Systems*, IEEE Standard C37.118-2005 (Revision of IEEE Standard 1344-1995), 2006.
[27] SEL-401, *Protection, Automation, and Control Merging Unit Instruction Manual*, 1 ed. NE Hopkins Court Pullman, Pullman, WA, USA, 2022, p. 18.8.
[28] S. R. Firouzi, L. Vanfretti, A. Ruiz-Alvarez, H. Hooshyar, and F. Mahmood, "Interpreting and implementing IEC 61850-90-5 routed-sampled value and routed-goose protocols for IEEE c37. 118.2 compliant wide-area synchrophasor data transfer," *Electric Power Syst. Res.*, vol. 144, pp. 255–267, 2017.
[29] R. Garcia-Valle, G.-Y. Yang, K. E. Martin, A. H. Nielsen, and J. Østergaard, "Dtu PMU laboratory development - testing and validation," in *Proc. IEEE PES Innov. Smart Grid Technol. Conf. Europe*, 2010, pp. 1–6.

Daniel Baltensperger received the Master of Science degree in engineering with specialisation in energy and environment UAS from the Zurich University of Applied Sciences, Zurich, Switzerland, in 2019. He is currently working toward the Ph.D. degree in electric power system engineering with the Norwegian University of Science and Technology, Trondheim, Norway. His research interest include the optimal coordination of system protection schemes, and focuses on wide-area monitoring, protection, and control.

Santiago Sanchez-Acevedo received the B.Sc. and M.Sc. degrees in electrical engineering from the Universidad Tecnológica de Pereira, Pereira, Colombia, in 2006 and 2008, respectively, and the Ph.D. degree in electric power engineering from the Norwegian University of Science and Technology (NTNU), Trondheim, Norway, in 2015. In 2016, he joined as a Postdoctoral Research Fellow with NTNU, where he was the main academic Researcher in the Project CLUDGRID for interoperability of high-voltage DC transmission systems. Since 2019, he has been a Research Scientist with SINTEF Energy Research, Trondheim, Norway, where he is involved in projects regarding power system stability, HVdc transmission systems, laboratory analysis of digital substations, validation of cyber-physical power systems, and cybersecurity.

Salvatore D'Arco received the M.Sc. and Ph.D. degrees in electrical engineering from the University of Naples "Federico II," Naples, Italy, in 2002 and 2005, respectively. From 2006 to 2007, he was a Postdoctoral Researcher with the University of South Carolina, Columbia, SC, USA. In 2008, he joined ASML, Veldhoven, the Netherlands, as a Power Electronics Designer Consultant, where he wtill 2010. From 2010 to 2012, he was a Postdoctoral Researcher with the Department of Electric Power Engineering, Norwegian University of Science and Technology (NTNU), Trondheim, Norway. In 2012, he joined SINTEF Energy Research where he currently a Senior Research Scientist. He is the author of more than 130 scientific papers and is the holder of one patent. His main research interests invlude control and analysis of power-electronic conversion systems for power system applications, real-time simulation, and rapid prototyping of converter control systems.

Kjetil Uhlen (Member, IEEE) received the Ph.D. and M.Sc. degrees in control engineering from the Norwegian University of Science and Technology (NTNU-former NTH), Trondheim, Norway. He is currently a Professor with the Department of Electrical Power Engineering, NTNU). He is also the Head of Research with the Department of Electric Energy. He is Special Adviser with STATNETT (the Norwegian TSO - Transmission System Operator). His main research interests include power system operation and control offshore grids and wind integration.

Paper IV

Optimal and predictive under-frequency load shedding against critical islanding contingencies

Daniel Baltensperger[1], Kjetil Uhlen
Department of Electric Power Engineering
Norwegian University of Science and Technology
Trondheim, Norway
[1]daniel.s.baltensperger@ntnu.no

***Abstract*—Grid separation is a dangerous and often severe contingency. For this reason, ensuring a secure N-1 operation with regard to the potential electric islands is of great importance. Nevertheless, situations appear where operating the system closer to its limits is more effective, and consequently, grid operators are challenged to perform a difficult risk assessment. This paper proposes a procedure that could assist the operator in deciding whether the system can be operated in the so-called N-1/2 secure state (with respect to grid islanding) or not. The proposed method is a model-based procedure that pre-calculates the optimal amount of under-frequency load shedding for a known potential grid separation. It is based on a simplified dynamic model, and a sensitivity-based optimal power flow as presented in [1]. The functionality is evaluated with two scenarios in the IEEE 39 bus system and has shown satisfactory results.**

***Index Terms*—Under-frequency Load Shedding, System Protection Schemes, Optimal power flow**

I. Introduction

Under-frequency load shedding (UFLS) has long been used to protect the electrical power system from sudden critical frequency drops and, consequently, from total collapse.

The driving force for a severe drop in frequency is a sudden mismatch between power generation and load. The severity of the frequency drop depends on the size of the power imbalance, the system inertia, and the response of the primary reserves.

Conventional UFLS relays protect the system against dangerous situations and shed loads according to a pre-determined frequency threshold. This response-based manner has the following drawbacks. The frequency must be low to shed load, which is dangerous because if the imbalance still exists after load shedding (LS), the frequency will continue to drop, increasing the risk of further generator disconnection [2]. Furthermore, the location and the amount of deficit need to be sufficiently taken into account [2].

The rate of change of frequency (ROCOF) is examined in various papers as a quantity that can indicate the power mismatch in the very beginning. Therefore, this quantity can be used for predictive UFLS, which are better with respect to the disadvantages just described. In [3], for example, the ROCOF was used together with a single machine equivalent model to estimate the frequency trajectory. Voltage and frequency dependencies of the loads are estimated online. Using this knowledge, the required load to be shed can be calculated. To decide the right location to shed these loads, an iterative method is proposed. Another advantage of predictive UFLS is that typically less load needs to be shed, which motivates even more, to identify the imbalance as early as possible. [1] proposes a sensitivity-based OPF that considers post-contingency line currents and nodal voltages. Furthermore, a second-order dynamic model is used in the optimization to predict the frequency trajectory. [4] extended this idea and proposed an improved governor model that leads to a third-order model. Hydro turbines, in particular, can be better approximated in this way. The model's parameters are identified according to a special least squares method presented in [5]. In addition, [4] considers low inertia aspects and includes, besides load shedding also, large battery storage units for fast frequency reserves in the optimization.

A predictive UFLS scheme that considers interaction with the conventional UFLS relays is described in [6], where a model predictive method was proposed to determine the amount of initial load shedding for a controlled islanding (CEI) scheme. In addition to the CEI described in [6], electrical islanding (EI) can occur uncontrolled at any point. Consequently, situations can occur where an (N-1) contingency leads to an electrical EI. In this situation, an optimal control action can be pre-calculated for this particular contingency, and the system operates in the so-called N-1/2 secure state. How this can be done optimally is the main objective of the method presented in this paper.

The optimization procedure follows the main idea presented in [1] and [4]. While [1] and [4] pre-calculate the optimal UFLS for generation outages, is the focus of this paper on the imbalance caused by islanding. The objectives of this paper and the development of the method can be summarised as follows:

1) Presenting a procedure that can assist the operator in deciding whether the system can be operated in the N-1/2 secure state with respect to EI. 2) Like [1], [4] and [6], this paper has the objective to predict the frequency trajectory with a simple but sufficiently accurate dynamic model and integrate it into the optimization for UFLS. Two different models are

This work was supported by the project SynchroPhasor based Automatic Real-time Control (SPARC), funded by the ENERGIX Program of the Research Council of Norway, under Project 280967, and the industry partners, Statnett, Fingrid, Energinet, Svenska Kraftnät, Landsnet and GE.

2023 IEEE Belgrade PowerTech | 978-1-6654-8778-8/23/$31.00 ©2023 IEEE | DOI: 10.1109/POWERTECH55446.2023.10202682

compared. First, the same second-order system that [1] used, but here three parameters are identified instead of two. In the following this model is called the single machine single governor model (SiGo). The second model that is examined is a single-machine multi-governor model (MuGo) in which each governor is individually approximated with a first-order model. This was done to see how far the two models differ in the event that multiple governor limiters are reached. 3) As proposed in [2], the sum of all pre-contingency line flows to the EI can be used as an indicator for the power deficit. However, voltage and frequency-dependent loads influence the correctness [3]. In this paper, we use an example to investigate how accurate and valuable this estimation is in the case of assuming constant power loads. 4) In addition to the costs for UFLS, an indicator for the line losses is used in the objective function of the optimization.

The following assumptions are made in this paper. 1) A contingency analysis continuously checks and reports all N-1 contingencies leading to a critical grid separation. 2) In the case of a cascade, it is assumed that there is sufficient time for the pre-calculation before the final contingency separates the grid. 3) A sufficiently detailed dynamic model is available that allows an RMS simulation of the critical contingencies. Furthermore, we assume that the initial conditions are known by means of a dynamic state estimator. 4) Generator terminal voltages remain constant. The loads are assumed to be constant power loads (in the optimization as well as in the RMS evaluation). 5) One generator can act as a slack and does not participate in frequency control. 6) Droop settings, individual machine inertia, and all mechanical power limits are available from a lookup table. 7) No interaction with conventional UFLS relays. If the reader is interested in this topic, we refer to [6].

II. Methodology

In the first part of this section, the technical relevant aspects for understanding the purpose of the method and the paper are introduced. In the second part, the optimization is explained in detail.

A. Relevant technical aspects

a) The N-1/2 secure operation state: Market liberalization and the capital-intensive nature of the transmission business force the grid operator to increase the utilization of existing transmission assets for a limited period of time, carefully considering tailored reliability and security restrictions [7]. Based on risk analysis, the system operator must decide whether an operation between normal and alert is justifiable or not. This is called N-1/2 secure operation and is typically reached if a specifically tailored system protection schemes is armed for the detected critical contingency.

It can be seen as a controlled relaxation of the N-1 secure system state. In this work, the critical contingency is a grid separation that follows after a line trip (as it can be seen in figure 2). If the imbalance after the loss of line is large enough, the system is in an alert state since the frequency in the EI would drop critically low. To bring the system back to its normal state, some actions have to be triggered by the operator, although the islanding has not yet taken place. If, in such a case, instead, an optimal amount of UFLS can be pre-calculated, that can be triggered directly after the contingencies would appear. The system would be in an N-1/2 secure state, which can be financially beneficial. This is an essential part of the proposed method of this paper.

b) Imbalance and Spinning reserves: To estimate the imbalance in a future EI, the sum of all line flows connecting the EI to the rest of the system is calculated. This is here referred to as the cut flow or the flow through the cut ($\Delta P_{cut} = \sum_{i \in \mathcal{T}} P^0_{line,i}$). Spinning reserves are relevant for frequency stability. Since they dictate how much power can be fed in by the individual generators connected in the EI.

c) Dynamic aspects: When dealing with UFLS, not only the equilibrium is relevant to be considered. Often the frequency nadir is of interest. The nadir is influenced by the power deficit, the system inertia, and the governor's connected to the EI. As mentioned before, two different dynamic models will be compared in this paper. Both with the aim of achieving the simplest possible and sufficiently reasonable modeling of the frequency behavior. SiGo model substitutes all connected governors in a single first-order model, which is linked to the swing equation, as it can be seen in equation (13) and (14). The MuGo, on the other hand, approximates all governors in the EI individually as a first-order model. Basically, there are N first-order models of equation (14) and one swing equation as equation (13). Non-linearities due to limiters are approximated in the optimization model with binary values (in the differential equations).

d) Parameter identification: In this paper, the parameters are identified for a single specific grid separations contingency. This is because the topology of the system and the number of generators can vary greatly depending on the respective grid separation. An RMS simulation is carried out as a first step to simulate the contingency. Based on this solution, a least-square parameter identification is made in matlab-simulink.

In the case of the MuGo model, the particular governor time constants are identified using the individual simulated mechanical powers. In the case of the SiGo model, three parameters are estimated. Firstly, the time constant of the governor (T_{eq}) and the damping constant (D). If the individual governors reach their limit, the composite droop gain is no longer a constant. This is why in this paper, it is proposed to identify (Kp) as a third parameter as well.

e) The procedure: For implementing the method the following procedure illustrated in 1 is proposed.

If the contingency analyses detect a critical cut, the state estimator will forward a snapshot of the current system. Based on this information, the cut flow ΔP_{cut} is calculated, and a counter i is initialized. Afterward, an RMS simulation of the critical EI is triggered. If the resulting frequency trajectory is unstable, a pre-optimization is done. This is implemented because it cannot be assumed that the EI has sufficient spinning reserves. The pre-optimization decides, based on ΔP_{cut}, where and how much load to shed in the simulation

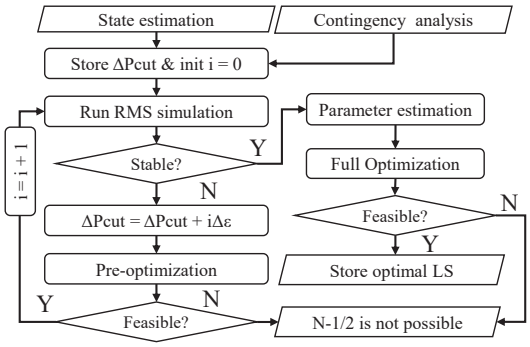

Fig. 1. Flow chart representing the basic method

such that an RMS simulation can be performed and, secondly, whether it is possible at all (i.e. whether a solution to the problem does exist). In case it is not feasible, it means that it is not possible to run the system in N-1/2 secure state. Otherwise, the first solution typically leads to a stable equilibrium, but since ΔP_{cut} is just an estimation and my be incorrect, it cannot be guaranteed that the frequency is stable after the first pre-optimization step. For this reason, ΔP_{cut} is increased in the loop successively by $\Delta\epsilon$. In case there are enough reserves $\Delta P_{reserve} > \Delta P_{cut}$, the RMS simulation produces a representative trajectory. Based on this trajectory, the parameters of the simplified dynamic model are identified. Consequently, full optimization can be computed to find the optimal load shedding. If such a solution does exist, it is stored and is ready in case the contingency appears.

B. The optimization

The pre-optimization method is explained in the first step, which does not consider any dynamic aspects. Later this optimization model is extended to the full-optimization, which includes static restrictions and dynamic aspects. To calculate the sensitivities for the approximation of the powerflow equations, [1] and [4] use a method presented in [8]. In contrast, this paper uses an automatic differentiation method to find the sensitivities. [9] was used to implement this in Python.

The objective function (1) includes prices for load shedding as well as an approximation of the line losses (equation (19) to (21)). $V_{k,m}$ is the voltage phasor between bus k and m and $g_{k,m}$ is the series line conductance. Equation (2) approximates the node voltage change at bus i. Equation (3) and (4) are analogous to (2) but approximate the change in the active and reactive power line flows. Note to save space and keep the equations minimal, the notation for the input is replaced by $\Delta u = [\Delta P_{cut}, \Delta Q_{cut}]^T$ and the variables by $\Delta x = [\Delta P_G, -\Delta P_L, -\Delta Q_L]$. The line apparent power flow limit is described as non-linear constraints in (5) and implemented with the help of piecewise linearization. The voltage limits are noted in (6). Constraint (8) ensures that the steady-state output power of all machines is equal to the sum of all pre-contingency line flows through the cut (i.e., the imbalance) minus the number of loads subject to be shed. The losses are neglected in the constraints. If the active output power is less than the maximum generator power, the active output power is calculated using its droop characteristic. Otherwise, the output power is the maximum power of the machine. This distinction is implemented with binary variables β_i as it can be seen in equation (9) to (11).

$$\min \left(\sum_{i \in \mathcal{L}} C_{load,i} \Delta P_{L,i} + \sum_{i \in \Omega_{Nl}} C_{loss,i} P_{loss,i} \right) \tag{1}$$

$$\begin{aligned} \text{s.t. } \Delta|V_i| = {} & \frac{\partial |V_i|}{\partial P_G} \Delta P_G - \\ & \left(\frac{\partial |V_i|}{\partial P_L} \Delta P_L + \frac{\partial |V_i|}{\partial Q_L} \Delta Q_L \right) + \\ & \left(\frac{\partial |V_i|}{\partial P_{L,k}} \Delta P_{cut} + \frac{\partial |V_i|}{\partial Q_{L,k}} \Delta Q_{cut} \right) \end{aligned} \tag{2}$$

$$\Delta P_{i,j} = \frac{\partial P_{i,j}}{\partial x} \Delta x + \frac{\partial P_{i,j}}{\partial u} \Delta u \tag{3}$$

$$\Delta Q_{i,j} = \frac{\partial Q_{i,j}}{\partial x} \Delta x + \frac{\partial Q_{i,j}}{\partial u} \Delta u \tag{4}$$

$$\sqrt{(P^0_{i,j} + \Delta P_{i,j})^2 + (Q^0_{i,j} + \Delta Q_{i,j})^2} \leq |S^{max}_{i,j}| \tag{5}$$

$$\Delta|V_i|^{min} \leq \Delta|V_i| \leq \Delta|V_i|^{max} \tag{6}$$

$$\Delta x^{min} \leq \Delta x \leq \Delta x^{max} \tag{7}$$

$$\sum_{i \in M} \Delta P^i_{Gen} = \Delta P_{cut} - \sum_{i \in \mathcal{L}} \Delta P_{L,i} \tag{8}$$

$$\Delta P^i_{Gen} = (-Kp_i \Delta f_{ss})\, \beta_i + \Delta P^{max}_{Gen,i} (1 - \beta_i) \tag{9}$$

$$M \beta_i \geq \Delta P^{max}_{Gen,i} + \Delta f_{ss} Kp_i \tag{10}$$

$$M (1 - \beta_i) \geq -\Delta f_{ss} Kp_i - \Delta P^{max}_{Gen,i} \tag{11}$$

The optimization problem (1) to (11) is the pre-optimization problem illustrated in the flow chart 1. In the full optimization model, the equations 1 to 11 are solved for the post-contingency steady-state. Depending on the model used, the differential equations 13 and 14 or 13 and 15 to 18 are included as additional constraints, and calculated over the entire prediction horizon. For the SiGo model, the single machine swing equation written in constraint (13) and (14) must be additionally considered:

$$f^{t \in [t_1,t_2]}_{\min} \leq f(t) \leq f^{t \in [t_1,t_2]}_{\max} \tag{12}$$

$$\begin{aligned} \Delta \dot{f}(t) = {} & \frac{1}{2H} \left(\Delta P^{tot}_{mech}(t) - D \Delta f(t) \right) + \\ & \frac{S_B}{2H S_{B,\,\text{tot}}} \left(\sum_{i \in \mathcal{L}} \Delta P_{L,i} - \Delta P_{cut} \right) \end{aligned} \tag{13}$$

$$\Delta \dot{P}^{tot}_{mech}(t) = -\frac{1}{T_{eq}} \left(\Delta P^{tot}_{\text{mech}}(t) + K_p \frac{S_B}{S_{B,\,\text{tot}}} \Delta f(t) \right) \tag{14}$$

Where S_B is the system base, $S_{B,i}$ is the rated power of generator i, and $S_{B,tot} = \sum S_{B,i}$ is the total rating. H is the total

inertia constant and calculated as $H = (\sum_i H_i S_{B,i})/(S_{B,tot})$. The three model-specific parameters (Teq,D and Kp) are only used in the dynamic model. The original individual droop used in the static equations remains the same. This is done because the differential equations are used for the approximation of the nadir and not for the static solution.

$$\hat{P}_{mech,i,t} = \left(\Delta \dot{P}_{mech,i,t} \Delta t + \Delta P_{mech,i,t}\right) \quad (15)$$

$$\Delta P_{mech,i,t+1} = \beta_{i,t} \hat{P}_{mech,i,t} + (1 - \beta_{i,t}) \Delta P^{max}_{mech,i} \quad (16)$$

$$M \beta_{i,t} \geq \Delta P^{max}_{mech,i} - \hat{P}_{mech,i,t} \quad (17)$$

$$M (1 - \beta_{i,t}) \geq \hat{P}_{mech,i,t} - \Delta P^{max}_{mech,i} \quad (18)$$

If a multi-machine multi-governor model is considered, each governor is approximated separately with a first-order model. To consider the limiters individually, the main idea is to set for each governor i and each time step t a binary variable $\beta_{i,t}$, which provides information on whether the governor has reached the limit or not. This can be seen in equations (15) to (18) and is done over the whole prediction horizon. One consequence is that the longer the prediction horizon, the smaller the time steps, and the more governors are chosen, the more binaries are needed.

As described in more detail later, the estimation $\Delta Pcut$ is rather pessimistic in this paper. Therefore, the use of this quantity in the differential equations would always tend to shed too much load, and it is, therefore, difficult to conclude anything about the accuracy of the two models. For this reason, a $\Delta Pcut$ known from the RMS simulation (the true deficit) is used in the differential equations in this paper.

Note, for simplicity, the apparent line flow constraint equation (5) was neglected in the optimization with MultiGov.

$$P_{loss,i} = P_{m,k} + P_{k,m} \approx \quad (19)$$

$$g_{k,m} \left(V^{Re}_{k,m,0} + \frac{\partial V^{Re}_{k,m}}{\partial u} \Delta u \right)^2 \quad (20)$$

$$+ g_{k,m} \left(V^{Im}_{k,m,0} + \frac{\partial V^{Im}_{k,m}}{\partial u} \Delta u \right)^2 \quad (21)$$

III. Results

In this section, the results are presented. First, the reader is introduced to the two different test scenarios, and secondly, the test results are discussed.

A. Introduction to the test scenarios

The IEEE39 model shown in figure 2 is considered. The line connecting bus 26 to 27 is assumed to be out of service. The contingency used in both scenarios is the sudden outage of the transmission line connecting buses 2 and 25. This separates the grid into two EIs and causes the frequency in the magenta-colored (lower, large) area to drop critically. In scenario one, enough spinning reserves are available; in scenario two, the power deficit is larger than the spinning reserves. Looking at the flow chart in Fig 1, it becomes clear

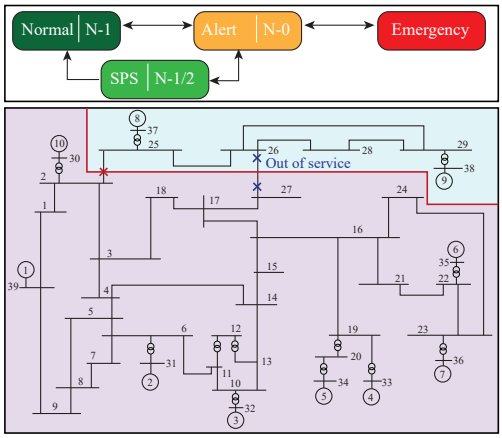

Fig. 2. Test model IEEE 39 Bus New England

how far the two scenarios differ. Scenario 1 does not require a pre-optimization step. In scenario 2, on the other hand, a pre-optimization step is needed because otherwise, there would be no representative trajectory to estimate the parameters of the model. All governors are replaced by "TGOV 1" in the considered model. In the context of this paper, some tests were performed and showed that this model could be approximated very well with a first-order model, especially when governor limits are not exceeded. To obtain a more serious frequency response, the steam bowl time constant (T1) was deliberately chosen to be very slow ($T1 = 3s$, $T2 = 1s$, $T3 = 2s$). The droop of all machines is set to 5% except the machine at bus number 39. This machine will not participate in frequency regulation in either scenario one or scenario 2. All machines are equipped with a "SEXS" exciter model.

B. Scenario 1: Spinning reserves are larger than the cut flow

Figure 3 shows on the y-axis the frequency deviation and on the x-axis delta mechanical power. The right-hand side shows the individual droop characteristics for all machines connected. The left-hand side shows in black solid the composite droop characteristic. The frequency trajectories plotted versus the total mechanical power can be seen in different colors. First, the solid magenta trajectory is considered. It represents the true center of inertia frequency deviation without triggering any load-shedding actions. The frequency drops significantly and exceeds the critical limit of -0.5 Hz. The generators connected at buses 32, 33, 34, 35 and 36 reached their limits clearly before the frequency nadir was reached. This can be seen by comparing the individual limits on the right-hand side with the magenta solid trajectories on the left-hand side. These non-linearities influence the frequency minimum (nadir) significantly. The solid blue, red, and green trajectories show the actual dynamic behavior of the system for different amounts of load shedding. The green curve shows the system's

behavior if the MuGo is used to determine the load-shedding action. A total amount of 69.595 MW and 33.706 MVar are recommended to be shed on bus 27. The plotting result indicates that minimally too little load is shed. The blue curve shows the behavior in the case of load shedding, where the amount was selected based on a SiGo. In this case, the parameters were determined using a frequency trajectory based on an RMS model that does not consider the governor limiters. Consequently, the basic composite droop is identified without any limits considered. The blue dashed curve is the dynamic response of the SiGo model used in the optimizer. The optimizer behaved correctly and kept the frequency of the simplified model within the acceptable range. The steady-state equilibrium is on the original composite droop curve (flattest gray dashed line). However, too little load is being shed, and since the system is in the N-1/2 secure state, a rather critical situation may appear.

The red trajectory shows the solution considering the amount of load shedding determined based on a SiGo model whose parameters were determined using the magenta trajectory. The parameter estimation recommends selecting a composite droop that deviates from the original (flattest gray dashed line). The SiGo behavior used in the optimizer can be seen as a red dashed trajectory. Enough loads are shed to keep the frequency nadir within the limit. Note the limiters are not explicitly modeled in the differential equation but considered since the parameters are tuned based on an RMS simulation that considers limiters. In the equations describing the static behavior, the limiters are modeled, on the other hand, with binaries. The optimizer calculated steady-state solution is the two light red lines whose intersection is on the composite droop curve (black solid). This deviates slightly from the true steady-state solution (red solid equilibrium) because the estimated power deviates from the true power deficit (see cyan line and black dashed line). Losses before islanding are different from those after because the power flows change. Since constant power loads were chosen, it can be assumed that this is the explanation for the estimation error of the power deficit. Figure 4 below shows the voltages for the different nodes. Magenta is the pre-contingency voltage magnitude for all nodes in the considered EI. Blue is the true post-contingency nodal voltage, and red is the calculated solution in the optimizer. The figure shows furthermore that the considered contingency does not lead to critical voltages. The amount of load shedding (with SiGo with limiters considered) is listed in table I.

A selection of apparent power flows are illustrated in figure 4 above. They represent the flows close to the line-tripping contingency. For detailed scenarios considering the interplay of thermal overload and UFLS in the optimization, see [1].

C. Scenario 2: Spinning reserves are smaller than the cut flow

In this scenario, the active power deficit exceeds the limited spinning reserves of 430.05 MW. In this case, a pre-optimization step is required (see figure 1) to obtain a reliable trajectory that can be used for parameter identification.

TABLE I
LOAD SHEDDING RESULTS FOR BOTH SCENARIOS

Scenario 1					
Bus Nr	4	12	15	27	
ΔP[MW]	70.743	7.5	0.204	12.489	
ΔQ[MVAr]	34.263	3.632	0.0986	6.049	
ΔP_L^{tot}	90.936	ΔQ_L^{tot}	44.043	ΔP_{mech}^{tot}	373.946
Scenario 2					
Bus Nr	7	8	16	24	27
ΔP[MW]	7.672	16.581	0.527	9.237	61.023
ΔQ[MVAr]	3.716	8.030	0.255	-4.474	29.555
ΔP_L^{tot}	95.441	ΔQ_L^{tot}	37.276	ΔP_{mech}^{tot}	368.918

Figure 5 shows the relevant aspects and results of scenario 2. The vertical black dashed line shows the estimated power deficit, determined via the pre-contingency line flows. With around 488 MW this is outside the available spinning reserves. The RMS simulation without UFLS (magenta solid) confirms this because the frequency is unstable. The pre-optimization recommends dropping around 58.8 MW on different buses to stabilize the frequency. In fact, this leads to a solution that is within the range of available reserves (light magenta curve). Unfortunately, this trajectory still exceeds the limit of -0.5 HZ. This is true because no dynamic model has been used in the pre-optimization process. Nevertheless, we use this now-generated trajectory to identify the parameters of the SiGo model needed for the full optimization (see figure 1). The solid red trajectory shows the final solution. Both steady-state frequency and limitations regarding frequency nadir are fulfilled. The solid green trajectory shows the result of the MuGo model. The optimizer recommends shedding 72.458 MW and 35.092 MVar at bus 27, which is slightly insufficient. The detailed numeric results are shown for the SiGo model in table I.

IV. CONCLUSION AND FUTURE STEPS

A model-based procedure that can assist in deciding whether N-1/2 secure operation would be possible concerning sudden grid islanding is presented. An RMS simulation is part of the procedure and is used to identify the parameters of a simplified dynamical model. This is used to decide where and how much UFLS must be armed. The paper follows the main idea proposed in [1] and [4]. But here, it is explicitly used for islanding, which leads to somewhat different challenges. The power mismatch is the driving force for the drop in frequency. The sum of the pre-contingency line flows to the EI was chosen as the indicator for the imbalance. Even with the assumption of 100% constant power loads, a significant estimation error due to changes in losses was found. This shows that reserves are essential when using such an estimator. Two simplified dynamical models were compared. The first model (MuGo) considers each governor individually and models their limiters with binary variables over the entire prediction horizon. For the case under consideration, the simulation was too optimistic. Furthermore, the optimization model quickly becomes extremely difficult to solve and complex, as many

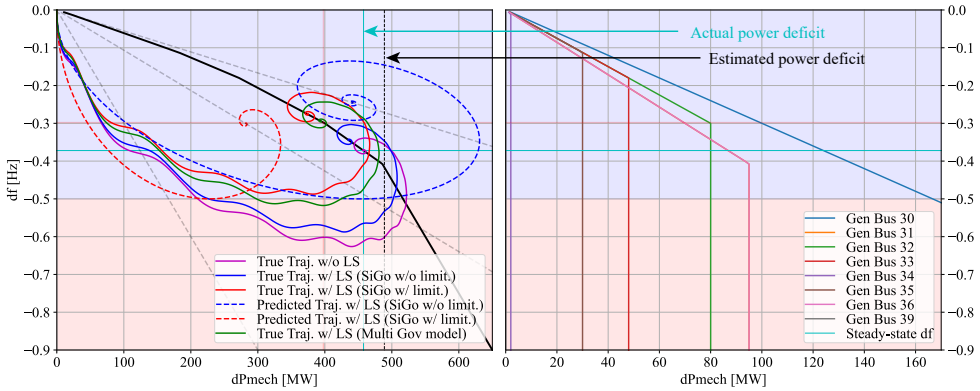

Fig. 3. left: The composite response of all machines in the EI. Right: Individual droop characteristic

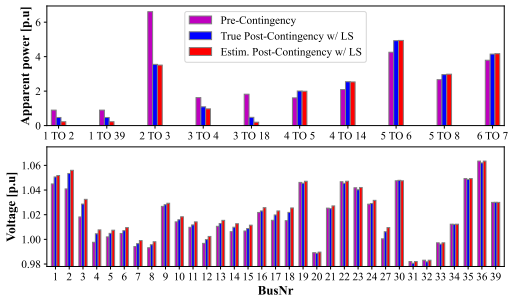

Fig. 4. Nodal voltages, and line apparent flows. For a optimization based on the SiGo (red trajectory in the fig:3)

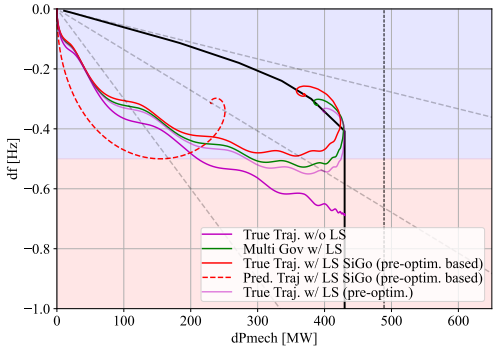

Fig. 5. The composite response of all machines in the EI

binaries have to be considered. In the presented example, about 850 binary values (prediction horizon of 12 seconds) were used. In contrast, the SiGo showed better results for the scenario studied. It is mainly because it is simple, fast in optimization, and accurate (at least in the model studied). However, it turned out that the accuracy was only achieved when the parameters were chosen with respect to a reliable trajectory that includes details such as limiters. Since, in the example shown, several governor limiters were reached, the composite droop was included in the parameter estimation. Consequently, three parameters were estimated. In the current state, the individual relevant blocks, as illustrated in figure 1 are implemented in Python and Matlab Simulink, and tests, as shown in this paper, can be carried out. Full automation, in the sense that the procedure automatically performs all steps as an independent program, will be implemented in future work.

REFERENCES

[1] Q. Walger, Y. Zuo, A. Derviškadić, G. Frigo, and M. Paolone, "Opf-based under frequency load shedding predicting the dynamic frequency trajectory," *Electric Power Systems Research*, vol. 189, p. 106748, 2020.

[2] D. T. Duong and K. Uhlen, "A topology-based scheme for adaptive underfrequency load shedding," in *2017 IEEE Manchester PowerTech*, 2017, pp. 1–6.

[3] M. Larsson and C. Rehtanz, "Predictive frequency stability control based on wide-area phasor measurements," in *IEEE Power Engineering Society Summer Meeting,*, vol. 1, 2002, pp. 233–238 vol.1.

[4] Y. Zuo, A. Derviškadić, and M. Paolone, "Opf-driven under frequency load shedding in low-inertia power grids hosting large-scale battery energy storage systems," in *2021 IEEE Madrid PowerTech*, 2021, pp. 1–6.

[5] F. Conte, S. Massucco, M. Paolone, G. P. Schiapparelli, F. Silvestro, and Y. Zuo, "Frequency stability assessment of modern power systems: Models definition and parameters identification," *Sustainable Energy, Grids and Networks*, vol. 23, p. 100384, 2020.

[6] M. Vrakopoulou and G. Andersson, "An Adaptive Load Shedding Technique for Controlled Islanding." Citeseer, 2010. [Online]. Available: https://citeseerx.ist.psu.edu/\document?repid=rep1&type=pdf&doi=60f2e8c56aa4c2f0eca7b865c057871564ead2b9

[7] O. Breidablik, F. Giaver, and I. Glende, "Innovative measures to increase the utilization of norwegian transmission," in *2003 IEEE Bologna Power Tech Conference Proceedings,*, vol. 1, 2003, pp. 8 pp. Vol.1–.

[8] K. Christakou, J.-Y. LeBoudec, M. Paolone, and D.-C. Tomozei, "Efficient computation of sensitivity coefficients of node voltages and line currents in unbalanced radial electrical distribution networks," *IEEE Transactions on Smart Grid*, vol. 4, no. 2, pp. 741–750, 2013.

[9] J. Bradbury, R. Frostig, P. Hawkins, M. J. Johnson, C. Leary, D. Maclaurin, G. Necula, A. Paszke, J. VanderPlas, S. Wanderman-Milne, and Q. Zhang, "JAX: composable transformations of Python+NumPy programs," 2018. [Online]. Available: http://github.com/google/jax

Paper V

Baltensperger, Daniel Simon; Uhlen, Kjetil Obstfelder; Stanković, Stefan; Ackeby, Susanne.
An Optimal Arming Technique for System Protection Schemes.
This paper is under review for publication and is therefore not included.

ISBN 978-82-326-7576-0 (printed ver.)
ISBN 978-82-326-7575-3 (electronic ver.)
ISSN 1503-8181 (printed ver.)
ISSN 2703-8084 (online ver.)

NTNU

Norwegian University of
Science and Technology